The Investigation of the Anticancer Effect of Artemisinin as Monotherapy and Combination Therapy in Cervical Cancer Cell Line

Sara MAGURA GAMAETHIGE

Submitted in accordance with the requirements for the degree of

MASTERS BY RESEARCH

Faculty of Health, Science, Social Care and Education

Department of Biomolecular Sciences

Kingston University

October 2024

Declaration of work

I hereby confirm that the thesis entitled “The Investigation of the Anticancer Effect of Artemisinin as Monotherapy and Combination Therapy in a Cervical Cancer Cell Line” is the result of my own independent research, conducted at the Department of Biomolecular sciences, Kingston University London, between October 2023 and October 2024. All sources consulted have been duly acknowledged and properly referenced within the thesis. I also affirm that this work has not been submitted for any degree at this or any other institution.

Acknowledgements

The completion of this study would not have been possible without the immense support I received from my supervisors Dr Ahmed Elbediwy and Dr Nadine Wehida. Their expertise, encouragement and constructive feedback were invaluable to the completion of this thesis. I am truly grateful for the opportunity to work under their supervision.

Thank you to the Department of Biomolecular Sciences at Kingston University for providing the necessary resources and facilities to conduct my experiments, which were essential for the completion of my experiments.

On a personal note, I am infinitely grateful to my parents and my brother for their constant encouragement and patience, even from afar and to my other half, Vimukthi, for his unwavering support and motivation, which has made all the difference.

A wholehearted appreciation goes to my lab partner Natalia Haddad, who helped me immensely throughout the course of this study and became a lifelong friend.

A heartfelt thank you to everyone, I appreciate you all!

Table of Contents

Table of Figures

Abstract

Cancer cell migration and proliferation are critical processes in metastasis, making them important targets for therapeutic intervention. Despite advances in chemotherapy, effective treatments with minimal side effects are still required. Evidently, drug repurposing offers a promising approach for discovering new therapeutic uses for existing drugs, reducing development time and costs. This study investigates the potential of antimalarial drugs artemisinin (ARTM) and artesunate (ART) singly and in combination with cisplatin (CIS) on HeLa cell behaviour, focusing on cell viability, migration, apoptosis and YAP localisation. HeLa cells were treated with ARTM, ART and CIS at specific concentrations. Cellular survival and proliferative potential of HeLa cells were measured using cell viability and MTT assays, while migration was assessed using a scratch wound assay. YAP translocation was examined by seeding cells at different densities to have varying localisation and staining them for imaging using a confocal microscopy. Results showed that ARTM and ART significantly reduced cell viability and inhibited migration at specific concentrations, particularly when combined with CIS. Nuclear YAP levels were decreased following treatment with ARTM and ART singly and in combination with CIS. However, phosphorylation levels analysed from Western blots did not indicate YAP phosphorylation at the LATS dependant S127 site. This raised the possibility that YAP regulation may occur via the non-canonical integrin-activated SRC signalling pathway rather than through the canonical Hippo signalling pathway.

Abbreviations

ART	Artesunate
ARTM	Artemisinin
ATR	Ataxia Telangiectasia Rad-3 Related
c-MYC	Cellular Myelocytomatosis Oncogene
CTGF	Connective Tissue Growth Factor
CYR61	Cysteine-rich Angiogenic Inducer 61
DMSO	Dimethyl sulfoxide
GAPDH	Glyceraldehyde 3-phophate dehydrogenase
HCC	Hepatocellular Carcinoma Cells
HeLa	Human Cervical Cancer Cells
HPV	Human Papillomavirus
HSP	Hippo Signalling Pathway
IF	Immunofluorescence
LATS ½	Large Tumour Suppressor Kinase ½
mAb	Monoclonal Antibodies
MAPK	Mitogen-Activated Protein Kinases
MOBKL1A/B	Mps One Binder Kinase Activator-like 1
MST ½	Mammalian STE20-like kinase ½
SAV1	Protein Salvador Homologue 1
SRC	Proto-oncogene tyrosine-protein kinase
TAZ	Transcriptional Coactivator
TEAD	Transcriptional Enhanced Associated Domain Family
Wnt	Wingless-related Integration Site
YAP	Yes-associated Protein

CHAPTER 1

Introduction

1.1 Cancer

Cancer is a debilitating disease and is one of the leading causes of deaths (Cancer Research UK, 2020). The disease accounts for more than 10 million mortalities worldwide. In the UK alone, 18.1 million new cases of cancer were reported as of 2020 (Cancer Research UK, 2020). It is identified as a disease causing severe changes to the metabolism and signalling of cells ultimately leading to uncontrollable growth and survival of cell clusters called neoplasms (Upadhyay, 2021). These cell clusters can develop into either benign tumours, which remain localised at the primary site or malignant tumours, which have the capacity to invade surrounding tissues and metastasise to other parts of the body resulting in patient death. It has been hypothesised that there are many triggers for the development of cancer, primarily resulting in alterations to DNA leading to defects in cell function in various parts of the body. Equally, the drastic dissimilarities between specific cancers make it more challenging for one particular cause to be identified. The variation in the incidence of certain cancer types and mortality across countries can be attributed to differing levels of exposure to environmental factors such as cigarette smoking, unhealthy dietary habits, hazardous chemical exposure and radiation. These disparities are particularly highlighted when comparing low-income and high-income countries (Bataouli *et al.,* 2024). Most cancers are classified into three primary categories: carcinomas, sarcomas and leukaemias or lymphomas. Carcinomas account for roughly 90% of human cancers and are malignancies originating from epithelial cells. Leukamias and lymphomas together account for about 8% of cancers, arising from blood and immune system cells, respectively. Sarcomas, which are solid tumours of connective tissues, are relatively rare in humans (Cooper, 2000). Key hallmarks of cancer include accelerated cell proliferation, evasion of apoptosis, heightened cell motility and invasiveness and the promotion of angiogenesis. These biochemical and physical properties of cancer cells can be impacted by biomechanical properties such as stiffening of the ECM, modification of collagen

reticulation etc. As a result, the activation of molecular pathways such as Wnt and The Hippo Pathway can occur (Runel *et al.,* 2021).

1.1.1 Cervical Cancer

Cervical cancer ranks as the fourth most prevalent cancer affecting women worldwide, with approximately 660,000 new diagnoses and 350,000 fatalities reported in 2022 (WHO, 2024). This cancer originates in the cervix, specifically within its layers and is often linked to infection with high-risk strains of human papillomavirus (HPV), particularly types 16 and 18 (NCI, 2023). The persistent presence of high-risk HPV strains, along with the activity of viral proteins E5, E6 and E7, interacts with host cellular factors to initiate and sustain a malignant state. Early detection plays a crucial role in preventing this type of cancer as well as being vaccinated against HPV (Burmeister *et al.,* 2022). The oncogenic pathways associated with cervical cancer are closely related to the E6 and E7 viral proteins which not only drive malignancy but also facilitate the accumulation of genetic mutations and viral integration into the host genome. Consequently, detecting HPV E6/E7 mRNA has emerged as a promising strategy in cervical cancer screening, utilising techniques like RT-PCR and nucleic acid sequence-based amplification (Zhang *et al.,* 2020). Additional screening approaches include Pap smears, visual inspection with acetic acid or Lugol's iodine, liquid-based cytology and HPV testing (Bouvard *et al.,* 2021).

1.2 The Hippo Signalling Pathway

One of the main themes that persist amongst all cancers is the atypical regulation of signalling pathways that leads to the generation, invasion and metastasis of malignant cancers. As mentioned, the most common signalling pathways altered in malignant cancers include: Wnt/β-catenin, PI3K/AKT/mTOR, Notch, Nf-κB and the Hippo signalling pathway (He *et al.,* 2021). The Hippo Signalling Pathway (HSP) is found to be dysregulated

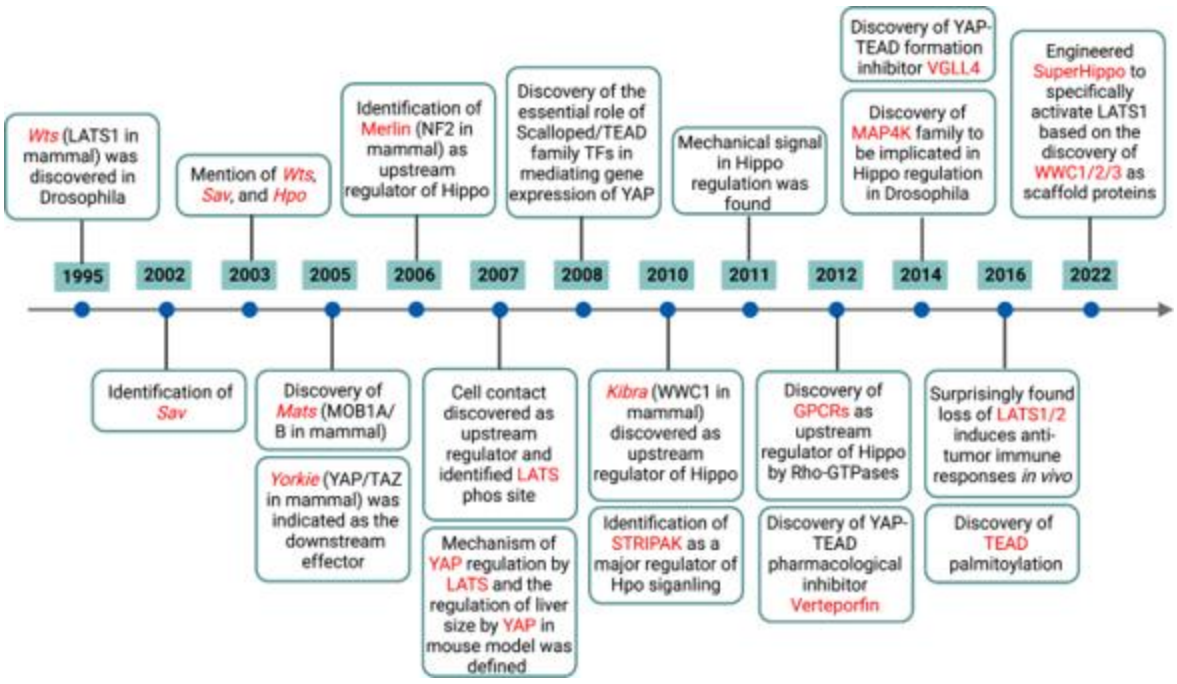

Figure 1.1: *Timeline of the Hippo signalling pathway (Fu et al., 2022).*

in a wide range of cancers (Lv and Zhou, 2023). The Hippo pathway also known as the Salvador-Warts-Hippo is a commonly known and highly conserved pathway that controls growth regulation, organ size, tissue homeostasis and regulation of stem cell pluripotency (Wang and Baker, 2019; Xiao and Dong, 2021). It was initially discovered in *Drosophila melanogaster* and different components of the pathway are constantly discovered (Figure 1.1).

The mammalian HSP is consisted of roughly 30 proteins amongst which are the key components such as mammalian STE20-like kinase ½ (MST ½), protein Salvador homologue 1 (SAV1), MOBKL1A/B, large tumour suppressor kinase ½ (LATS ½), Yes-associated protein (YAP), WW-domain-containing transcription regulator 1 (TAZ) and the

transcriptional enhanced associated domain (TEAD) family (Fu *et al.,* 2022). The different components of the pathway are categorised into upstream regulatory proteins, main core kinases and downstream transcriptional mechanisms. The HSP is activated by numerous external stimuli including cell-cell adhesion, mechanotransduction, extracellular signalling, cell polarity and G-coupled protein receptor (GPCRs) complexes. Once activated, the phosphorylation of YAP and TAZ is increased by a kinase cascade formed by the association of MST ½ with SAV1 to phosphorylate and activate LATS ½ involved with MOB1A/B. Consequently, YAP and TAZ are excluded from the nucleus by degradation by proteosomes in the cytoplasm or through interactions with 14-3-3 proteins. In turn the transcriptional activity of TEAD is decreased. As a result, gene expression in downstream genes such as CTGF, c-MYC and CYR61 is suppressed by the activation of the HSP (Pan, 2010) (Figure 1.2).

1.2.1 Yes-associated Protein (YAP)

YAP is a one of the two transcriptional coactivators and the main effector protein of the HSP. Numerous studies have suggested that a wide range of malignancies exhibit accumulation and activation of YAP. Overexpression of YAP is a prevalent characteristic across various cancers, including glioma, lung, pancreatic, colorectal, breast and prostate cancers among others (Lv and Xiangxiang, 2023). The HSP is a serine/threonine kinase module which phosphorylates YAP on serine residues leading to YAP isolation in the cytoplasm, essentially preventing YAP from entering the nucleus ultimately regulating YAP function by restricting its coactivating transcriptional function (Werneburg *et al.,* 2020). In normal tissue YAP is continually regulated and kept inactive, the activation of YAP is essential for embryonic development and non-homeostatic conditions such as wound healing and regeneration in such areas where rapid cell division is experienced. YAP can be regulated through non-canonical pathways involving various cellular signalling mechanisms, including the epidermal growth factor receptor (EGFR), Rho-GTPases and

integrin-activated SRC kinases. SRC kinases can directly phosphorylate YAP on tyrosine residues, specifically Y341, Y357 and Y394. This phosphorylation not only regulates YAP activity but also alters its interactions with other cellular proteins. In addition to direct phosphorylation, SRC kinases can inhibit LATS½, key regulators of YAP within the canonical HSP. This inhibition prevents YAP phosphorylation, thus promoting YAP's nuclear localisation and transcriptional activity, further enhancing its role in regulating cellular proliferation and differentiation (Elbediwy *et al.,* 2016; Li *et al.,* 2016).

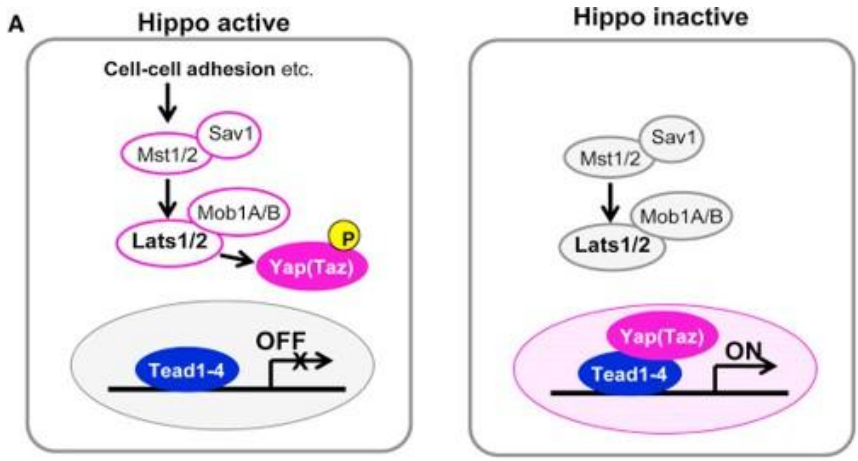

Figure 1.2: *The Hippo signalling pathway regulates gene transcription via YAP/TAZ (Sasaki, 2015).*

Hippo active (left): LATS ½ phosphorylates YAP, preventing its nuclear entry and keeping gene expression 'OFF'. Hippo inactive (left): YAP enters nucleus, binds TEAD 1-4 and activates target gene transcription 'ON'.

1.3 Treatments

The intricate nature of cancer has made it challenging to develop effective treatments. The most common forms of treatment are surgery, chemotherapy, radiotherapy and hormonal therapy. With recent advancements more precise treatment methods including immunotherapy, stem cell therapy, ablation therapy, radionics, natural antioxidants, and chemodynamic therapy have been introduced for the treatment of different types of cancers (Debela *et al.,* 2021) Advancements in treatment have also elevated survival rates and made managing terminal conditions more feasible.

The most frequently used treatment for hormone-dependent cancers such as breast, uterine, prostate and endometrial is hormone therapy. It is a non-toxic and efficient form of therapy especially for cancers which are oestrogen and progesterone receptor positive such as breast or prostate cancers. This form of therapy acts by either modifying activity of the receptors or hindering the hormone production. However, with metastatic cancers, almost all different types of therapies including hormonal therapy have to be administered either as a pre-surgery treatment (neoadjuvant), after surgery (adjuvant) or as a treatment to relieve symptoms (palliative) (Abraham and Staffurth, 2020).

Additionally, more precise therapies such as immunotherapy are treatments that directly targets cells at the tumour site unlike traditional treatment methods that affect the adjacent healthy cells. Targeted therapy as such minimises damage to healthy cells and often results in lesser side effects compared to chemotherapy. Immunotherapy primarily works by engaging with the patient's immune system, boosting its capacity to recognise, attack and eliminate cancerous cells. Similarly, treatments such as monoclonal antibodies (mAbs), immune checkpoint blockers, cytokines and cancer vaccines function by limiting the scope of action of specifically targeted proteins (Puhalla *et al.,* 2021).

Compared to conventional treatment methods, targeted therapy proves more effective by minimising the unwanted side effects commonly associated with cancer treatments (Zhou and Li, 2022). Another newer common mode of treatment and prevention used for diseases is vaccination. Vaccines have also been developed for cancers which can either be prophylactic or therapeutic. Despite having researched for numerous years, only a few vaccines are available to fight against cancers (Kaczmarek *et al.,* 2023). Therapeutic vaccines are developed to induce an immune response against antigens of specific tumours whereas prophylactic vaccines function by hindering and deferring the development of cancer by killing viruses that can cause cancer or enhancing the immune response against premalignant lesions (Grimmett *et al.,* 2022). Various factors such as the tumour

microenvironment, antigen type, immune landscape are responsible for the invention of a successful vaccination.

Given the wide range of side effects associated with traditional treatment methods, non-toxic alternatives are increasingly being developed to treat cancers as well as other diseases. UV rays, pollution and tobacco smoke are external stressors that result in the formation of reactive species including oxidants and free radicals which are responsible for the development of an array of diseases including cancer. In addition to these, our bodies naturally create such stressors from metabolism or macrophages, aerobic processes, mitochondria and peroxisomes. Oxidative stress and reactive oxygen species can profoundly impact the regulation of transcription factors by inducing damage to DNA and other biomolecules. As a result, transcription factors responsible for the gene expression of growth, repair and differentiation may be adversely affected. Natural antioxidants such as vitamins, polyphenols and plant-derived bioactive compounds can be used as therapeutic and preventative drugs against such molecules. Compounds including curcumin, berberine, quercetin are natural antioxidants that can be used for the treatment of various tumours including brain, lung, pancreatic and leukaemia (Debela *et al.,* 2021; Marino *et al.,* 2023).

1.3.1 Chemotherapeutic Agents

Chemotherapy is the most widespread treatment used for cancers which is also typically used in conjunction with surgery. Chemotherapeutic agents are used to evade invasion and metastasis by inhibiting cell proliferation and reducing tumour growth. While chemotherapy remains a highly effective treatment, its severe cytotoxic effects, particularly on adjacent healthy cells, present significant challenges.

Conventionally, chemotherapeutic agents operate by disrupting the synthesis or function of DNA, RNA and proteins, thereby affecting the macromolecular processes essential for the survival and proliferation of neoplastic cells. Thus, triggering apoptosis (cell death) in the cells. Traditional drugs can also induce cell death; however, the process is often delayed

since only a fraction of cells die at a time, requiring repeated treatments to achieve the desired therapeutic response (Amjad *et al.,*, 2023). There are multiple groups of chemotherapeutic agents differed by their primary mechanism of action, such as alkylating agents, platinum analogues, antimetabolites and topoisomerase inhibitors. The secondary mechanisms of action of these drugs contribute to the cytotoxic effects of chemotherapies by impeding mitochondrial biogenesis and producing reactive oxygen species (Tilsed *et al.,* 2022).

Topoisomerases (Top) such as irinotecan, topotecan, doxorubicin, etoposide and teniposide create a drug/enzyme complex insinuating DNA in order to bind to Top, essentially intruding the normal function of the Top enzymes to cause cell death. Antimetabolites such as 5-fluorouracil, cytarabine, gemcitabine and clofarabine act by integrating DNA to inhibit synthesis and causing premature chain termination. Alkylating agents such as mitomycin, streptozocin, dacarbazine transfer alkyl groups to DNA, subsequently causing DNA damage by generating covalent adducts (Gilbert *et al.,* 2012). The most commonly used group of alkylating agents are their platinum analogues namely, cisplatin, carboplatin and oxaliplatin. Platinum-based chemotherapies form crosslinks between DNA to induce DNA damage and hinder DNA repair, replication and transcription to halt any cell growth in a tumour (Tilsed *et al.,* 2022)

Chemotherapy can be administered orally, intravenously, subcutaneously and by intramuscular shots. Despite the several methods of administration, intravenous chemotherapy is classed as the most effective and efficient due to its 100% absorption rate (Amjad *et al.,* 2023).

Although chemotherapy is highly effective and efficient in treating cancer, it is well-documented that this treatment is associated with numerous side effects that can significantly impact patient health. The most frequently seen side effects of chemotherapy include nausea, vomiting fatigue, loss of appetite (and weight loss), hair loss, altered bowel habits, pain and depression (Akashdeep *et al.,* 2020). Chemotherapy not only induces a

range of physiological effects but also contributes to DNA damage in the healthy tissue around, leading to genomic instability, causing toxicity and increased aging (Boogard and Komnios, 2022).

Cisplatin or cisplatinum scientifically known as cis-diamminedichloroplatinum (II) belongs to the alkylating class of chemotherapeutic agents. It is a first-generation platinum-based drug characterised by two chloride ligands arranged in a cis configuration (Figure 1.3) (Berdnarska and Krol, 2022). Despite its high toxicity, it is one of the most commonly used chemotherapeutic agents for solid tumour malignancies. Cisplatin is clinically approved to be used against cancers in the ovaries, lung head and neck, although its therapeutic applications extend to various other cancer types (Gold and Raja, 2023) In the bloodstream, the structure of cisplatin is distinctly stabilised due to the presence of a high concentration of chloride ions. Cisplatin only undergoes biochemical transformations only after being absorbed by the cell. Although the transport mechanism of cisplatin has not been fully deciphered, some studies suggest that it penetrates the plasma membrane through passive diffusion while others suggest partial uptake may be facilitated by protein transporters such as ATPases (Ciarimboli, 2012; Spreckelmever *et al.,* 2014).

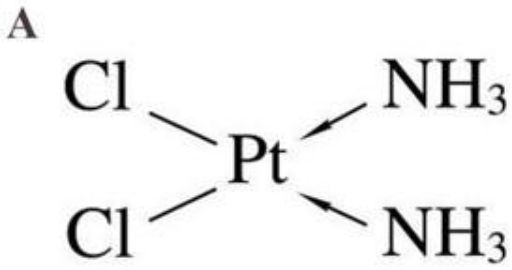

Figure 1.3: *Chemical structure of cisplatin (Dai et al., 2017).*

1.4 Drug Repurposing

The concept of drug repurposing also known as drug repositioning has emerged as a widespread approach, which uses a previously approved drug for a different indication than its original application (Kulkarni *et al.,* 2023) In the concept of systematic drug repurposing strategies, pharmaceutical companies typically employ three primary approaches: drug, disease and target centric. Drug centric approach involves repurposing existing drugs by

exploring their pharmacological profiles for new therapeutic indications. It focuses on revisiting drugs that initially failed to demonstrate sufficient efficacy for their intended indication or did not obtain approval. By re-examining their mechanisms of action or targeting different conditions, these drugs may be repurposed for alternative therapeutic uses. Moreover, the drug centric approach also looks at drugs that were pulled from the market due to safety concerns to then identify alternative dosing or different patient populations to find renewed therapeutic value. The disease centric approach focuses on finding drugs that can modulate pathways or mechanisms central to the pathology of a specific disease. Finally, the target-centric approach revolves around identifying and validating biological targets, typically proteins or genes implicated in disease processes. The objective is to repurpose drugs that can modulate these targets, regardless of the original indication of the drug (Pushpakom *et al.,* 2018).

Drug repurposing offers several significant advantages over conventional drug development, with one of the primary benefits being the substantial reduction in development time. Since repurposed drugs have already undergone extensive testing for safety, pharmacokinetics and toxicology in their original indications – much of the early-stage development work such as preclinical studies and Phase I clinical trials – have already been completed. This allows the focus to shift more rapidly to evaluating efficacy for the new indication, often bypassing several time-consuming steps in the traditional drug development route (as shown in Figure 1.4). As a result, the overall time to market can be significantly shortened, enabling quicker access to potentially life-saving treatments for patients (Rao *et al.,* 2022).

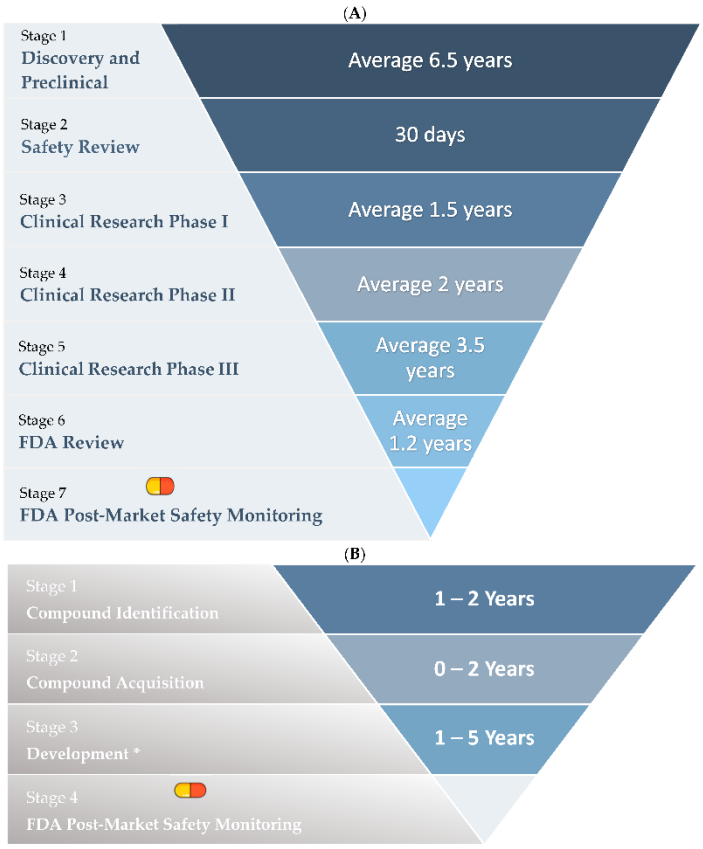

Figure 1.4: *Timeline of drug repurposing compared to traditional drug development (Haddad et al., 2024)*

Thus, this approach typically reduces the development timeline to approximately 3-12 years in contrast to the 13-17 years often required for new drug development. This accelerated timeline not only speeds up the availability of treatments but also significantly lowers the financial burden associated with drug development which makes drug repurposing an attractive strategy for developing new therapies with less investment (Hua *et al.,* 2022).

1.4.1 Metformin

A good example of a successful repurposed drug for cancer is metformin, which is the widely prescribed agent for type 2 diabetes. Metformin functions by inhibiting the activity of mTOR which in turn activates ataxia telangiectasis mutated (ATM) and LKB1 (liver kinase B1). This cascade ultimately triggers the adenosine monophosphate-activated kinase (AMPK) pathway leading to impeding protein synthesis and cell growth (Saraei *et al.,*

2019). Elevated mTOR-dependent protein synthesis is a key pathway in breast tumorigenesis in humans. The antitumour properties of metformin may also arise from its ability to lower blood glucose levels and reduce insulin resistance. This reduction leads to decreased levels in insulin and insulin-like growth factor 1 (IGF-1), which can subsequently inhibit cancer cell proliferation. (Daugan *et al.,* 2016).

Additionally, natural compounds such as curcumin, ginger and Vernonia amygdalina have also proven effective for the treatment of various cancers, alone and in combination with chemotherapeutic agents such as cisplatin (Dasari *et al.,* 2022).

1.5 Antimalarial Drugs

Frequently used antimalarial drugs such as chloroquine and its derivative hydroxychloroquine have been effectively repurposed for the treatment of autoimmune diseases such as rheumatic arthritis and systemic lupus erythematosus. Numerous studies have also confirmed their effectiveness towards the treatment of different solid and haematological tumours (Abdel-Aziz *et al.,* 2022; Agalakova, 2024; Kamat and Kumari, 2021). Chloroquine is often employed to enhance the sensitivity of tumour cells to chemotherapy and radiotherapy, making it a commonly used agent in combination therapy for cancer. It has been shown to regulate various cellular signalling pathways involved in inflammation and cancer, surpassing other significant natural agents like curcumin in this regard (Zhou *et al.,* 2020) Tumour cells rely on autophagy as an essential adaptive mechanism for their survival. Thus, when sensitising cancer cells against chemotherapy autophagy is inhibited. However, this may also lead to the sensitization of kidney cells to chemotherapy resulting in acute kidney injury (Kimura *et al.,* 2013). Indeed, when administered on different types of cultured cancer cells such as human cervical cancer (HeLa), melanoma (SK-MEL23), triple negative breast cancer (Hs578t) cells autophagy had decreased and a decrease in cell viability and increase in apoptosis were also observed

in glioma (U87MG), melanoma (SK-MEL23) and breast cancer (MCF-7) cells (Agalokova, 2024).

1.5.1 Artemisinin

Deriving from sweet wormwood extracts, Artemisia annua, commonly known as artemisinin (ARTM) is a widely used drug against malaria, even the highly drug-resistant strains unlike conventionally used agent chloroquine (Krishna *et al.,* 2008)**.** ARTM is a short acting tetracyclic endoperoxylactone (Figure 1.5) which exhibits nanomolar potency in combating resistant strains of malaria (Jahan *et al.,* 2021). ARTM exhibits activity against a range of parasite species *in vitro,* including protozoa that are phylogenetically distinct from apicomplexan parasites like *Plasmodium* species, which cause malaria. Additionally, ARTM is effective against metazoan parasites such as *Schistosoma spp* (Krishna *et al.,* 2008). This broad-spectrum antiparasitic activity underscores the potential of artemisinin as a potent anticancer agent. According to numerous studies, ARTM has demonstrated therapeutic efficacy against a variety of tumour types including breast, ovarian, pancreatic and lung cancers (Zhou *et al.,* 2017). Artemisinin exerts its anticancer effects through multiple mechanisms, including the induction of apoptosis and ferroptosis (iron dependent non-apoptotic cell death) by generating reactive oxygen species (ROS) and causing cell cycle arrest (Willoughby *et al.,* 2009; Wong *et al.,* 2017; Zhu *et al.,* 2021) (Figure 1.6).

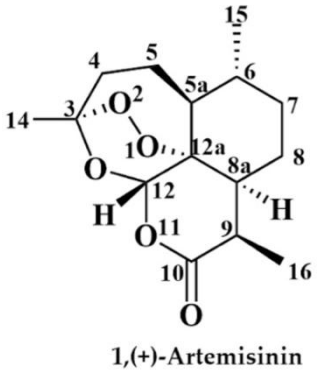

Figure 1.5: *Chemical structure of artemisinin*

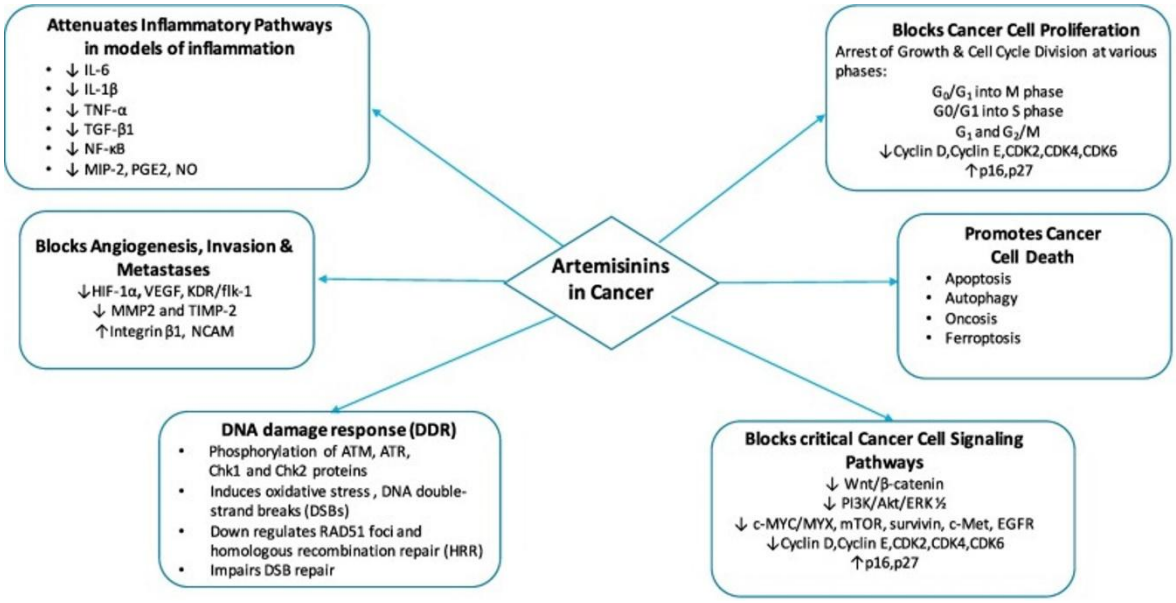

Figure 1.6: *Antitumour effects of artemisinin (Augustin, Staines and Krishna, 2020).*

ARTM exerts its antitumour effects by disrupting various stages of the cell cycle, primarily targeting the G0/G1 or S phases. This disruption is achieved through modulation of the activity and expression of key cell cycle regulatory enzymes. Additionally, ARTM impairs glycolytic metabolism by decreasing glucose uptake, which is mediated by reduced expression of the glucose transporter GLUT1. This inhibition affects lactate production and decreases ATP synthesis in non-small cell lung cancer cell lines (Kiani *et al.,* 2020) As mentioned, ARTM induces apoptosis through the generation of ROS which damage cellular organelles, DNA and proteins ultimately leading to cancer cell death. ROS-mediated apoptosis is primarily caused through Bax-dependent intrinsic pathway (Jia *et al.,* 2016). In Huh7 and Hep3B cells treated with ARTM this pathway is activated, resulting in mitochondrial dysfunction, the release of cytochrome c and subsequent activation of capase-9 (Pang *et al.,* 2016). This activation cascades to caspase-3, an executioner caspase that targets and degrades critical cell components contributing to cell death (Chen *et al.,* 2017). Furthermore, ARTM treatment has been shown to cause dose-dependent increase in caspase-3 cleavage in HepG2 hepatocellular carcinoma cells as well as in K562 leukaemia cells and pancreatic cells, reinforcing its role in promoting apoptosis (Hou *et al.,* 2008; Zhou *et al.,* 2007). Consequently, ARTM can target various cellular processes and impact

several signalling pathways involved in cancer progression. Indeed, ARTM has shown to inhibit cell proliferation and metastasis. ARTM interferes with Wnt/β-catenin signalling pathway in lung cancer cells, resulting in increased expression of E-cadherin, a protein crucial for cell-cell adhesion. Enhanced E-cadherin expression promotes strong cell-cell adhesion and hinders epithelial to mesenchymal transition which is a hall mark of metastasis (Tong *et al.,* 2016; Xu *et al.,* 2015).

1.5.2 Artesunate

Artesunate (ART) is the semisynthetic derivative of ARTM, which is also a commonly used treatment against malaria. Similarly, in addition to its antimalarial properties, ART has demonstrated significant biological activity against various types of cancers (Ruwizhi *et al.,* 2022). ART is a semisynthetic compound characterised by its peroxide-bridged sesquiterpene lactone structure also referred to as dihydroartemisinin-12-α-succinate (Aprioku and Obianime, 2011) (Figure 1.7). Compared to ARTM, ART exhibits superior adsorption, solubility and pharmacokinetic properties. ART can be administered through multiple routes including intramuscular, oral, rectal and intravenous. When administered orally, ART has relatively short half-life of 20 to 45 minutes (Ismail *et al.,* 2018) ART induces cell death through mechanisms similar to those of ARTM, including autophagy, oncosis and ferroptosis in addition to its non-apoptotic effects (Jiang *et al.,* 2018; Ooko *et al.,* 2015). Moreover, ART influences multiple critical processes in cancer progression. It impedes tumour cell proliferation and invasion, induces cell cycle arrest and disrupts crucial cancer signalling pathways. It also induces oxidative stress leading to cellular damage and triggers apoptotic cell death. Additionally, it exerts anti-angiogenic effects and

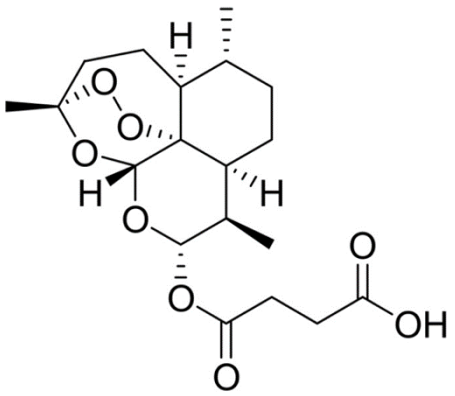

Figure 1.7: *Chemical structure of artesunate (Chung et al., 2013)*

has been shown to inhibit metastasis, further proving its potential as a complex anticancer agent (Xu *et al.,* 2020; Zhao *et al.,* 2013). Indeed, research indicates that ART is the more potent agent as a cancer therapy in comparison to ARTM. It targets major pathways such as NF-κB to achieve its anti-angiogenic effect by targeting VEGF, VEGFR and EGF and also supresses Wnt/β-catenin through β-catenin downregulation hindering proliferation, invasion and angiogenesis (Kiani *et al.,* 2020). It has also been reported that ART inhibits cell proliferation by stimulating the ROS-mediated activation of the AMPK-mTOR signalling pathway in glioblastoma cells (Strik *et al.,* 2024).

1.6 Aims

The aim of this project was to evaluate the anticancer effects of artemisinin and artesunate on human cervical cancer (HeLa) cells, both individually and in combination with the chemotherapy cisplatin. The primary goal is to assess whether the drugs inhibit cancer growth, survival and metastasis and if this is due to the drugs' inhibition of the HSP effector YAP.

1.7 Objectives

- To determine the anticancer effects of ARTM and ART by assessing their effects on cell proliferation, migration and apoptosis.
- To determine ARTM and ART's effect on the HSP effector YAP and if its activation is affected.
- To determine if ARTM and ART influences any downstream regulatory genes of the HSP.

CHAPTER 2

Material and Methods

2.1 Experimental Procedures

Cell culture processes carried out as part of this thesis were performed in a laminar flow hood and handled with aseptic techniques. Cell culture media (RPMI) was supplemented with 10% Fetal Bovine Serum (FBS) and 1% penicillin streptomycin (Pen-Strep) and thawed at 37°C prior to use.

2.1.1 Cell Culture Maintenance of Cervical Cancer (HeLa) Cells

Human Cervical Cancer cells (HeLa) supplied by Kingston University, London, were maintained in 75cm^3 Nunc EasYFlask Cell Culture Flasks from ThermoFisher Scientific and maintained with RPMI supplemented with 10% FBS (Fetal Bovine Serum) and 1% Pen-Strep. Cells were then incubated for growth at 5% carbon dioxide (CO_2) at 37°C using a Thermofisher HERACELL 150i CO_2 incubator.

At 70-80% confluency cells were briefly passaged by aspirating the supernatant and washing with 5mL of PBS. Upon removal of PBS, 6mL of 0.05% Trypsin was added and incubated for 5-10 minutes in 5% CO_2 at 37°C. Once the cells have fully trypsinised and detached, 1mL of cells were aspirated out and suspended in a 75cm^3 flask with fresh RPMI in a 1:6 split for stock. For experimental purposes, cells were seeded in 6, 12, 24 or 48 well plates. Seeded cells were then returned to the incubator with 5% CO_2 at 37°C.

2.2 Artemisinin, Artesunate and Cisplatin Treatments

HeLa cells were treated with antimalarial drugs artemisinin and its semi-synthetic derivative artesunate and chemotherapeutic agent cisplatin at different concentrations alone and in combination purchased from Sigmas Aldrich (see appendix Table II).

2.2.1 Scratch Assay

HeLa cells were seeded in 6, 12 or 24 well plates at a density of 0.03 x 10^6, 0.01 x 10^6 and 0.005 x 10^6 in RPMI media to achieve increased confluency to perform a scratch assay

analysis. When cells reached around 95-100% confluency forming a complete monolayer, the edge of a p200 pipette tip was used to form a scratch diagonally across the middle of each well before treating with different concentrations of already prepared artemisinin, artesunate, cisplatin and 0.1% DMSO in the control wells. Images were taken at time 0, 24 and 48 hours after treatment to observe migration using Invitrogen EVOS Imaging System.

2.2.2 Viability Assay

HeLa cells were seeded in 6, 12 or 24 well plates at a density of 0.03×10^6, 0.01×10^6 and 0.005×10^6 in RPMI cell culture medium overnight in 5% CO_2 at 37°C to achieve 40-50% confluency to perform a cell viability assay. When desired confluency was reached, control wells were treated with 0.1% DMSO and the rest were treated with already prepared concentrations of artemisinin, artesunate and cisplatin. Images were taken at time 0, 24 hours and 48 hours after treatment to observe the proportion of live and healthy cells within the population using an Invitrogen EVOS Imaging System.

2.2.3 MTT Assay

HeLa cells were seeded into a 96 well microplate at a density of 0.01×10^6 in RPMI cell culture medium and incubated to grow up to 40-60% confluency overnight in 5% CO_2 at 37°C. The following two days were used to treat the cells with 0.1% DMSO, artemisinin, artesunate and cisplatin at 48- and 24-hours intervals. 48 hours after treatment, 10µL of Roche MTT labelling reagent was added and incubated for 4 hours in 5% CO_2 at 37°C. Following the incubation, 100µL of solubilisation buffer was added to each well and incubated overnight in 5% CO_2 at 37°C.

The following day, the spectrophotometric absorbance was measured using the Infinite M200 Pro microplate (ELISA) reader with a wavelength of 580nm and reference wavelength of 680nm.

2.2.4 Caspase-3 Assay

To measure cell death (apoptosis), a colorimetric assay kit from Millipore (see appendix Table IV) was used. HeLa cells were plated in a 6 well plate and incubated over night to achieve 80-85% confluency. Cells were then treated with the desired drug concentrations and one control well with 0.1% DMSO.

Treated cells were harvested and resuspended in 150µL of cell lysis buffer (Part No. 90065) in Eppendorf tubes 24 hours later . Subsequently, the samples were centrifuged in a microcentrifuge for 5 minutes at 10,000 rcf. The supernatants of the samples were then transferred to new Eppendorf tubes and incubated on ice. Following the incubation, 150µL of caspase-3 substrate (Ac-DEVD-pNA) (Part No. 90080) added to the supernatants and incubated for 2 hours at 37°C.

Consequently, samples were transferred to a 96 well microplate and read using an ELISA microplate reader (Infinite M200 Pro) at 405nm.

Experiment was repeated twice with 3 replicated each time. Mean caspase-3 activity was obtained and analysed on Microsoft Excel.

2.3 Western Blotting

2.3.1 Cell Lysis

HeLa cells were seeded on a 48 well plate at a concentration of 0.03 x 10^6 and incubated in 5% CO_2 at 37°C for 24 hours. Cells were treated with the desired drug concentrations and controls with 0.1% DMSO and incubated for another 24 hours. Lysis buffer was prepared with a 1 in 10 dilution of Sample Reducing Agent and 1 in 2 of lithium dodecyl sulphate (LDS). Sample buffer in distilled water. Wells were washed 3 times using PBS prior to adding 100µL of lysis buffer 24 hours post treatment.

Samples were heated at 95°C for 10 minutes for protein denaturation and further homogenised with a 25-gauge needle prior to loading on to the gel.

Lysed cells were stored in the 48 well plate at -20°C until western blot was performed.

2.3.2 SDS-PAGE

Preparation of gels were done using the following volumes of Ultra Pure ProtoGel A, Ultra Pure 4X ProtoGel Resolving Buffer, ProtoGel Stacking Buffer, distilled water, tetramethylethylenediamine (TEMED) and 2% ammonium persulphate APS (as shown in appendix Table VI)

To prepare gels, the Bio-Rad gel rack was assembled using a glass back plate and a short plate stacked on top of each other. Subsequently, the 10% separating gel was added until 75% of the gap had filled. Distilled water was added to get rid of any bubbles and discarded once gel had set. Roughly 30 minutes after the separating gel had set, 3% stacking gel was added till the top and a 1.0mm comb was inserted promptly ensuring no air bubbles were present.

. The glass with the gel was then fitted into the Bio-Rad electroporator tank filled with running buffer. PageRuler Plus Prestained Protein Ladder (10µL) was loaded followed by 20µL of samples and two controls of 15µL and 10µL into each well. The gel was then run for 1 hour or until the dye front runs off the bottom of the gel at 150V.

2.3.3 Gel Transfer

Once the run was completed, the gel was carefully placed in between the filter papers on top of the nitrocellulose membrane in the sandwich (made by placing a fibre foam pad, a filter paper, a nitrocellulose membrane another filter paper and a foam pad, starting from the red side of the cassette), making sure to dab away any bubbles formed before closing the sandwich and using a roller to release any further air bubbles left.

The sandwich was then placed in the buffer tank making sure the colours on the sandwich correspond the colours in the tank (i.e., red to red and black to black). The tank was plugged into the power unit and run for 120 minutes at 100V and 0.7A.

2.3.4 Western Blot

Following the transfer the membrane was carefully taken out of the sandwich and the excess membrane was cut and placed in a black cassette and stained with amido black for 20 seconds to check for protein bands. Subsequently, the membrane was washed with destain solution for 20 minutes ensuring to change the solution every 10 minutes. The membrane was then washed with PBS for 5 minutes to neutralise any acid left. Afterwards, the membrane was incubated in 5% milk/PBS-T for 15 minutes on a shaker to minimise non-specific binding of the antibody.

The membrane was then incubated in primary antibody (Phospho YAP Rabbit s127) in milk in a 1 in 500 dilution overnight at 4°C on a Stuart See-Saw rocker.

The following day, the membrane was washed 3 times in PBS-T for 10 minutes each time. Afterwards the membrane was incubated with the corresponding secondary antibody (donkey anti-rabbit 680, LI-COR) in PBS-T on a Stuart See-Saw rocker at room temperature in a black cassette in dark conditions for 120 minutes.

The membrane was then washed 3 times in PBS-T and 2 times in PBS for 10 minutes each time and viewed under a LI-COR Odyssey CLx Infrared Imaging System.

Total protein levels were quantified using ImageJ software and analysed on Microsoft Excel.

2.4 Immunofluorescence Microscopy

Coverslips were incubated in absolute ethanol for 30 minutes to sterilise and were then placed in between filter papers in a petri dish and taped up to be autoclaved at 125°C, 18psi for 45 minutes as a method of sterilising prior to use. Prior to seeding, coverslips were placed into a 48 well plate using a set of curved precision tweezers. Tweezers were sterilised with ethanol and flamed before placing a coverslip in each well. Cells were then seeded as normal in a 1:30 or 1:60 split (40,000 or 20,000 cells). Once cells have reached required confluency of around 40-50% they were treated with the desired concentrations

of the compounds and incubated overnight. The following day, media was discarded and cells were fixated using 4% formaldehyde (ThermoScientific) for 20 minutes. Formaldehyde was discarded and PBS was added for 5 minutes. PBS was then discarded and blocking buffer was added for 1 hour. Post incubation in blocking buffer, mouse monoclonal IgG_{28} YAP (63.7) primary antibody in a 1:200 dilution in blocking buffer with 0.2% triton was added and incubated over night at 4°C. The following day, the wells were washed three times in PBS. Fluorescent secondary antibody of Donkey anti-mouse CY3 in a 1:300 dilution and Hoechst (DAPI) in a 1:2000 dilution was added and incubated for 2 hours in the dark.

Wells were then washed 3 times with PBS. Following the last wash wells were filled with PBS to the top to allow the removal of coverslips to be mounted on the slides. Using a pair of bent tweezers coverslips were lifted out of the wells, dabbed on a towel to eliminate any residual PBS and mounted upside down on a microscopic slide with a drop of ProLong Gold Antifade Mountant. The coverslip was gently pressed using the tweezers to allow mountant to spread evenly across the coverslip. Slides were then placed in a slide folder and incubated at 4°C overnight. The following day images were taken using Zeiss LSM 980 at 20X magnification. Each experiment was replicated 3 times to achieve n=3.

2.5 qRT-PCR

2.5.1 RNA Extraction

Cells are seeded into a 6 well plate to achieve desired confluency and incubated in 5% CO_2 at 37°C for 24 hours. Once desired confluency had reached, cells were treated with treatments and incubated overnight.

RNA extraction was carried out using the RNeasy Mini Kit (see appendix Table X). Following with the drug treatment, the supernatant was removed and the wells were washed with PBS. Prior to adding the RLT lysis buffer, 70% ethanol was added and mixed well. 350µL of lysis buffer RLT was added to each well and cells were scraped using a cell scraper and the lysate was collected into Eppendorf tubes labelled with the corresponding

drug conditions. 350µL of 70% ethanol was added to the Eppendorf tubes and the total volume was brought to 700µL.

A 700µL volume of the mixture was transferred to RNeasy mini spin column and centrifuged for 15 seconds at 8000 rpm using a microcentrifuge. The flow through was discarded. A volume of 700µL of RW1 buffer was added to the spin column and centrifuged for another 15 seconds at 8000 rcf. Flow through was discarded before adding 500µL buffer RPE and centrifuging for 15 seconds at 8000 rpm. After discarding the flow through, 500µL of buffer RPE was added a second time and centrifuged for 2 minutes at 8000 rpm.

Lastly, the spin columns were placed in new labelled Eppendorf tubes and 50µL RNase-free water was added directly into the spin column membranes. Samples were incubated for 5 minutes at room temperature before centrifuging for 1 minutes at 10,000 rpm to elute the RNA.

The RNeasy spin columns were then discarded and the Eppendorf tubes were collected. Using a Bio-Drop Duo+ Micro Volume Spectrophotometer the concentrations of the extracted RNA and the purity at A260/A280 absorbance were measured. Eppendorf tubes containing the RNA extracts were then stored at -80°C.

2.5.2 cDNA Synthesis

Using the Applied Biosystem™ High-Capacity RNA to cDNA™ (catalogue 4387406), the RNA from the extracts were synthesised to single-stranded cDNA. To prepare 20µL of cDNA, 1µL of 20X RT enzyme and 10µL of RT buffer mix were added to each 20µL reaction tubes. Based on the RNA concentrations measured by the Bio-Drop, a calculation (dividing the RNA concentrations by 1000) was done to determine the volume of RNA to RNase free water ratio. Subsequently, dependent upon the calculations, RNA and RNase free water were added to the corresponding tubes to complete making the RT master mix as advised to in the manufacturers protocol.

Once the samples were ready, they were placed in the Thermo Scientific ProFlex PCR system thermocycler and run for approximately 1 hour and 10 minutes by setting the priming stage at 37°C for 60 minutes, followed by the reverse transcription at 95°C for 5 minutes and RT inactivation at 16°C for 3 minutes.

Once the cycle has finished, the samples were collected and stored at -20°C.

2.5.3 Quantitative Reverse Transcription Polymerase Chain Reaction (qRT-PCR)

Prior to preparing the samples for the RT-PCR run, the desired primers were reconstituted to a stock solution of 100μM in sterile Tris-EDTA (TE) buffer and centrifuged for 30 seconds to allow proper mixing. The reconstituted primers were diluted using sterile TE buffer a 1:25 ratio to bring working concentration to 4μM. Primers were incubated at room temperature for 15 minutes prior to use and stored at -20°C after.

All samples are to be kept in ice throughout the duration of the experiment. Each well on a 48 well PCR amplification microplate was filled with 0.5μL of yellow sample buffer, 0.5μL of forward and reverse primers, 2μL of cDNA, 6.5μL of nuclease free water and 10μL of SYBR green master mix. Therefore, on a separate Eppendorf tube a mixture of yellow sample buffer, SYBR green master mix and nuclease free water was prepared depending on the number of wells that were used (i.e., for 48 wells, 0.5μL x 48 of yellow sample buffer + 10μL x 48 of SYBR green master mix + 6.5μL x 48 of nuclease free water) and 17μL were added to each well. Depending on the plate plan the corresponding forward and reverse primers of 0.5μL were added for CTGF, c-MYC, Cyr61 and GAPDH (housekeeping) genes (appendix Table XIII). Finally, the corresponding cDNA samples were added to each well. The plate was then sealed using an adhesive cover ensuring no air bubbles were present. Subsequently, the plate was centrifuged to assure all components were mixed well using the Thermo Scientific Sorvall Legend RT+ Centrifuge, at 1000 rpm for 1 minute. Then, using an Eco PCRmax machine the plate was run for approximately 1

hour until all cycles mentioned below were completed 40 times. For each gene 4 replicates of each sample were run.

PCR Cycles:

Polymerase Activation	PCR Cycling			Melt Curve		
2 minutes at 95°C	15 seconds at 95°C	30 seconds at 60°C	15 seconds at 72°C	15 seconds at 95°C	15 seconds at 55°C	15 seconds at 95°C

Table 1: Cycle settings used for running a PCR.

Results were analysed by finding the ΔΔCt for each gene and normalising to corresponding values of the housekeeping gene – GAPDH using Microsoft Excel.

2.6 Co-Immunoprecipitation

Initially, 40µL of protein A/G magnetic beads (MCE ®) were washed using 500µL of wash buffer repeating the process 3 times by placing it on the magnetic rack to avoid beads being discarded. The magnetic beads were then incubated with 25µL of the selected antibody of YAP for 2 hours at room temperature on a rotator. Following the incubation, the tubes containing the antibody-magnetic bead complex were placed on a magnetic bead separating MagRack6 and any unbound antibody was discarded. The mixture was then washed with 500µL of wash buffer twice.

HeLa cells were plated in a 6 well plate and treated with the desired drug concentrations including a control well at 90% confluency. Cells were washed three times using ice cold PBS and placed on ice. Cells were scraped and then lysed using 1200µL of lysis buffer (0.5% Triton X-100 in PBS) containing 100µL of phosphatase and 100µL of protease inhibitors. Cells were further homogenised 6 times and placed in a 1.5 mL centrifuge tube ensuring to repeat the same process for each condition. 30µL of the prepared beads were

added to the cell lysates and incubated on ice for 30 minutes to inhibit non-specific binding ensuring to invert the tubes every 5 minutes. Thereafter, the beads were removed.

1mL of cell lysate was added to a centrifuge tube containing antibody-bead mixture and the lysate-antibody-bead mixture was resuspended. 1mL of cell lysate without antibody-bead mixture was added into a tube labelled as input. The mixture was then incubated for 90 minutes at 4°C on a Stuart See-saw rocker. Following the incubation, the beads were separated by placing the tubes on a separating rack (MagRack6) and any unbound sample was discarded. Thereafter, beads were washed 3 times with 500µL of lysis buffer followed by 3 times of wash buffer. 80µL of the sample buffer was added to the tubes containing the beads and the input. Samples were heated on a heat block for 10 minutes at 96°C-100°C. Afterwards, samples were stored at -20°C until used for SDS-PAGE analysis.

2.7 Mass Spectrometry

The samples were prepared for Mass Spectrometry using the co-immunoprecipitation process mentioned above. 4 tubes of YAP antibody-bead-lysate complexes and 1 tube with lysate and IgG (for negative control) were prepared. 3 of the tubes were treated with 75µM of ARTM, 50µM of ART and 100µM of ART and one tube with DMSO. The samples were then analysed using SDS-PAGE.

Samples were heated on a heat block at 96°C-100°C and loaded as usual (around 20µL of each sample per well) and run at 100V for 2-3 minutes. Once the sample has run for 2 minutes emptying the wells, more sample was added and run. The run was stopped as necessary until the entire sample was loaded. The gel was then run at 160V for about 1 hour. Following the run, the gel was treated with Commasie blue stain (0.75g Comassie brilliant blue R-250(VWR) + 60mL of methanol + 20mL of glacial acetic acid + 200mL of dH_2O) on a shaker for 30 minutes. The stain was then removed by rinsing with dH_2O twice for 5 minutes each time. Destain solution was added to the gel and incubated on a shaker

for another 30 minutes. Following the 30 minutes, new destain was added and incubated overnight on the shaker. The protein bands of interest were cut and placed in centrifuge tubes and sent off for mass spectroscopy analysis. The bands were sent to the Advanced Mass Spectrometry Facility at the University of Birmingham. A Cross Linking Mass Spectrometry (XL-MS) was performed to identify protein-protein interactions

CHAPTER 3

Effect of Artemisinin and Artesunate as Monotherapy and Combination Therapy on Cervical Cancer Growth and Migration

3.1 Effect of ARTM, ART and CIS on HeLa Cell Viability, Migration and Apoptosis

The first part of the project was to discover the optimum concentrations of artemisinin, artesunate and cisplatin to assess their effect on cancer on HeLa cells. To assess the efficacy of potential therapeutic agents reliable assays are required to evaluate cancer cell behaviour such as survival and migration. Cell viability assays are widely used to determine the cytotoxic effects of drugs by measuring the survival rate of treated cells in comparison to control. Monitoring cell viability provides direct evidence of the drug's ability to suppress or kill cancer cells, reflecting its potential therapeutic value (Mukherjee, 2019).

Scratch wound assay complements viability assays by focusing on cell migration, a key process in cancer metastasis. This assay involves introducing a gap in a monolayer of cancer cells (i.e., HeLa cells) and the ability of the cells to migrate and close the gap is monitored over time. The inhibition of cell migration by a drug suggests its potential to prevent cancer from spreading, a critical factor in improving patient outcomes (Kauanova, Urazbayev and Vorobjev, 2021; Liang *et al.,* 2007).

The MTT assay is another significant method in assessing drug efficacy. It is based on the reduction of MTT [3-(4,5-Dimethylthiazol-2-yl)-2,5-diphenyltetrazolium bromide] by metabolically active cells, producing a colour change that reflects cell viability. Drugs that reduce cancer cell metabolism and thus their viability will result in lower MTT activity resulting in a faint purple colour due to cells incapability to convert MTT into formazan as opposed to viable cells which turn MTT into purple formazan crystals. The MTT assay is widely used due to its quantitative nature and its ability to provide a more detailed understanding of drug's cytotoxic effects on cancer cells.

Finally, a caspase-3 assay plays a critical role in evaluating apoptosis, as caspase-3 is a key executor of programmed cell death. Therefore, an increase in caspase-3 activity following drug treatment indicates the drug is effectively inducing apoptosis in cancer cells (Mizukami *et al.,* 1999).

Previous studies suggest that ART and ART not only inhibit the growth of cancer cells but also enhance their sensitivity to traditional chemotherapeutic agents like CIS, promoting apoptosis and reducing cell viability (Augustin, Staines and Krishna, 2020; Ma *et al.,* 2021). In this chapter, a comprehensive evaluation of ARTM, and ART singly and in combination with CIS on HeLa cells will be conducted using a combination of cell viability, wound healing, MTT and caspase-3 assays.

3.2 Cell Viability

To assess the impact of ARTM, ART and CIS on proliferation and potential cytotoxicity in HeLa cells, a cell viability assay was performed. This assay involves assessing cell survival in cultured cells to study the effects of drugs *in vitro* to monitor proliferation. Various concentrations of each drug were tested on HeLa cells to identify the optimum doses for cell growth inhibition. Based on previous studies that utilised various concentrations for each drug, experiments were conducted using a range of concentrations starting at 25μM for both ARTM and ART and 1μM for CIS. This approach aimed to identify the most effective doses for inhibiting cell proliferation in HeLa cells.

3.2.1 Effect of Different ARTM Concentrations on Cell Viability

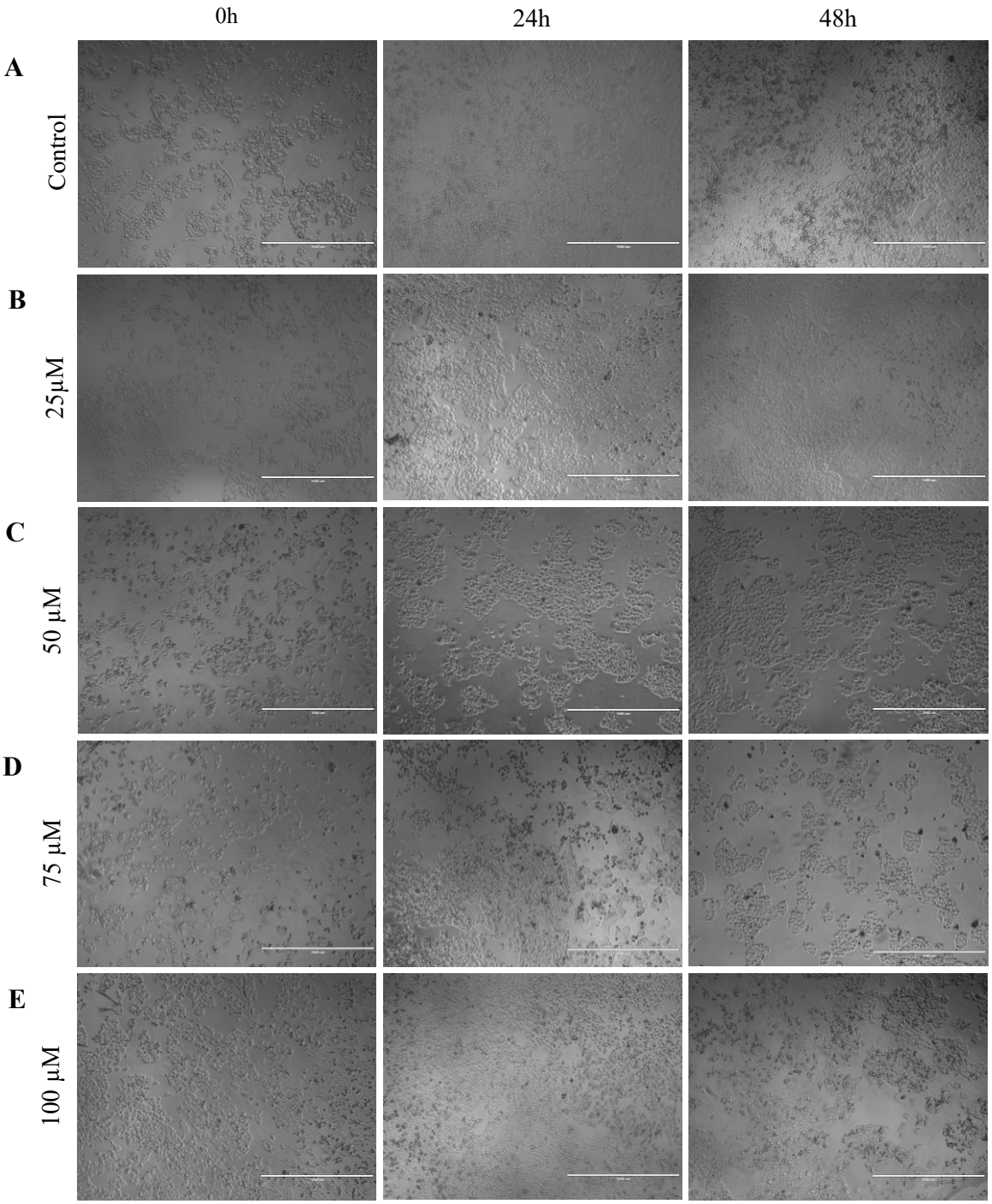

Figure 3.1: Cell viability analysis of different concentrations of ARTM treatment in HeLa cell line.

Brightfield images representing cells at 0-, 24- and 48-hours post treatment with (B) 25µM, (C) 50µM, (D) 75µM and (E) 100µM of ARTM compared to (A) control, treated with 0.1% DMSO. Illustrative images show N=3 experiments. Scale bars represent 1000µm.

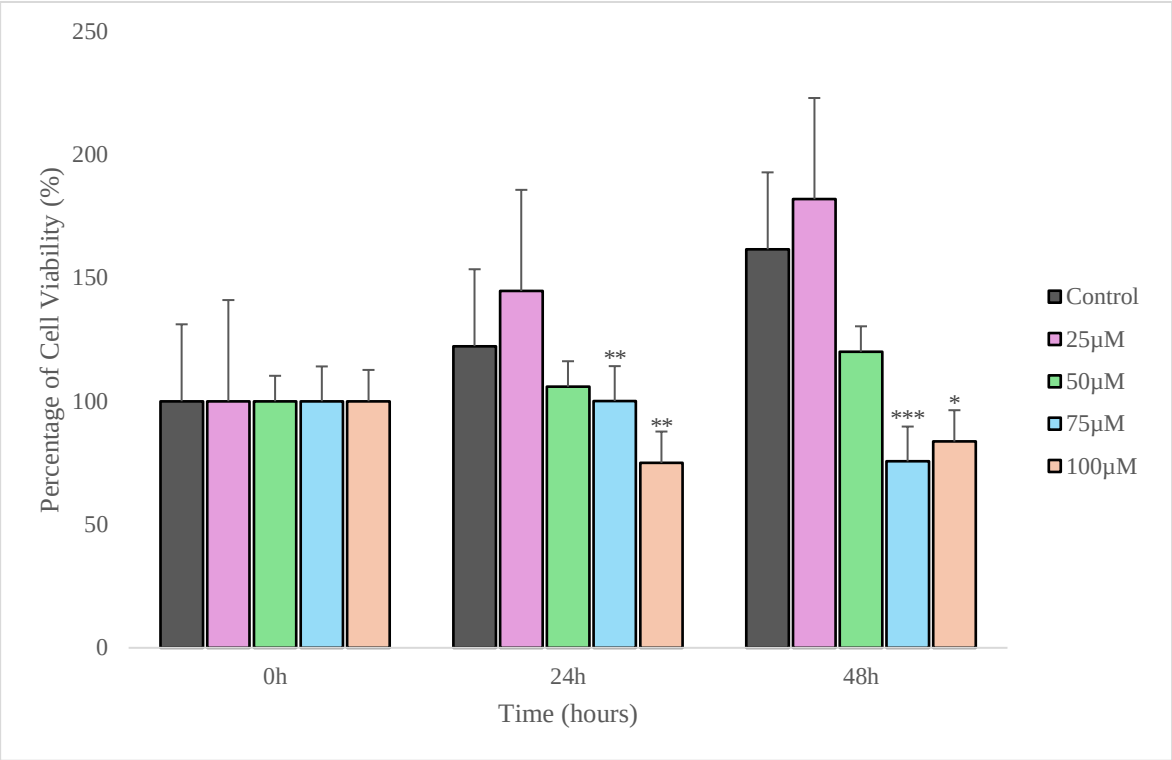

Figure 3.2: Graph representing the percentage of viable HeLa cells treated with 25µm, 50µm, 75µm and 100µm of ARTM.

Quantitative graph showing the number of viable cells present post treatment with 25µM, 50µM, 75µM and 100µM of ARTM compared to control treated with 0.1% DMSO.
*Graph was compiled using data generated from 3 independent experiments. Data is displayed as the ± standard deviation with N=3. The statistical significance between the control (treated with 0.1% DMSO) and ARTM concentrations was evaluated using a two-sample equal variance T-TEST with significance levels *p≤0.05, ** p≤0.01 and ***p≤0.0001.*

After treating HeLa cells with 25µM, 50µM, 75µM and 100µM concentrations of ARTM, Figure 3.2 shows that higher concentrations of ARTM, specifically 75µM and 100µM, had a significant impact on cell viability. Notably, 75µM had a more pronounced effect on cell viability, as illustrated in Figure 3.1(D) and further confirmed in the quantified graph in Figure 3.2, where 75µM treatment exhibited significance levels of 0.0005 at 24 and 0.000013 at 48 hours. In contrast, although 100µM showed a significant effect, it was less pronounced, with significance levels of 0.01 at 24 hours and 0.003 at 48 hours.

3.2.2 Effect of Different ART Concentrations on Cell Viability

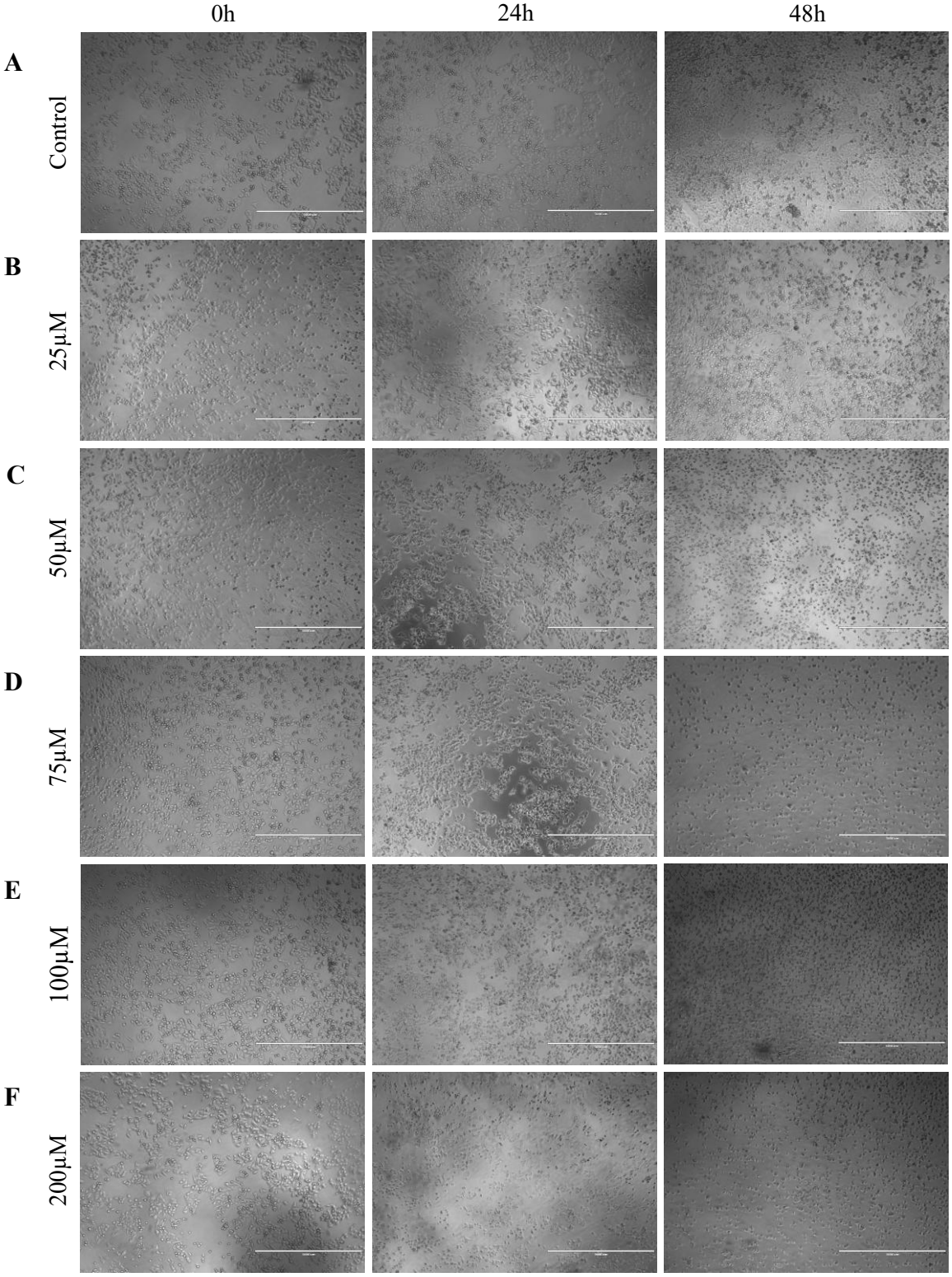

Figure 3.3: Cell viability analysis with different concentrations of ART treatment in HeLa cell line.

Brightfield images representing cells at 0-, 24- and 48-hours post treatment with (B) 25µM, (C) 50µM, (D) 75µM, (E) 100µM and (F) 200µM of ART compared to (A) control, treated with 0.1% DMSO. Illustrative images show N=3 experiments. Scale bars represent 1000µm.

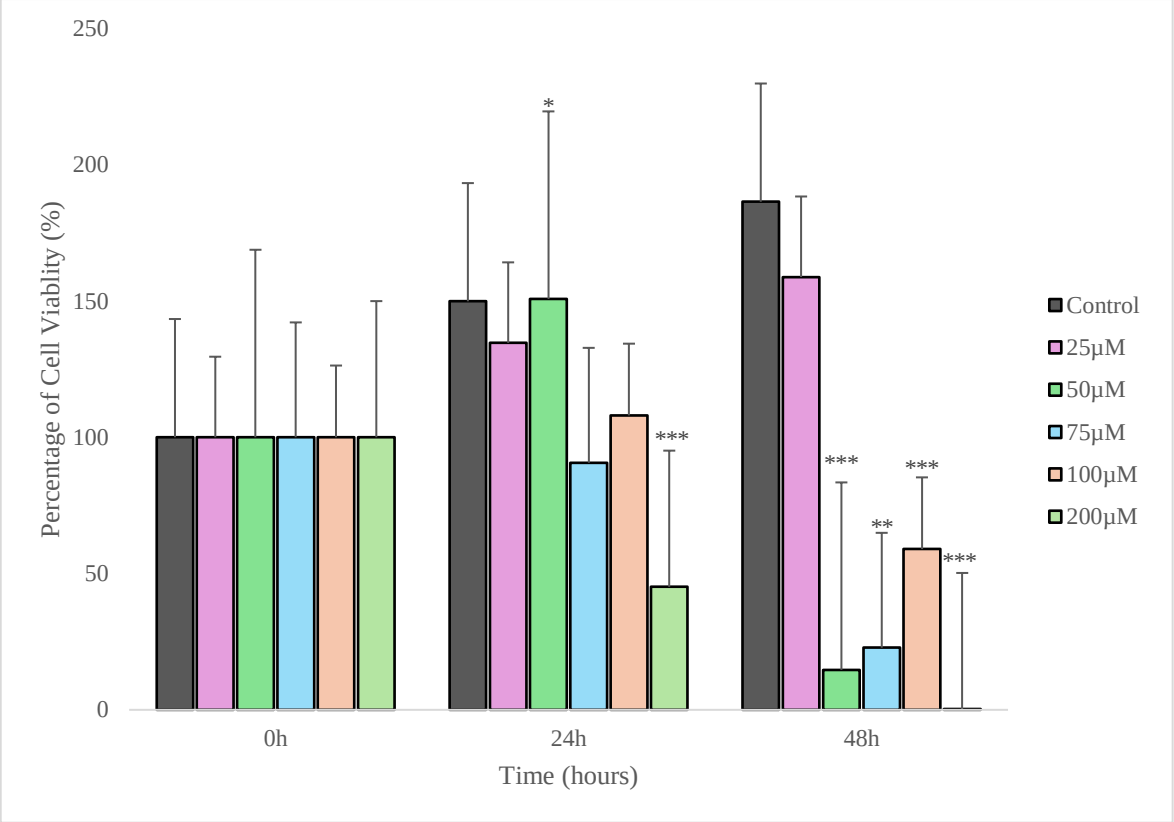

Figure 3.4: Graph representing the percentage of viable HeLa cells treated with 25µM, 50µM, 75µM, 100µM and 200µM of ART.

Quantitative graph showing the number of viable cells present post treatment with 25µM, 50µM, 75µM, 100µM and 200µM of ART compared to control treated with 0.1% DMSO.
*Graph was compiled using data generated from 3 independent experiments and. Data is displayed as the ± standard deviation with N=3. The statistical significance between the control (treated with 0.1% DMSO) and ART concentrations was evaluated using a two-sample equal variance T-TEST with significance levels *p≤0.05, ** p≤0.01 and ***p≤0.0001.*

Figure 3.3 illustrates HeLa cells treated with varying concentrations of ART: (B) 25µM, (C), 50µM, (D) 75µM, (E) 100µM and (F) 200µM, assessed at 24 and 48 hours post-treatment compared to untreated control cells (A). At higher concentrations, inlcuding 50µM, 75µM, 100µM and 200µM there is a notable increase in the number of dead cells observed at 48 hours with the 200µM treatment resulting in complete cell death. While the 50µM and 75µM treatments exhibit statistically significant effects on cell viability ($p \leq 0.05$ and $p \leq 0.0001$, respectively) according to Figure 3.4. Figure 3.3(C) and (D) at 48 hours illustrate that these concentrations have led to nearly complete cell death. However, despite being a higher dosage, the 100µM treatment still shows viable cells at 48 hours, while exhibiting a statstically significant effect ($p \leq 0.0001$).

3.2.3 Effect of Different CIS Concentrations on Cell Viability

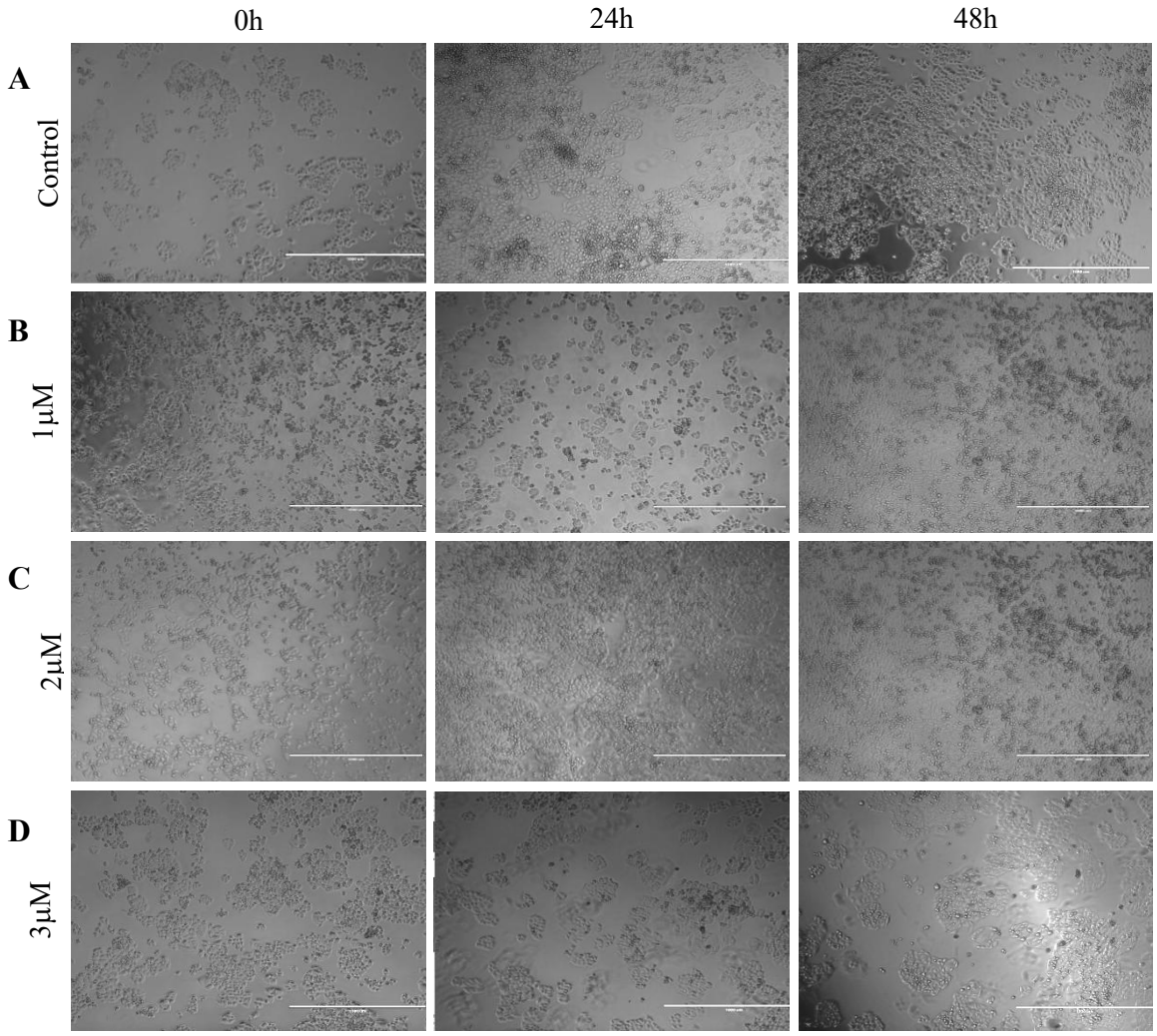

Figure 3.5: Cell viability analysis of different concentrations of CIS treatment in HeLa cell line.

Brightfield images representing cells at 0, 24 and 48 hours post treatment with (B) 1μM, (C) 2μM, (D) 3μM of CIS compared to (A) control, treated with 0.1% DMSO. Illustrative images show N=3 experiments. Scale bars represent 1000μm.

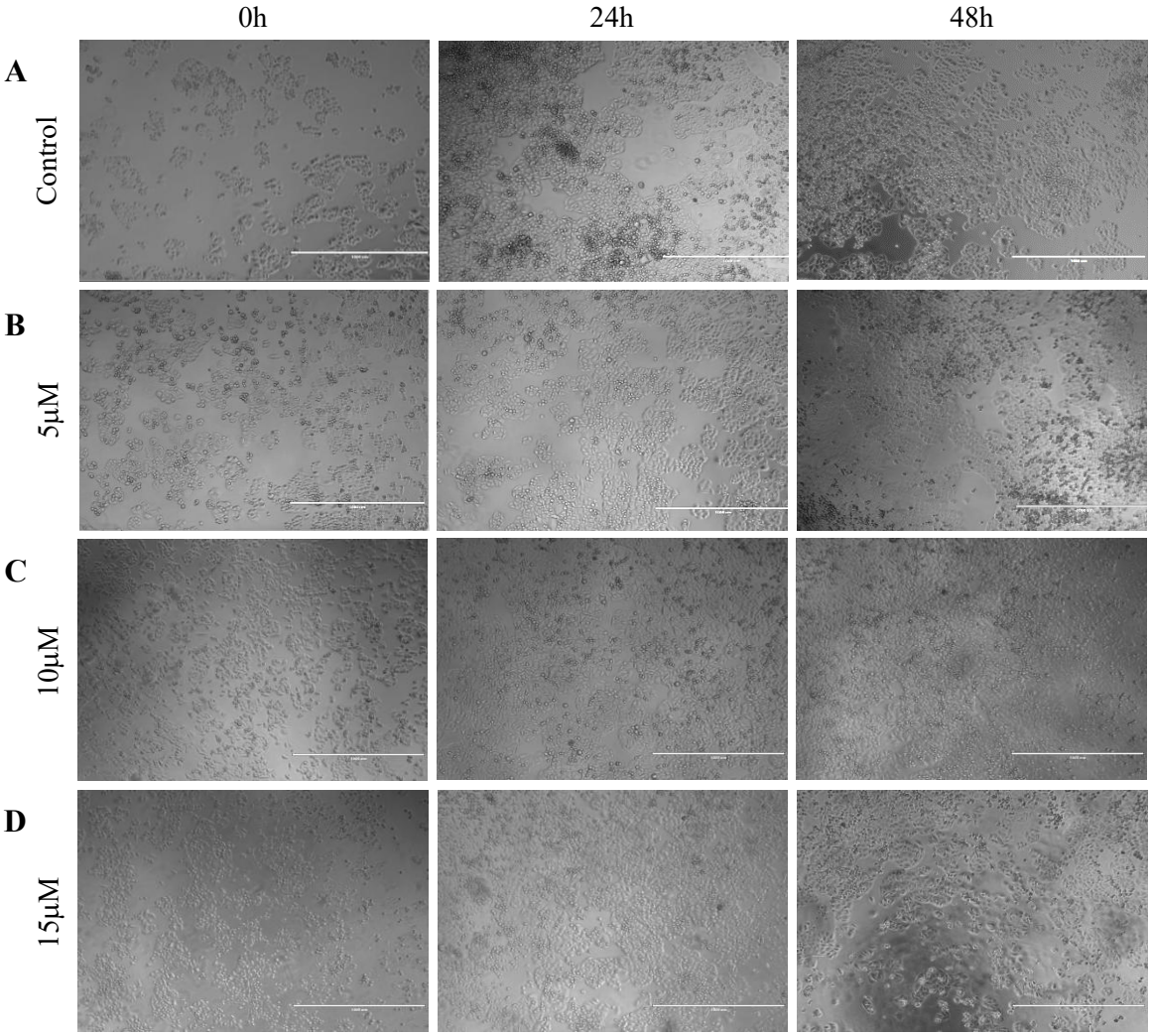

Figure 3.6: Cell viability analysis of different concentrations of CIS treatment in HeLa cell line.

Brightfield images representing cells at 0, 24 and 48 hours post treatment with (B) 5µM, (C) 10µM, (D) 15µM of CIS compared to (A) control, treated with 0.1% DMSO. Illustrative images show N=3 experiments. Scale bars represent 1000µm.

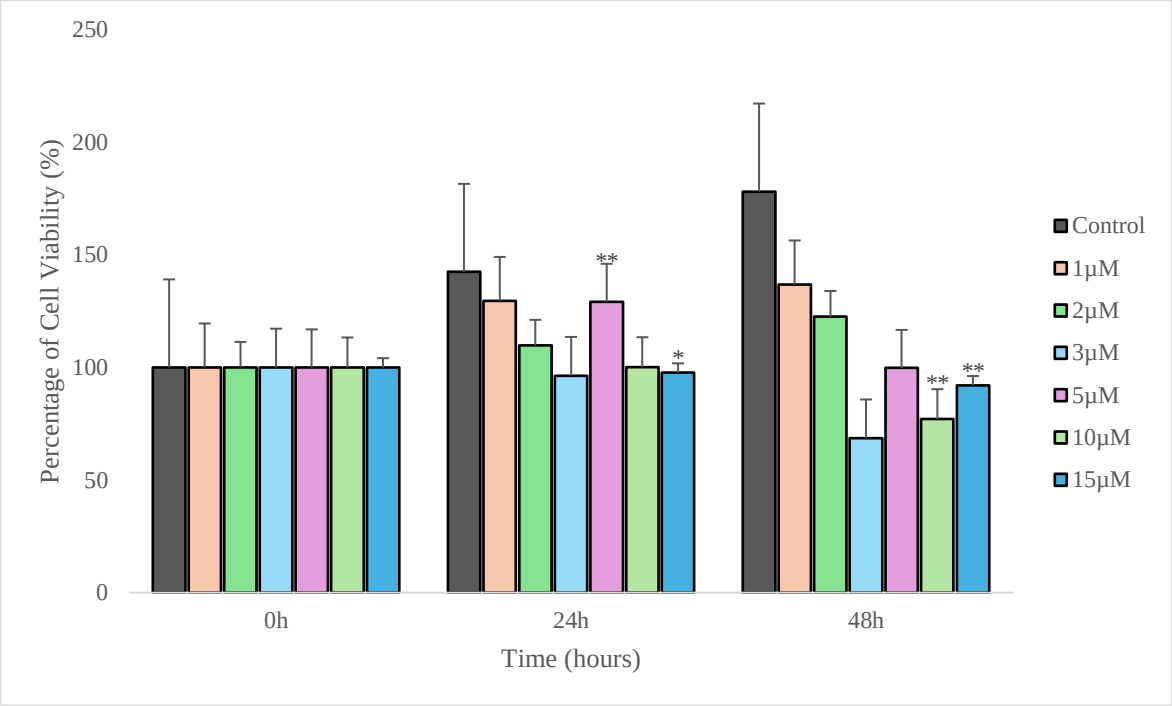

Figure 3.7: Graph representing the percentage of viable HeLa cells treated with 1µM, 2µM, 5µM, 10µM and 15µM of CIS

Quantitative graph showing the number of viable cells present post treatment with 1µM, 2µM, 5µM, 10µM and 15µM of CIS compared to control treated with 0.1% DMSO.
*Graph was compiled using data generated from 3 independent experiments. Data is displayed as the ± standard deviation with N=3. The statistical significance between the control (treated with 0.1% DMSO) and CIS concentrations was evaluated using a two-sample equal variance T-TEST with significance levels *p≤0.05, ** p≤0.01 and ***p≤0.0001.*

In addition to ARTM and ART, CIS was also tested individually on HeLa cells to determine the optimum concentration. Figure 3.5 and Figure 3.6 display HeLa cells treated with various concentrations of CIS: 1µM (Figure 3.5B), 2µM (Figure 3.5C), 3µM (Figure 3.5D), 5µM (Figure 3.6B), 10µM(Figure 3.6C) and 15µM (Figure 3.6D) in comparison to untreated control cells, assessed at 24 and 48 hours post-treatment. Based on the quantified data, the 10µM and 15µM concentrations of CIS demonstrated the most statistically significant cell viability shown in the graph Figure 3.7. Furthermore, Figure 3.6 (D) reveals that the 15µM concentration resulted in a notable higher number of dead cells compared to other concentrations. Although the 5µM concentration exhibited statistical significance at 24 hours post-treatment, this effect was not as noticeable in the images at 48 hours, indicating a diminished cytotoxic effect over time.

3.3 Scratch Wound

In the next assay, HeLa cells were treated with different concentrations of ARTM, ART and CIS, to assess the rate of cellular migration at 0-, 24- and 48-hours post-treatment. Treatment samples were compared to control samples treated with 0.1% DMSO. The control was expected to show complete closure at 48 hours, while treatments that did not achieve full closure were analysed to determine the optimum concentration of each drug, in correlation with cell viability results obtained for the same concentrations.

3.3.1 Effect of Different ARTM Concentrations on Cellular Migration

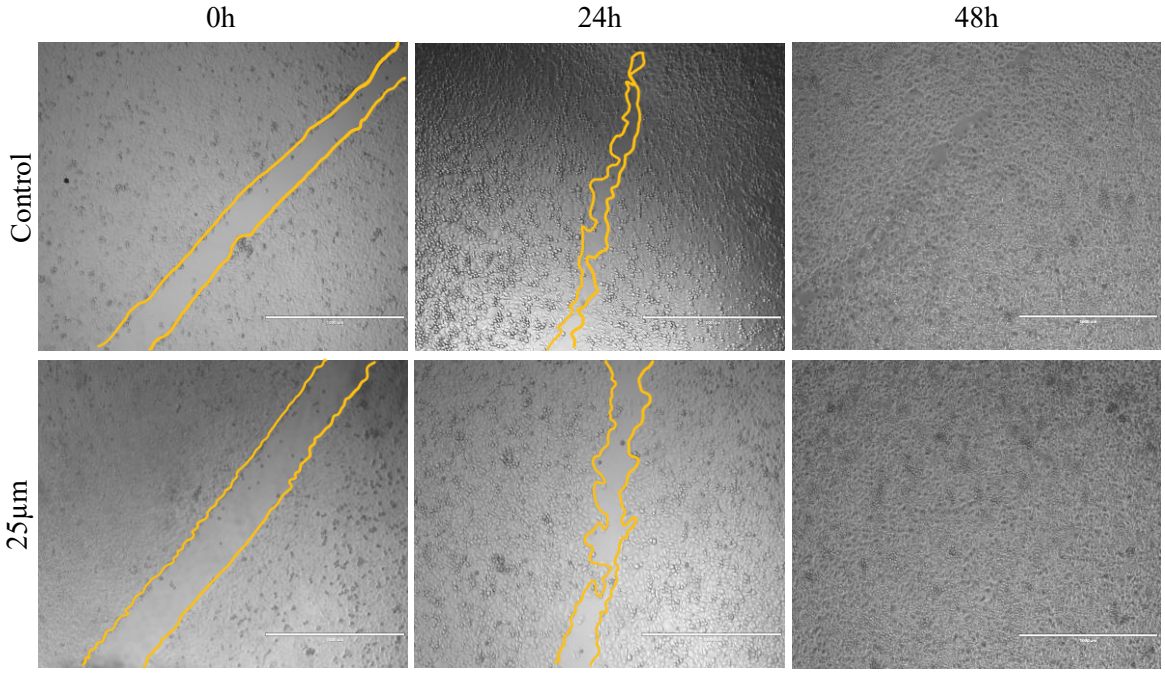

Figure 3.8: Scratch wound analysis of 25µM of ARTM treatment in HeLa cell line.

Brightfield images representing scratch wound closure at 0, 24 and 48 hours post treatment with 25µM of ARTM compared to control, treated with 0.1% DMSO. Illustrative images show N=3 experiments. Scale bars represent 1000µm.

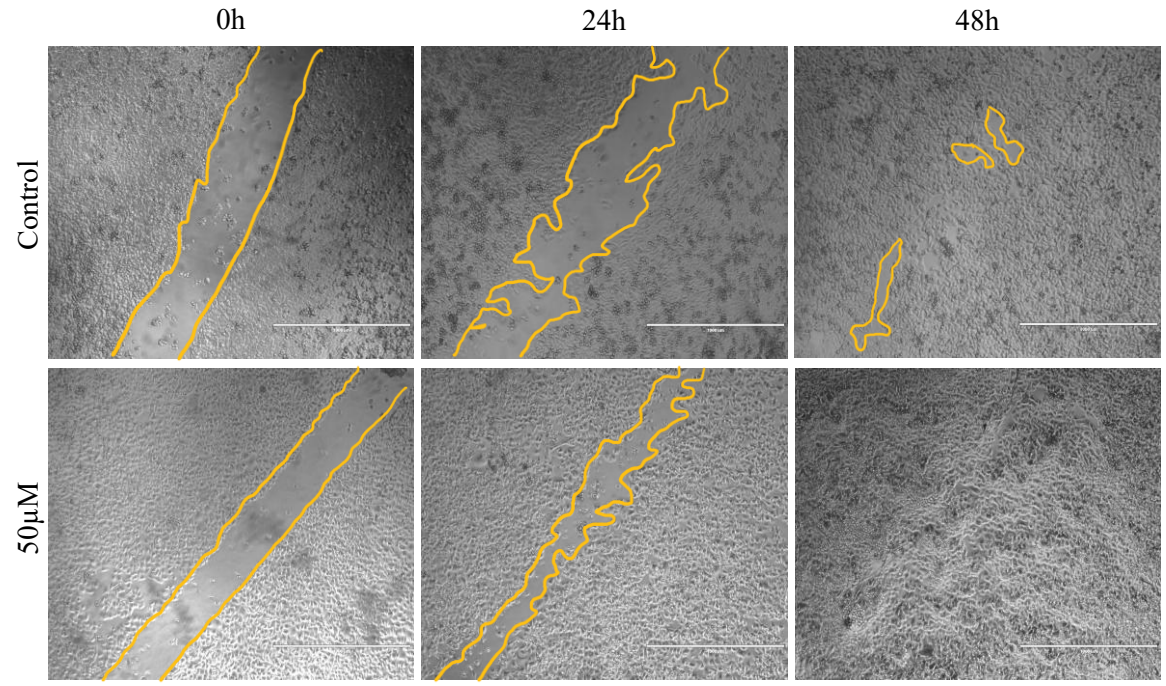

Figure 3.9: Scratch wound analysis of 50µM of ARTM treatment in HeLa cell line.

Brightfield images representing scratch wound closure at 0, 24 and 48 hours post treatment with 50µM of ARTM compared to control, treated with 0.1% DMSO. Illustrative images show N=3 experiments. Scale bars represent 1000µm.

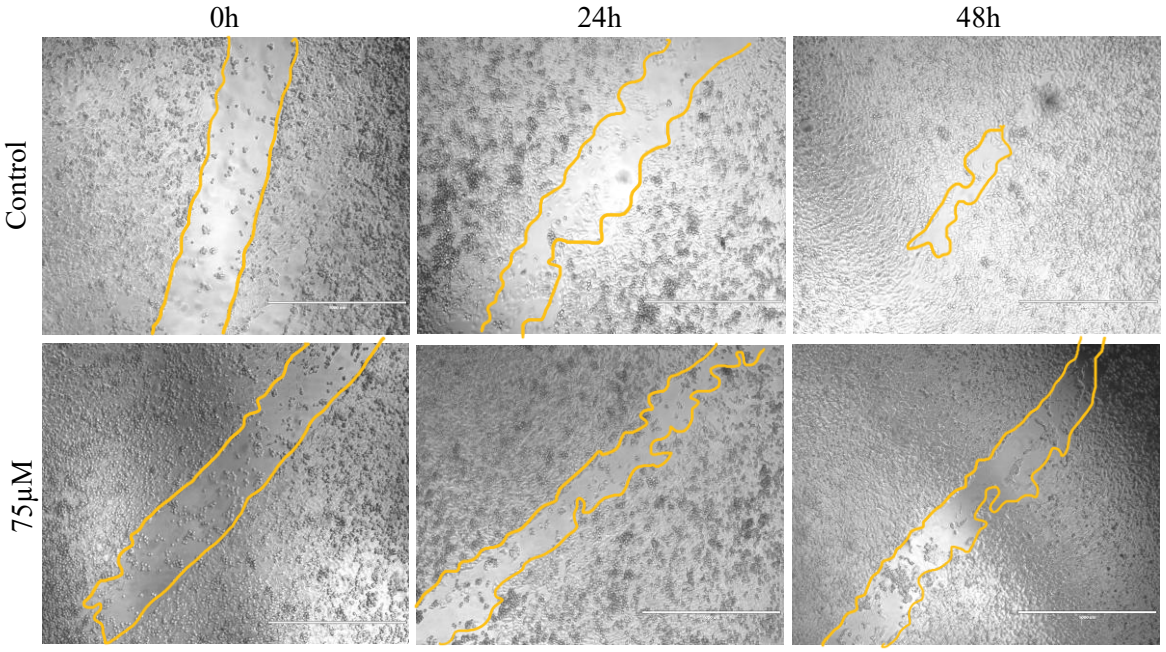

Figure 3.10: Scratch wound analysis of 75µM of ARTM treatment in HeLa cell line.

Brightfield images representing scratch wound closure at 0, 24 and 48 hours post treatment with 75µM of ARTM compared to control, treated with 0.1% DMSO. Illustrative images show N=3 experiments. Scale bars represent 1000µm.

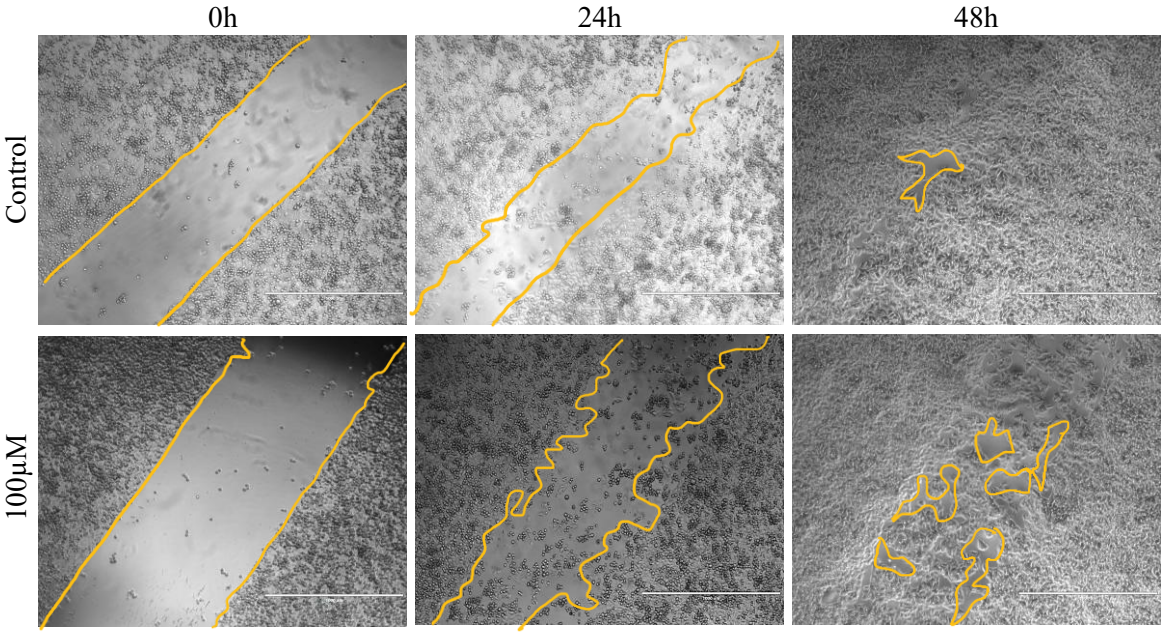

Figure 3.12: Scratch wound analysis of 100µM of ARTM treatment in HeLa cell line.

Brightfield images representing scratch wound closure at 0, 24 and 48 hours post treatment with 100µM of ARTM compared to control, treated with 0.1% DMSO. Illustrative images show N=3 experiments. Scale bars represent 1000µm.

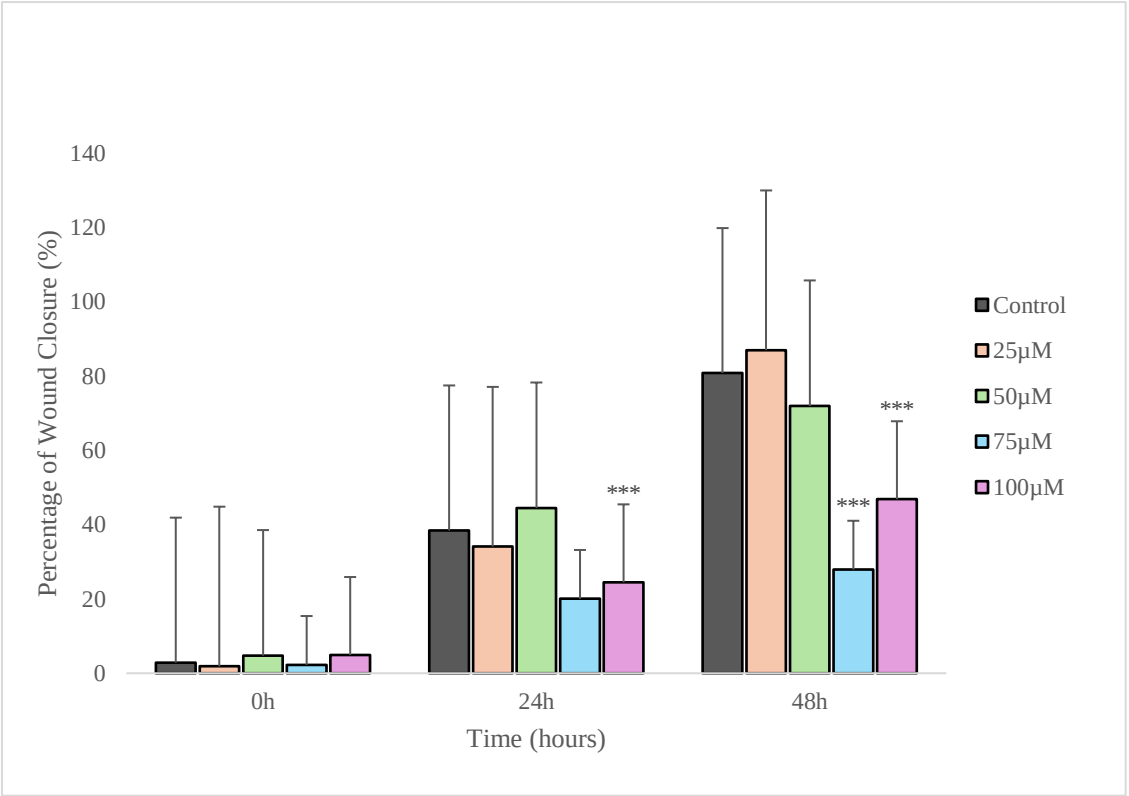

Figure 3.11: Graph representing the percentage closure of scratch wound in HeLa cells treated with 25µM, 50µM, 75µM and 100µM of ARTM.

Quantitative graph showing the percentage of scratch wound closure present post treatment with 25µM, 50µM, 75µM and 100µM of ARTM compared to control treated with 0.1% DMSO.
*Graph was compiled using data generated from 3 independent experiments. Data is displayed as the ± standard deviation with N=3. The statistical significance between the control (treated with 0.1% DMSO) and ARTM concentrations was evaluated using a two-sample equal variance T-TEST with significance levels *p≤0.05, ** p≤0.01 and ***p≤0.0001.*

After assessing cell viability, a migration assay was performed to evaluate wound closure following treatment with different concentrations of ARTM. Figure 3.8 - Figure 3.12 illustrate the wound healing assay at 24- and 48-hours post-treatment with 25µM, 50µM, 75µM and 100µM ARTM. No significant effect on wound closure was observed at 25µM and 50µM, as complete closure occurred similar to the untreated control images in Figure 3.8 and Figure 3.9. In contrast, treatments with 75µM and 100µM ARTM resulted in incomplete wound closure as depicted in the corresponding images in Figure 3.10 and Figure 3.12, respectively and further quantified in the graph in Figure 3.11. Statistical significance was noted at 75µM and 100µM, suggesting that these higher concentrations inhibit cell migration and wound closure more effectively than the lower concentrations.

3.3.2 Effect of Different ART Concentrations on Cellular Migration

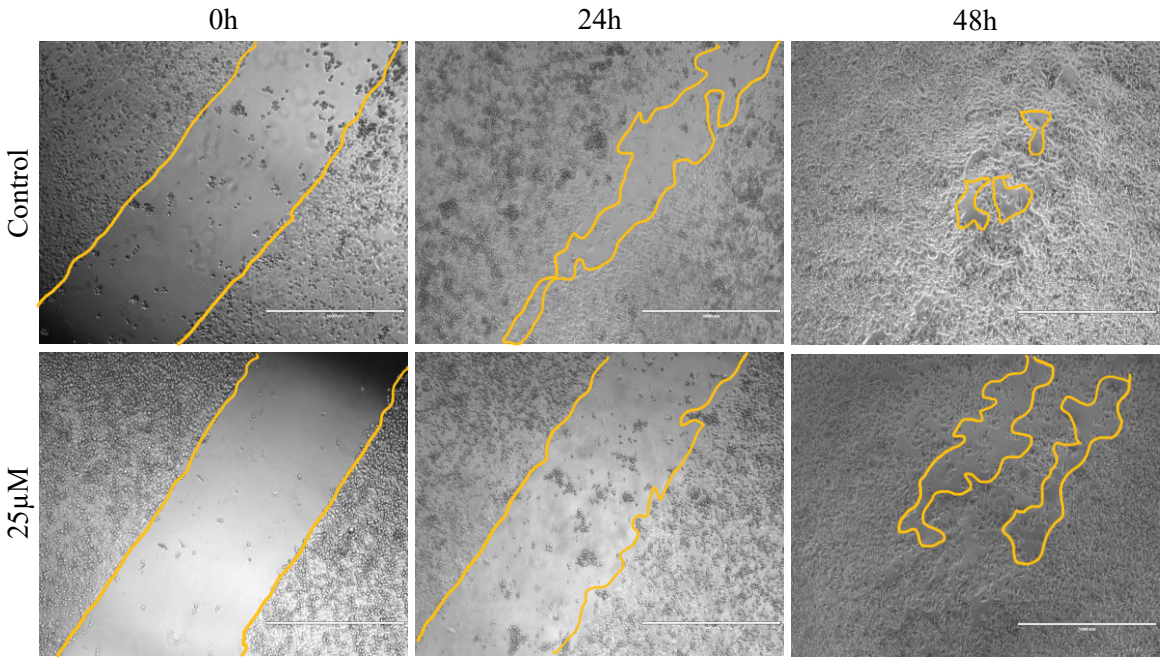

Figure 3.13: Scratch wound analysis of 25µM of ART treatment in HeLa cell line.

Brightfield images representing scratch wound closure at 0. 24 and 48 hours post treatment with 25µM of ART compared to control, treated with 0.1% DMSO. Illustrative images show N=3 experiments. Scale bars represent 1000µm.

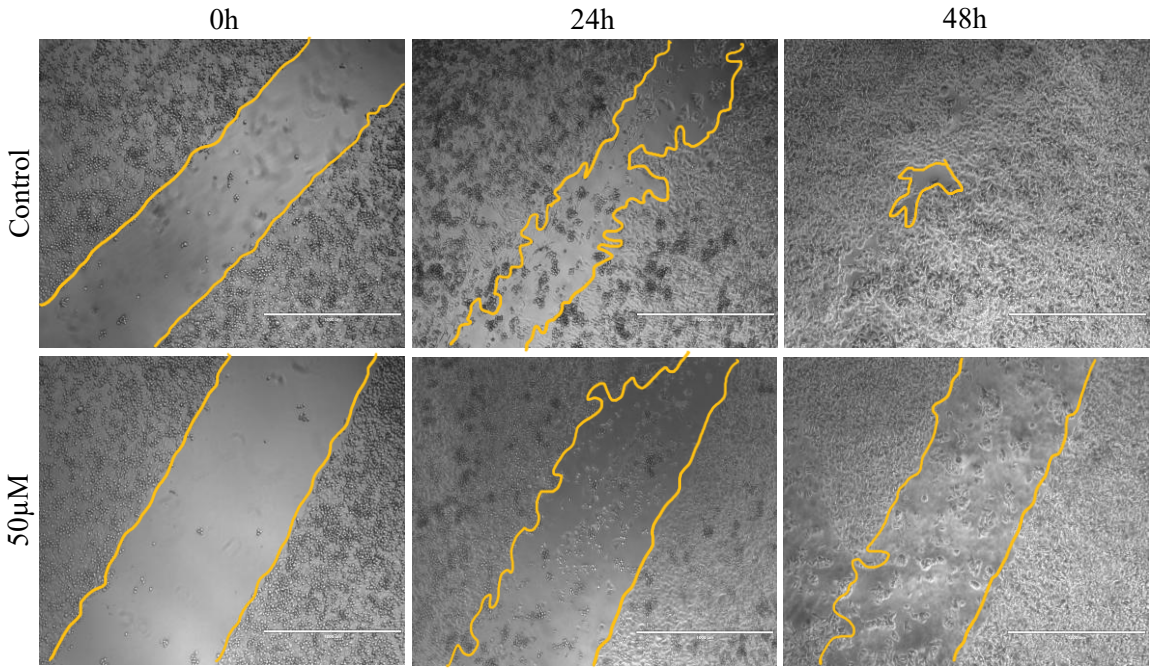

Figure 3.14: Scratch wound analysis of 50µM of ART treatment in HeLa cell line.

Brightfield images representing scratch wound closure at 0. 24 and 48 hours post treatment with 50µM of ART compared to control, treated with 0.1% DMSO. Illustrative images show N=3 experiments. Scale bars represent 1000µm.

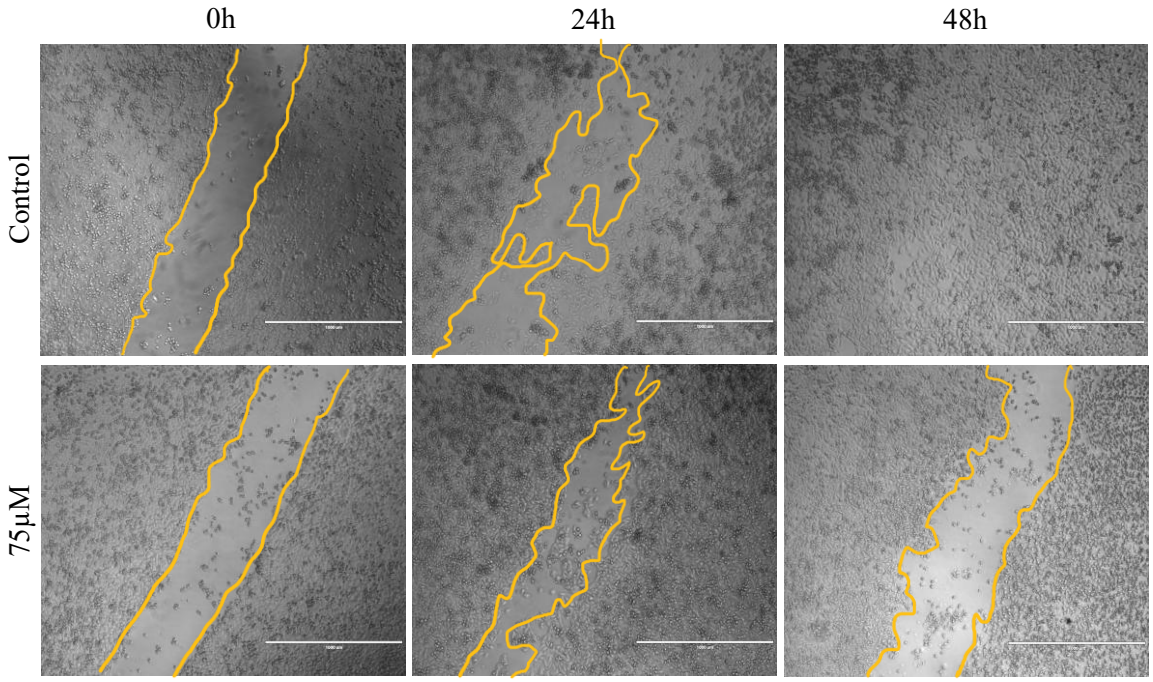

Figure 3.15: Scratch wound analysis of 75µM of ART treatment in HeLa cell line.

Brightfield images representing scratch wound closure at 0. 24 and 48 hours post treatment with 75µM of ART compared to control, treated with 0.1% DMSO. Illustrative images show N=3 experiments. Scale bars represent 1000µm.

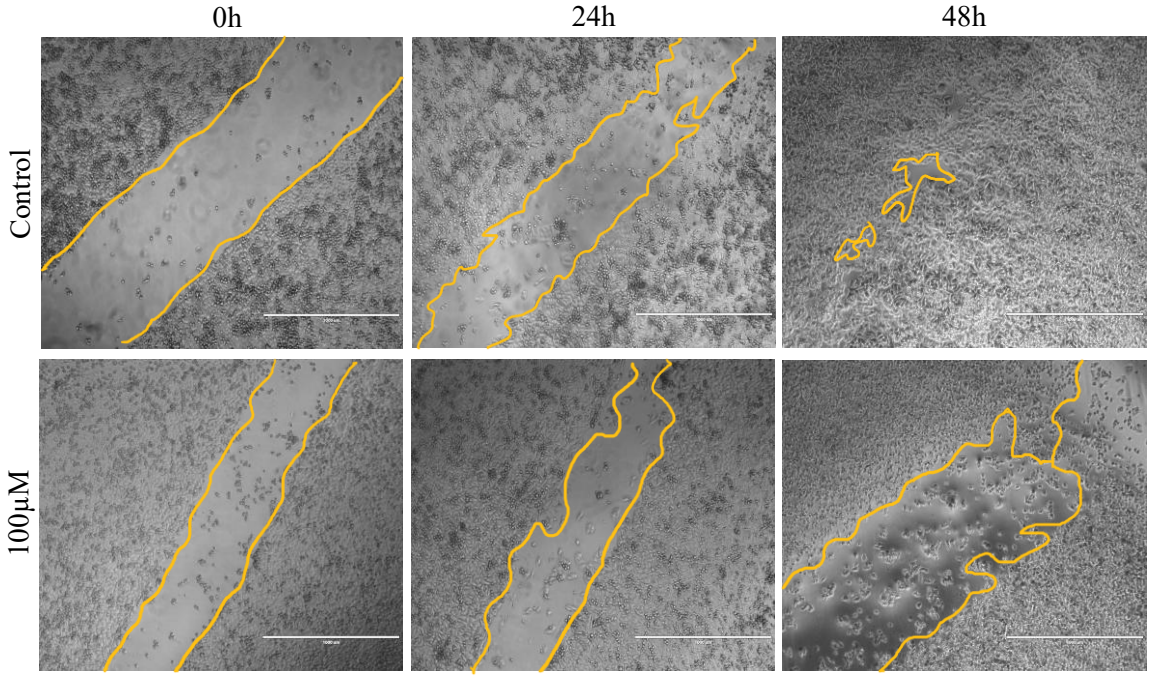

Figure 3.16: *Scratch wound analysis of 100µM of ART treatment in HeLa cell line*

Brightfield images representing scratch wound closure at 0. 24 and 48 hours post treatment with 100µM of ART compared to control, treated with 0.1% DMSO. Illustrative images show N=3 experiments. Scale bars represent 1000µm.

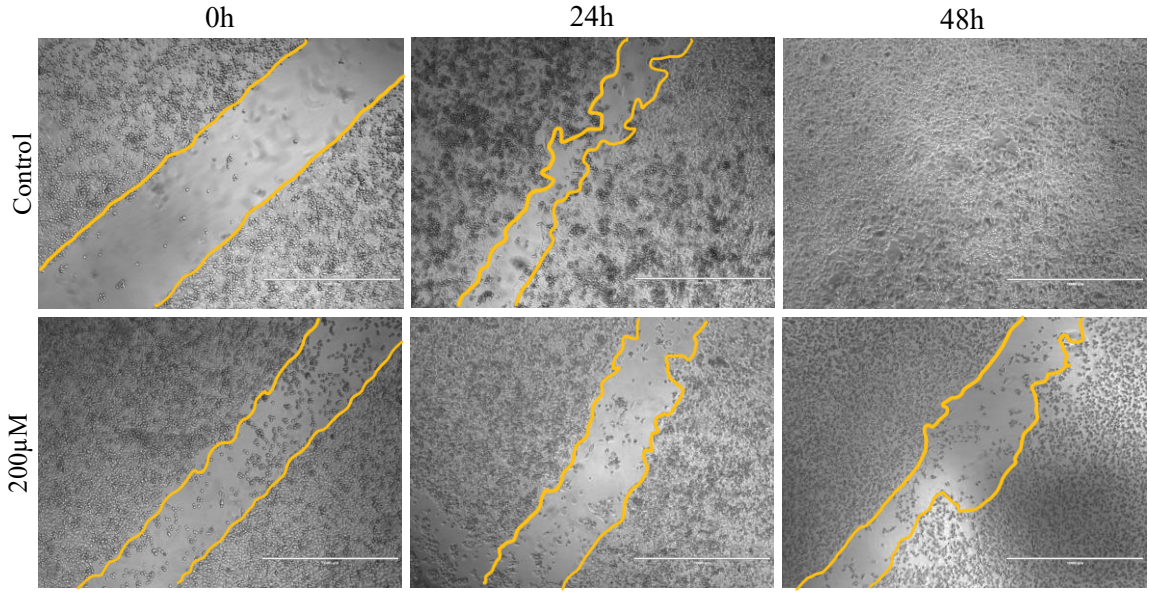

Figure 3.17: Scratch wound analysis of 200µM of ART treatment in HeLa cell line

Brightfield images representing scratch wound closure at 0. 24 and 48 hours post treatment with 200µM of ART compared to control, treated with 0.1% DMSO. Illustrative images show N=3 experiments. Scale bars represent 1000µm.

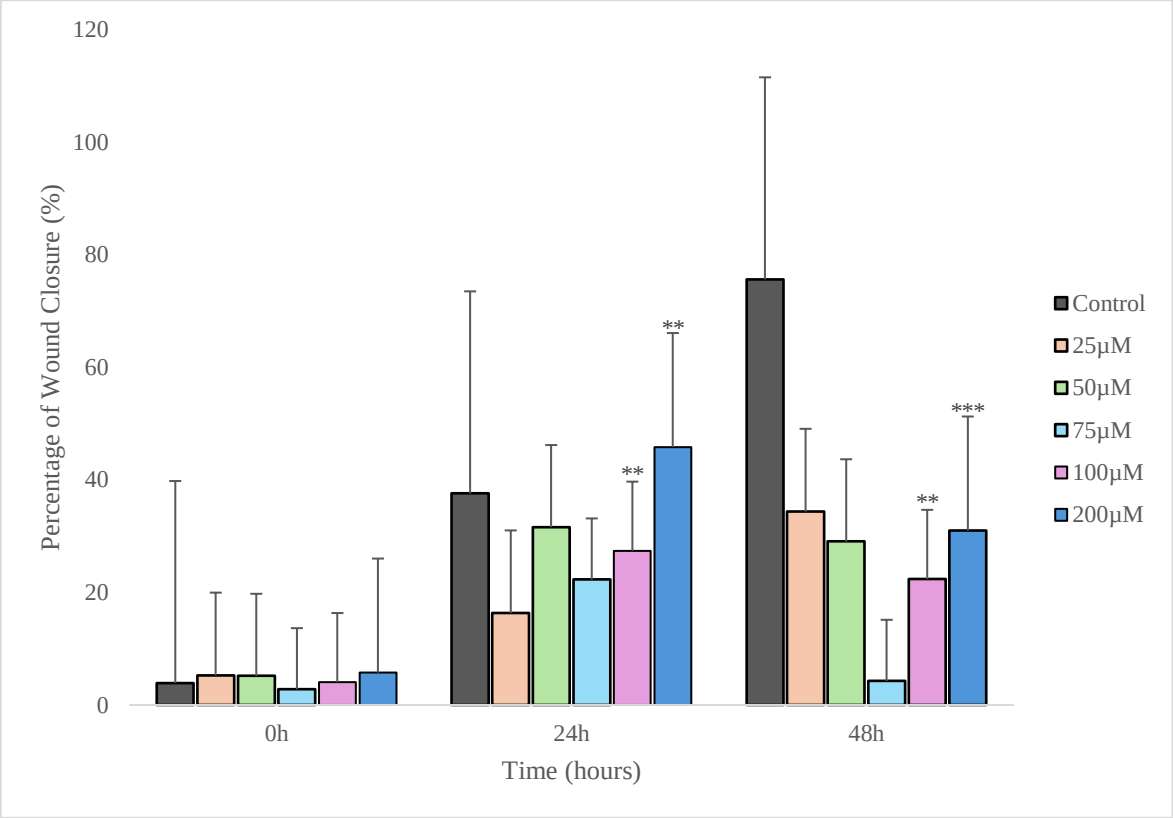

Figure 3.18: Graph representing the percentage closure of scratch wound in HeLa cells treated with 25µM, 50µM, 75µM, 100µM and 200µM of ART.

Quantitative graph showing the percentage of scratch wound closure present post treatment with 25µM, 50µM, 75µM, 100µM and 200µM of ART compared to control treated with 0.1% DMSO.
*Graph was compiled using data generated from 3 independent experiments. Data is displayed as the ± standard deviation with N=3. The statistical significance between the control (treated with 0.1% DMSO) and ART concentrations was evaluated using a two-sample equal variance T-TEST with significance levels *p≤0.05, ** p≤0.01 and ***p≤0.0001.*

Figures 3.13-3.17 illustrate the effects of ART treatment on HeLa cell migration across a range of concentrations: 25µM (Figure 3.13), 50µM (Figure 3.14), 75µM (Figure 3.15), 100µM (Figure 3.16) and 200µM (Figure 3.17) assessing cell migration at these different concentrations. At 25µM, ART treatment resulted in nearly complete wound closure at 48 hours, compared to the control. However, at higher concentrations (starting from 50µM to 200µM), incomplete wound closure was observed. Despite not completely closing, 50µM and 75µM show no significance in comparison to 100µM and 200µM which show statistical significance at both 24- and 48-hours post-treatment with $p<0.01$ (Figure 3.18). Additionally, Figure 3.17 demonstrates that ART 200µM led to near-total cell death by 48 hours, indicating a noticeable cytotoxic effect at this concentration.

3.3.3 Effect of Different CIS Concentrations on Cellular Migration

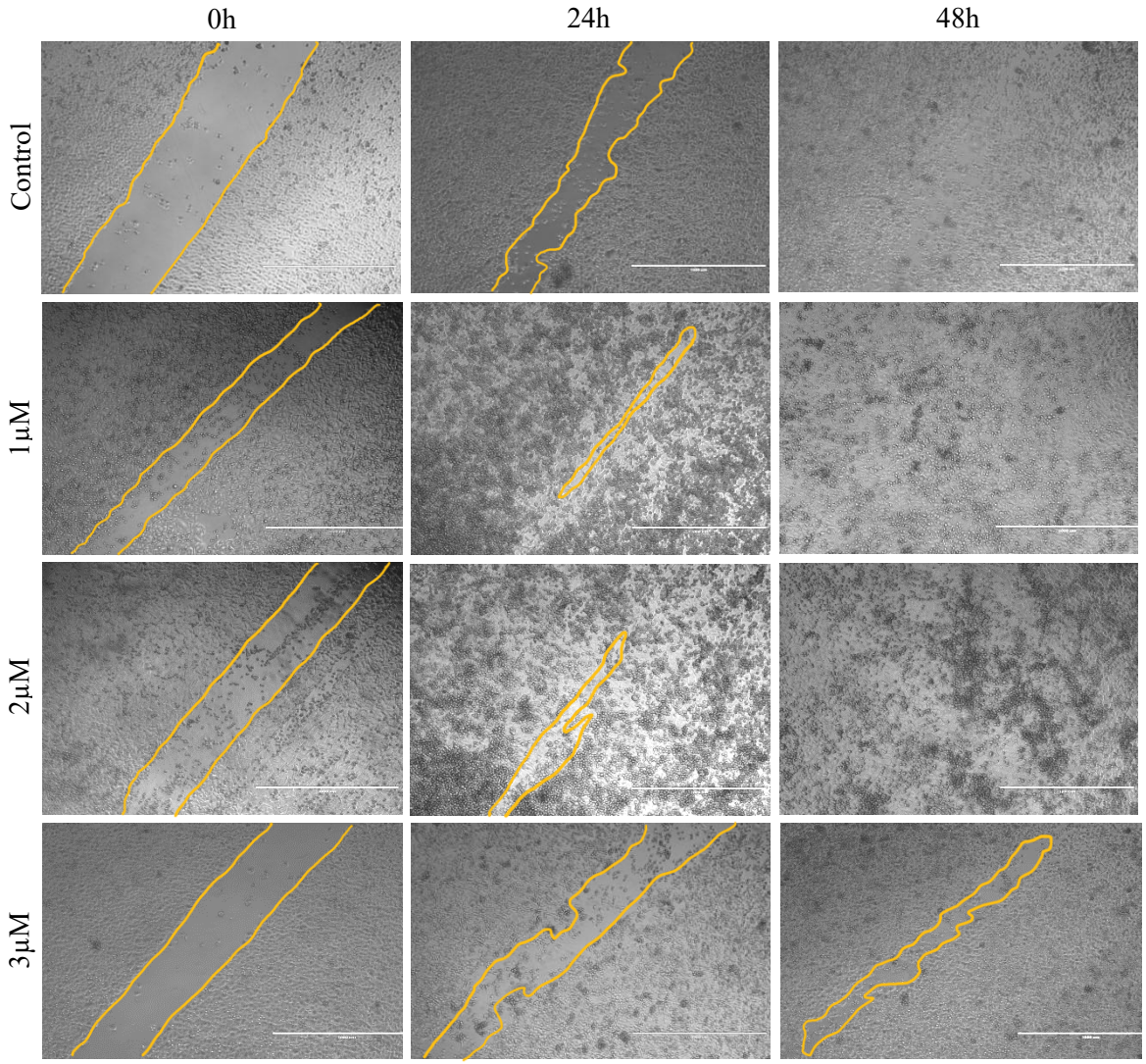

Figure 3.19: Scratch wound analysis with different concentrations of CIS treatment in HeLa cell line.

Brightfield images representing scratch wound closure at 0-, 24- and 48-hours post treatment with (B) 1µM, (C) 2µM and (D) 3µM of CIS compared to (A) control, treated with 0.1% DMSO. Illustrative images show N=3 experiments. Scale bars represent 1000µm.

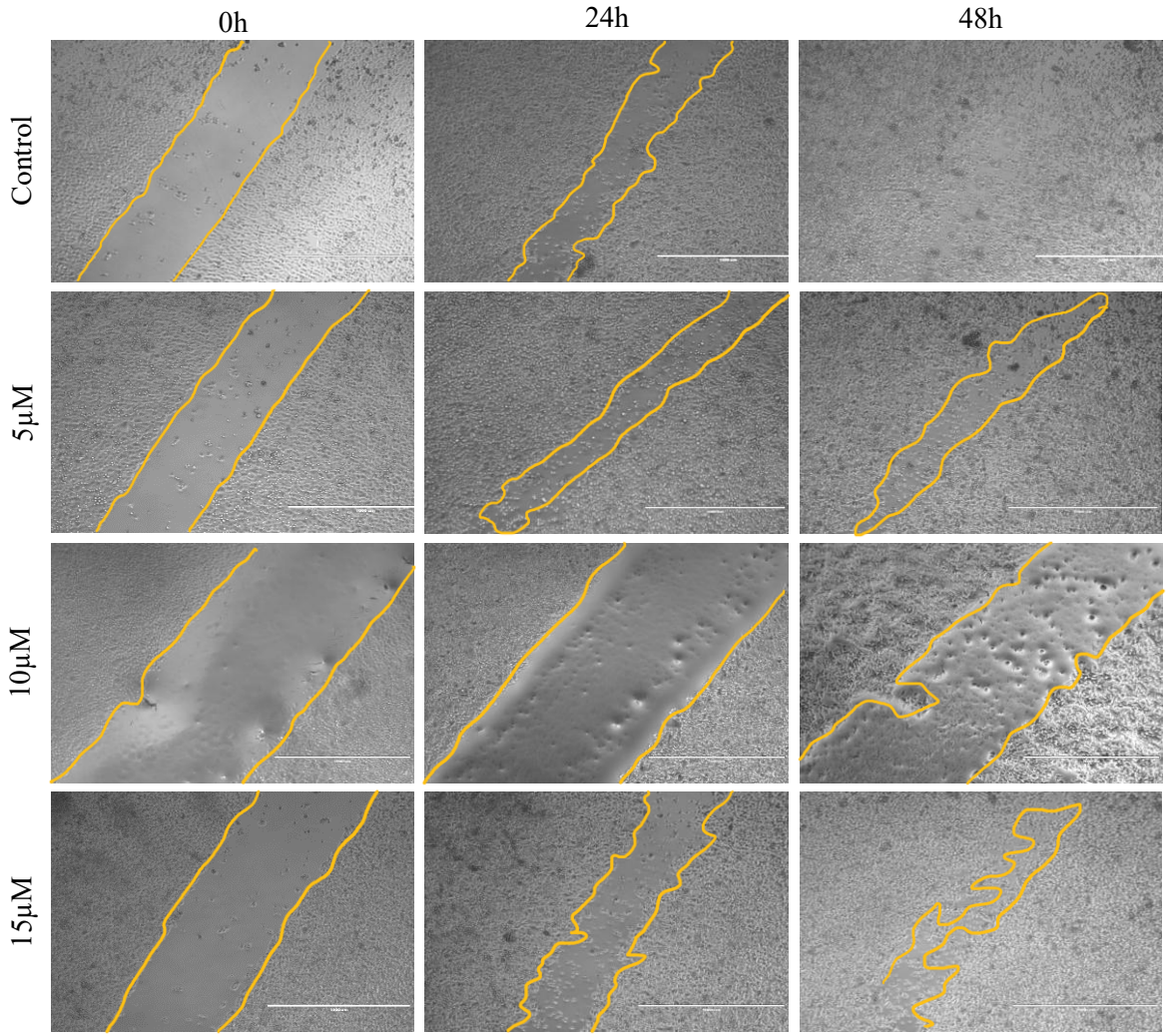

Figure 3.20: Scratch wound analysis with different concentrations of CIS treatment in HeLa cell line.

Brightfield images representing scratch wound closure at 0-, 24- and 48-hours post treatment with (B) 5µM, (C) 10µM and (D) 15µM of CIS compared to (A) control, treated with 0.1% DMSO. Illustrative images show N=3 experiments. Scale bars represent 1000µm.

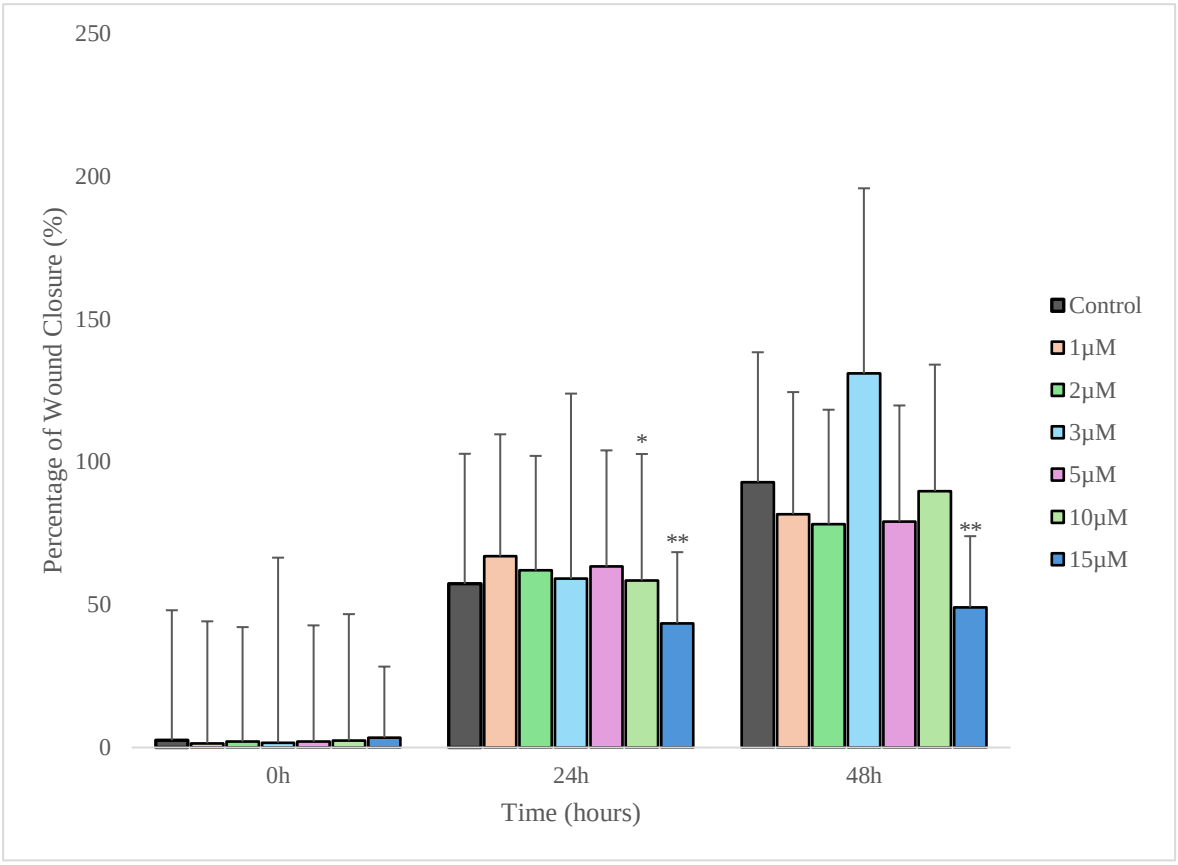

Figure 3.21: Graph representing the percentage closure of scratch wound in HeLa cells treated with 1µM, 2µM, 3µM, 5µM, 10µM and 15µM of CIS.

Quantitative graph showing the percentage of scratch wound closure present post treatment with 1µM, 2µM, 3µM, 5µM, 10µM and 15µM of CIS compared to control treated with 0.1% DMSO.
*Graph was compiled using data generated from 3 independent experiments. Data is displayed as the ±standard deviation with N=3. The statistical significance between the control (treated with 0.1% DMSO) and CIS concentrations was evaluated using a two-sample equal variance T-TEST with significance levels *p≤0.05, ** p≤0.01 and ***p≤0.0001.*

When CIS concentrations ranging from 1µM to 15µM were tested on HeLa cells for cell migration it is observed that at the lower concentrations of 1µM and 2 µM, there is complete wound closure, as shown in Figure 3.19 (B) and Figure 3.19 (C). However, starting at 3µM, there is a noticeable gap remaining in the scratch wound at 48 hours, indicating incomplete closure compared to the control group (Figure 3.19 (A)). This suggests that higher concentrations of CIS begin to inhibit cell migration and therefore, wound closure more effectively as the dose increases. As represented in the graph in Figure 3.21, the quantified data suggests that there is a statistically significant reduction in wound closure in 10µM and 15µM concentrations of CIS. These concentrations demonstrate a significant inhibitory effect on cell migration as visualised in Figure 3.20 (C) and (D) (10µM and 15µM, respectively), by exhibiting incomplete closure of the scratch wound.

3.4 Cell Proliferation Analysis utilising an MTT Assay

We next wanted to assess if the HeLa cells which were treated with a range of concentrations including 75µM and 100µM ARTM, 50µM, 75µM and 100µM ART and 10µM and 15µM CIS and displayed significance through cell viability and scratch wound assays, whether the same effect could be seen using an MTT assay to validate our previous findings.

3.4.1 Effect of Proliferation upon treatment with 75µM and 100µM of ARTM

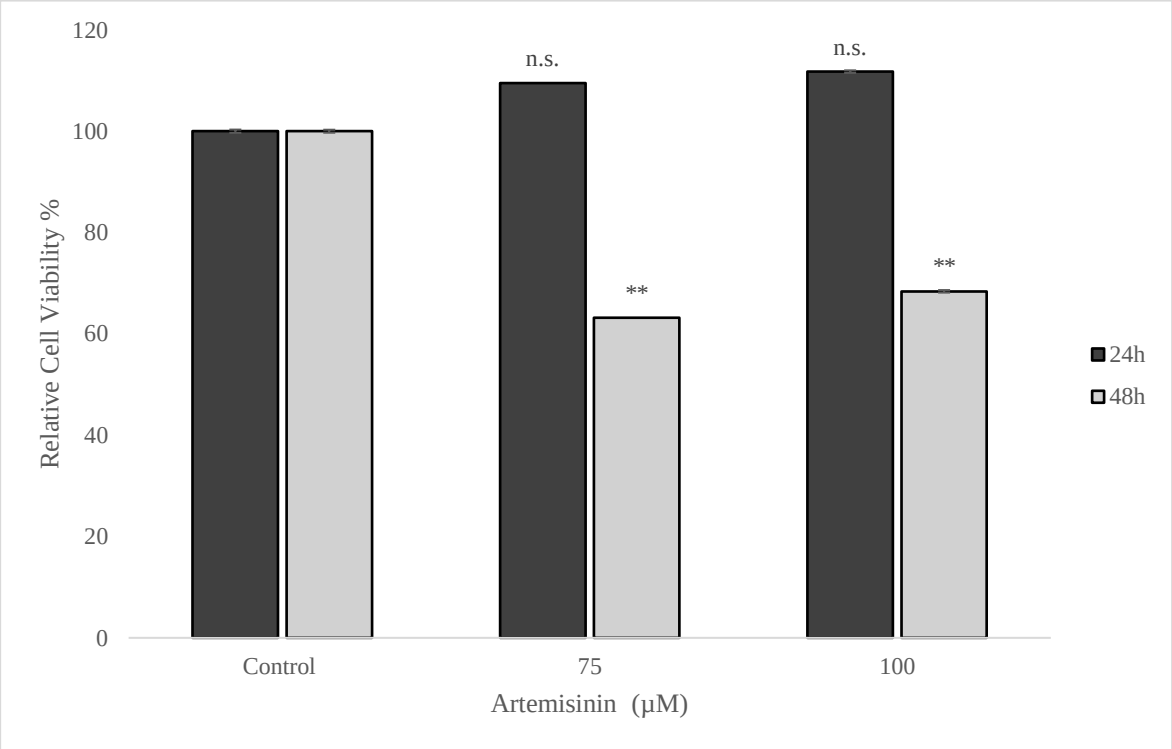

Figure 3.22: Graph representing the percentage of viable cells treated with 75µM and 100µM of ARTM

Quantitative graph showing the percentage of cell viability post treatment with 75µM and 100µM of ARTM compared to control treated with 0.1% DMSO.
*Graph was compiled using data generated from 2 independent experiments with 4 replicates. Data is displayed as the ± standard deviation with N=3. The statistical significance between the control (treated with 0.1% DMSO) and ARTM concentrations was evaluated using a two-sample equal variance T-TEST with significance levels *p≤0.05, ** p≤0.01 and ***p≤0.0001. No significance is represented as n.s.*

The MTT assay was used to confirm the results from the cell viability assay, which has shown significant effects in the graph presented in Figure 3.22. The MTT assay was conducted on the 75µM and 100µM concentrations of ARTM concentrations of ARTM. Figure 3.22 indicates that both concentrations exhibited similar patterns: neither showed

statistical significance at 24 hours, but at 48 hours post-treatment, both displayed statistical significance with p≤0.01. When comparing these results to the cell viability images in Figure 3.1, it was evident that 100μM ARTM resulted in a higher number of dead cells at 48 hours than 75μM. Given that both concentrations have similar effects in terms of efficacy, 75μM can be considered the optimum concentration, as it leads to fewer dead cells, thereby reducing cytotoxicity while maintaining effectiveness.

3.4.2 Effect of Proliferation upon treatment with 50μM, 75μM and 100μM of ART

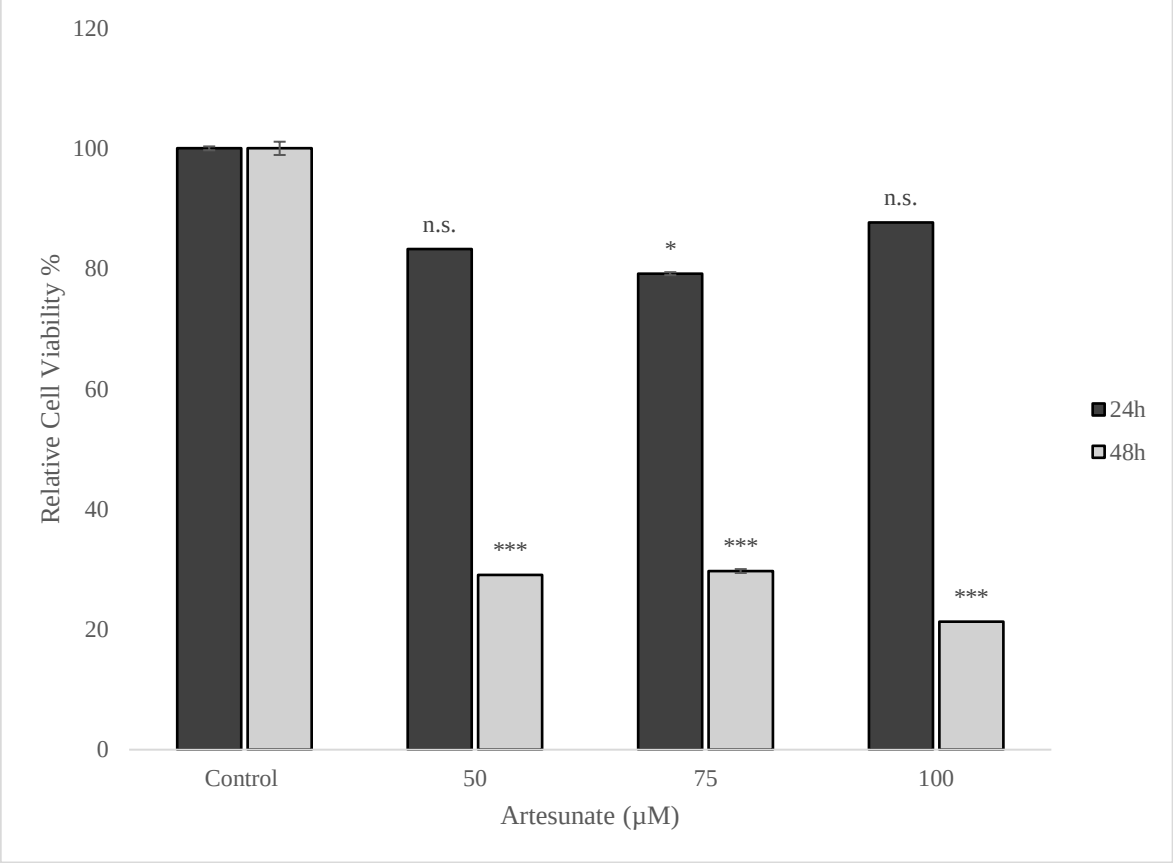

Figure 3.23: Graph representing the percentage of viable cells treated with 50μM, 75μM and 100μM of ART

Quantitative graph showing the percentage of cell viability post treatment with 50μM, 75μM and 100μM of ART compared to control treated with 0.1% DMSO.
*Graph was compiled using data generated from 3 independent experiments with 4 replicates. Data is displayed as the ± standard deviation with N=3. The statistical significance between the control (treated with 0.1% DMSO) and ART concentrations was evaluated using a two-sample equal variance T-TEST with significance levels *p≤0.05, ** p≤0.01 and ***p≤0.0001. No significance is represented as n.s.*

Similarly, ART was tested across a range of concentrations that demonstrated significance in cell viability previously from 50μM to 100μM. The MTT assay confirmed these findings, in the context of inhibition of proliferation, as shown in Figure 3.23, where the

concentrations of 50µM, 75µM and 100µM all exhibited statistical significance at 48 hours post treatment, while no significance was observed at 24 hours except for 75µM. Despite 75µM showing significance at both 24 and 48 hours, 100µM will be selected as the optimum concentration due to its more noticeable effects on both cell migration and cell viability. This makes 100µM ART the preferred choice for further experimentation.

3.4.3 Effect of Proliferation upon treatment with 10µM of CIS

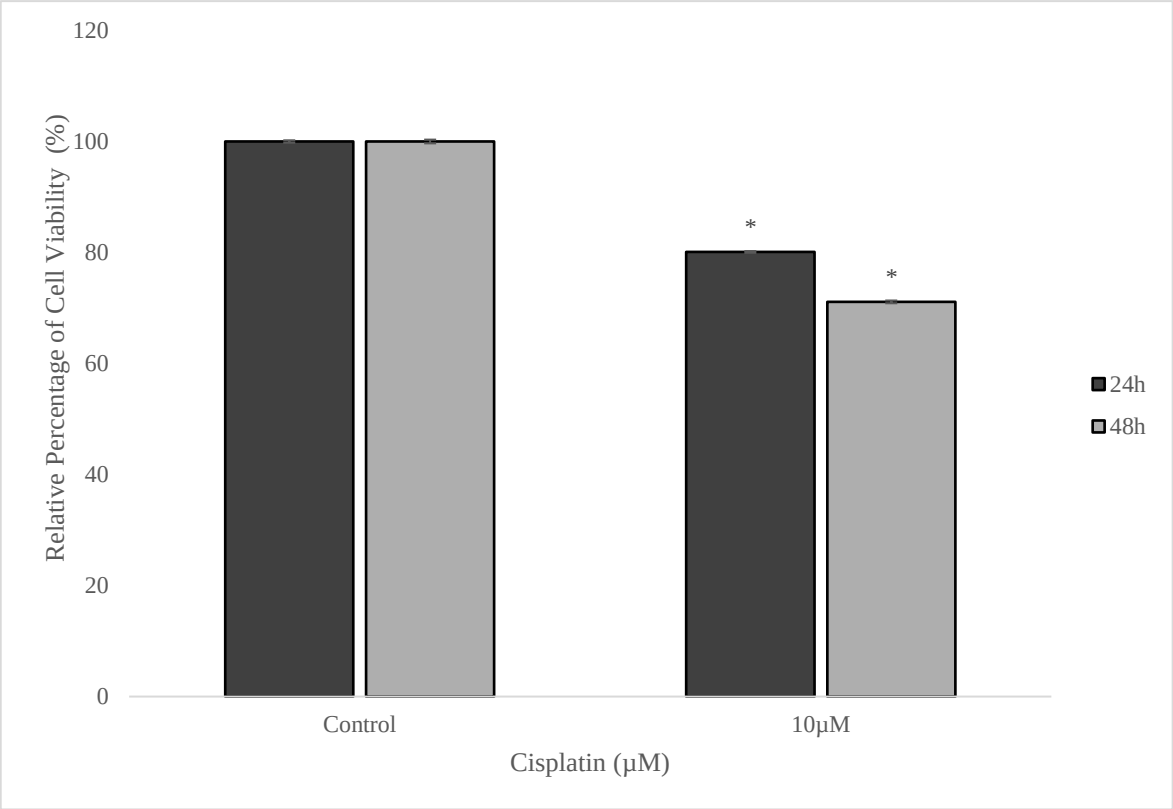

Figure 3.24: Graph representing the percentage of viable HeLa cells treated with 10µM of CIS

Quantitative graph showing the percentage of cell viability post treatment with 10µM of CIS compared to control treated with 0.1% DMSO.
*Graph was compiled using data generated from 2 independent experiments with 4 replicates. Data is displayed as the ± standard deviation with N=3. The statistical significance between the control (treated with 0.1% DMSO) and CIS concentrations was evaluated using a two-sample equal variance T-TEST with significance levels *p≤0.05, ** p≤0.01 and ***p≤0.0001. No significance is represented as n.s.*

Figure 3.24 represents the results of the MTT assay conducted to confirm the effect of 10µM of CIS on HeLa cell viability, supporting the findings from Figure 3.7. The MTT assay demonstrates a statistically significant reduction in cell viability at both 24- and 48-

hours post-treatment with 10µM CIS. This confirms that 10µM CIS effectively impacts cell viability over time, consistent with the previous viability assay results.

3.5 Caspase-3 Assay

Following the quantification of the previous assays, the concentrations of each drug that exhibited significance ($p \leq 0.05$, $p \leq 0.01$ or $p \leq 0.0001$) were further evaluated using a caspase-3 activity assay. This assay assesses the enzymatic activity of caspase 3, a key mediator of apoptosis. This method involves the use of Asp-Glu-Val-Asp p nitroanilide (Ac-DEVD-pNA) substrate, which is specifically cleaved active by caspase-3 resulting in the release of p-nitroaniline (pNA). The concentration of pNA is then determined by measuring its absorbance at 405nm.

3.5.1 Caspase-3 Activity on HeLa Cells Treated with ARTM

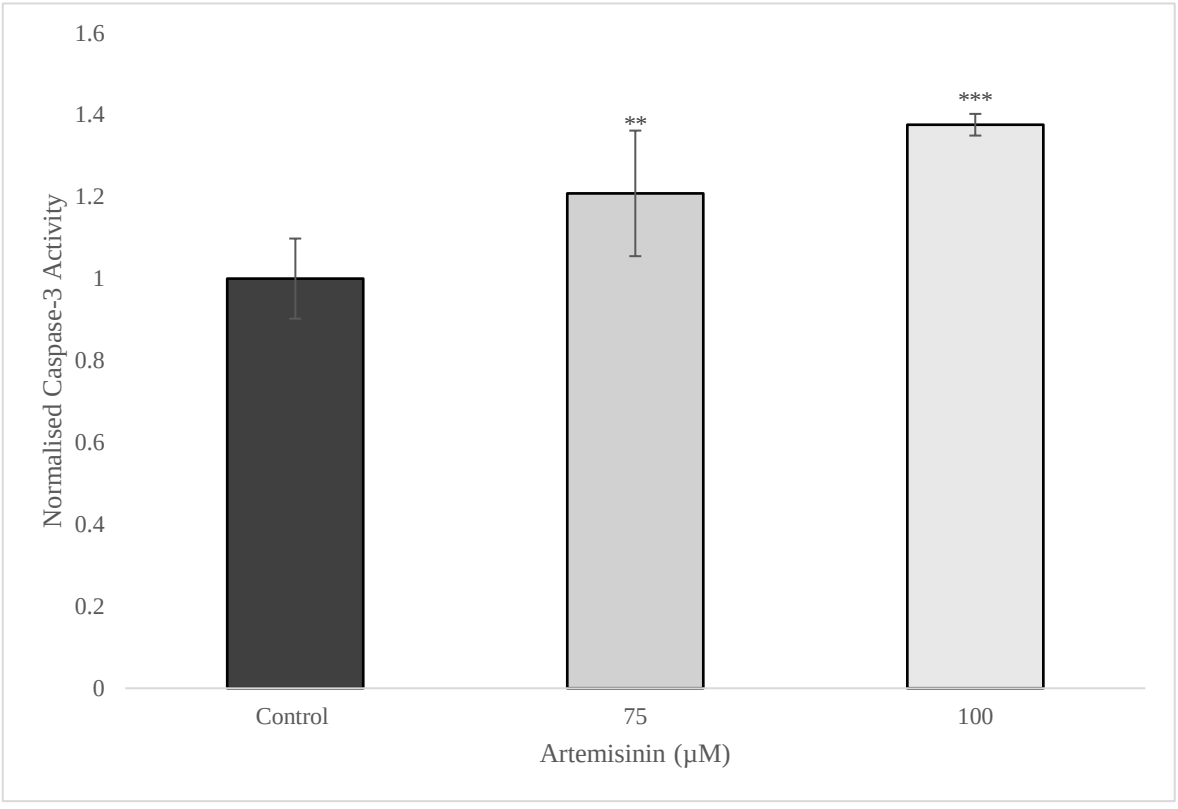

Figure 3.25: Graph representing caspase-3 activity of HeLa Cells treated with ARTM.

Quantitative graph showing the caspase-3 activity post treatment with 75µM and 100µM of ARTM compared to control treated with 0.1% DMSO.
*Graph was compiled using data generated from 2 independent experiments. Data is displayed as the ± standard deviation with N=3. The statistical significance between the control (treated with 0.1% DMSO) and ARTM concentrations was evaluated using a two-sample equal variance T-TEST with significance levels *p≤0.05, ** p≤0.01 and ***p≤0.0001. No significance is represented as n.s.*

3.5.2 Caspase-3 Activity on HeLa Cells Treated with ART

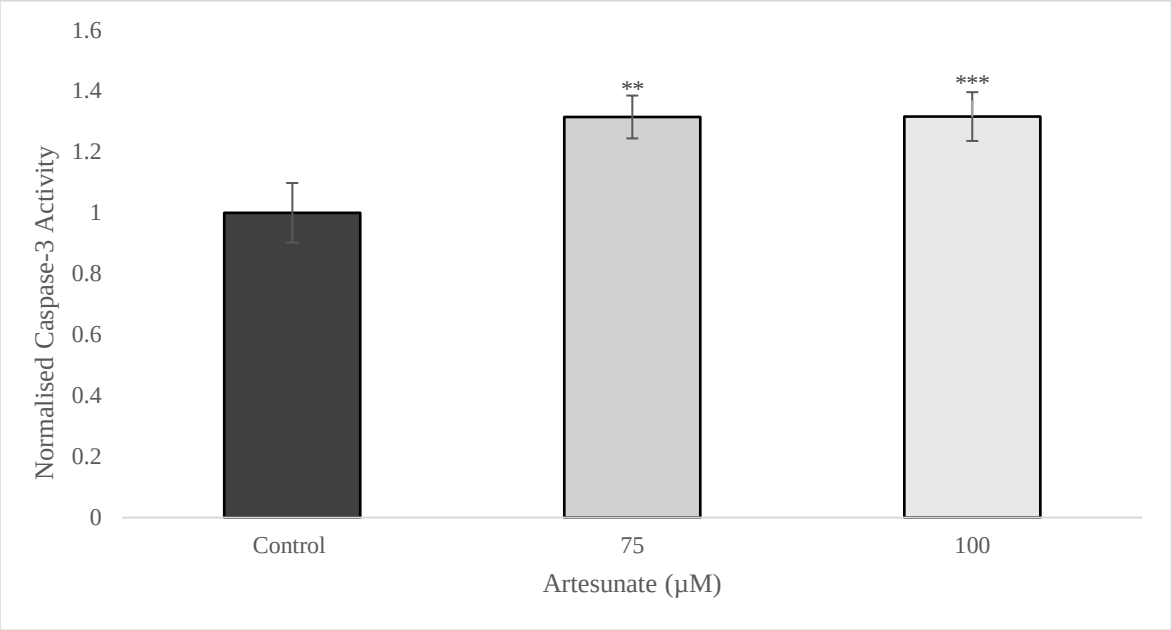

Figure 3.26: Graph representing caspase-3 activity of HeLa Cells treated with ART.

Quantitative graph showing the caspase-3 activity post treatment with 75µM and 100µM of ART compared to control treated with 0.1% DMSO.

*Graph was compiled using data generated from 2 independent experiments. Data is displayed as the ± standard deviation with N=3. The statistical significance between the control (treated with 0.1% DMSO) and ART concentrations was evaluated using a two-sample equal variance T-TEST with significance levels *p≤0.05, ** p≤0.01 and ***p≤0.0001. No significance is represented as n.s.*

3.5.3 Caspase-3 Activity on HeLa Cells Treated with CIS

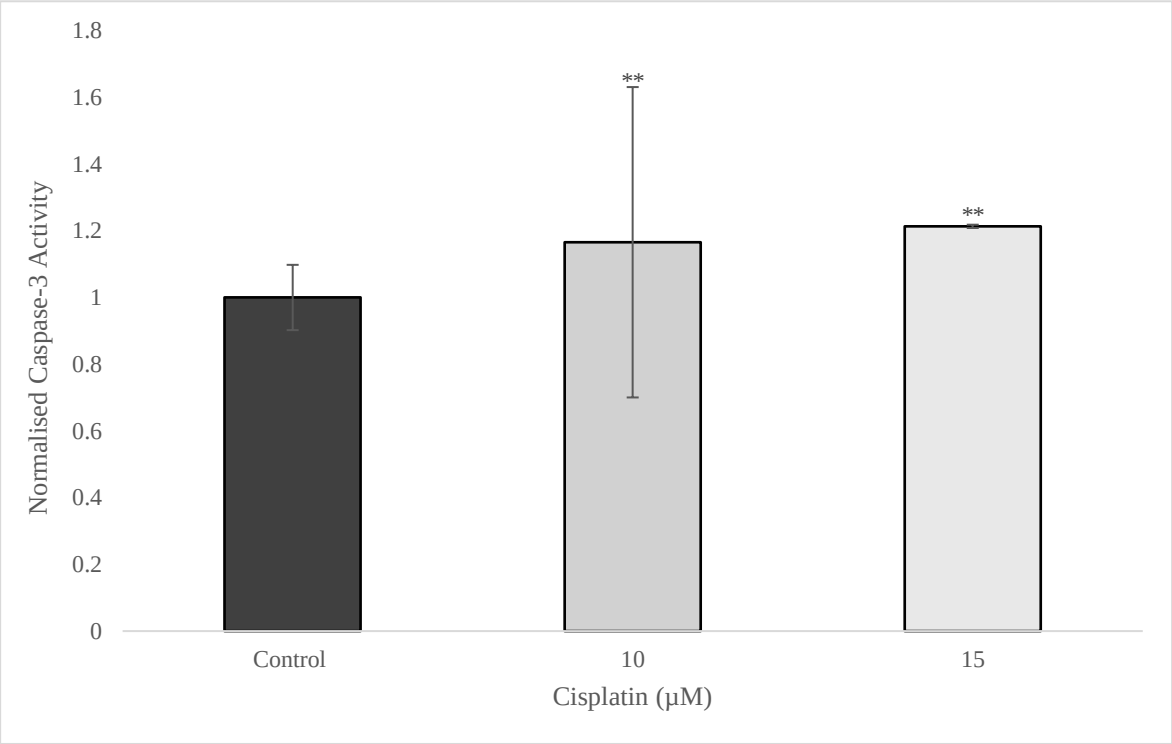

Figure 3.27: Graph representing caspase-3 activity of HeLa cells treated with CIS.

Quantitative graph showing the caspase-3 activity post treatment with 10µM and 15µM of CIS compared to control treated with 0.1% DMSO.

*Graph was compiled using data generated from 2 independent experiments. Data is displayed as the ± standard deviation with N=3. The statistical significance between the control (treated with 0.1% DMSO) and CIS concentrations was evaluated using a two-sample equal variance T-TEST with significance levels *p≤0.05, ** p≤0.01 and ***p≤0.0001. No significance is represented as n.s.*

As shown in Figure 3.25 - Figure 3.27, each concentration tested demonstrated a higher level of caspase-3 activity compared to the untreated control group, indicating increased apoptotic activity.

In Figure 3.25, HeLa cells treated with 75μM and 100μM ARTM exhibit significant caspase-3 activity. Notably, 100μM ARTM shows higher caspase-3 activity than 75μM, aligning with the cytotoxic effects observed in the cell viability assay, where more dead cells were seen at 100μM concentration. Both concentrations show statistical significance in their effects.

Similarly, ART-treated HeLa cells (75μM and 100μM) exhibited comparable effects, with ART 75μM displaying slightly higher caspase-3 activity than ART 100μM represented in Figure 3.26, although both concentrations demonstrated statistical significance with $p \leq 0.01$.

CIS treatments at 10μM and 15μM also induced higher caspase-3 activity compared to the control and both were statistically significant with the same p-value ($p \leq 0.01$) shown in Figure 3.27 confirming increased apoptosis at this concentration compared to control.

3.6 Combination Therapy Assays

3.6.1 Effect of ARTM and ART in combination with CIS on Cell Viability in HeLa Cells

Having established the optimum concentrations for both ARTM (75µM) and ART (100µM) from singular assays, we decided to use this in combination with 10µM CIS, which was found to be the statistically significant concentration of CIS in reducing HeLa cell viability and resulted in incomplete wound closure in the migration assay (Figure 3.21). Its efficacy was comparable to that of 15µM but given the goal of minimising cisplatin-induced cytotoxicity, the lower concentration of 10µM – while still effective – was selected as the optimum concentration to test for combination effects on HeLa cells with 1µM used as a lower range.

3.6.2 Effect of 75µM ARTM in Combination with CIS on HeLa Cell Viability

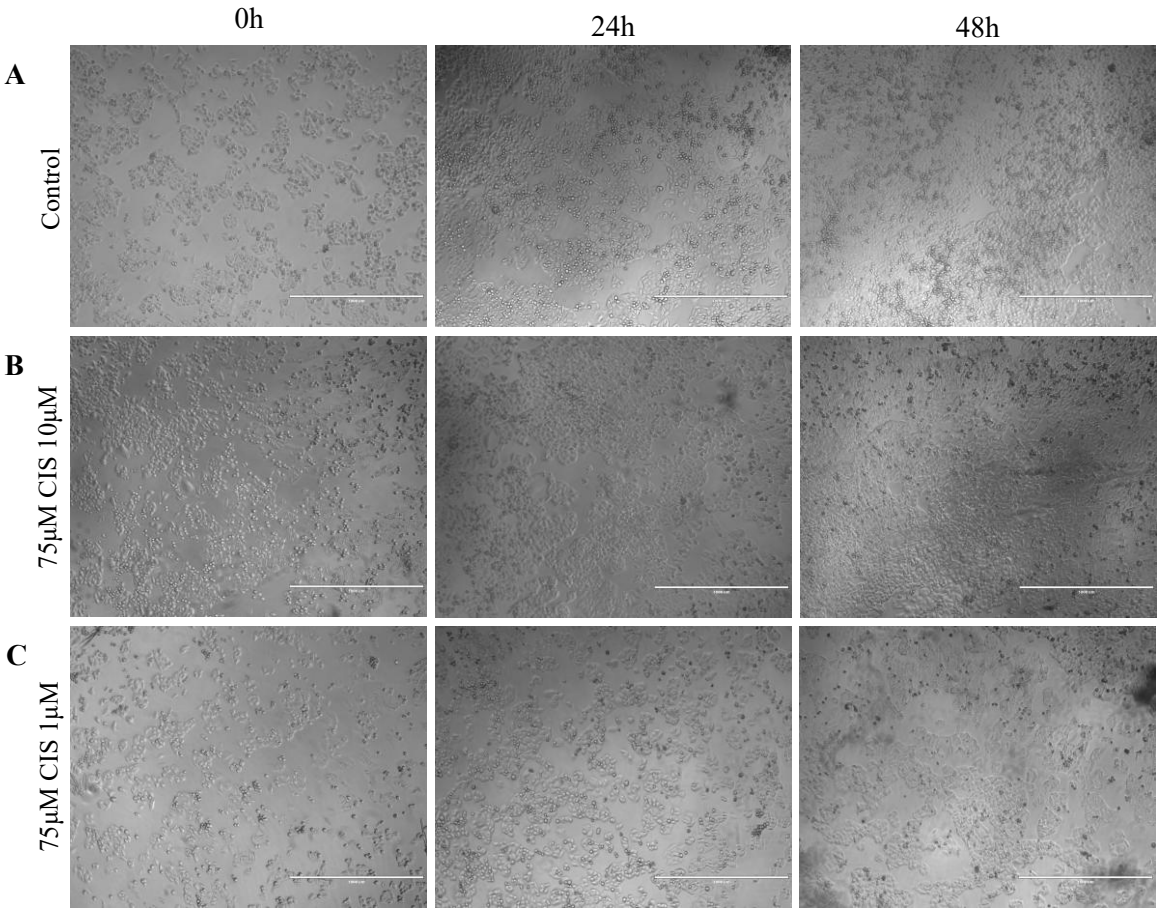

Figure 3.28: Cell viability analysis of HeLa cells treated with ARTM in combination with CIS.

Brightfield images representing cells at 0-, 24- and 48-hours post treatment with (B) ARTM 75µM CIS 10µM and (C) ARTM 75µM CIS 1µM compared to (A) control, treated with 0.1% DMSO. Illustrative images show N=3 experiments. Scale bars represent 1000µm.

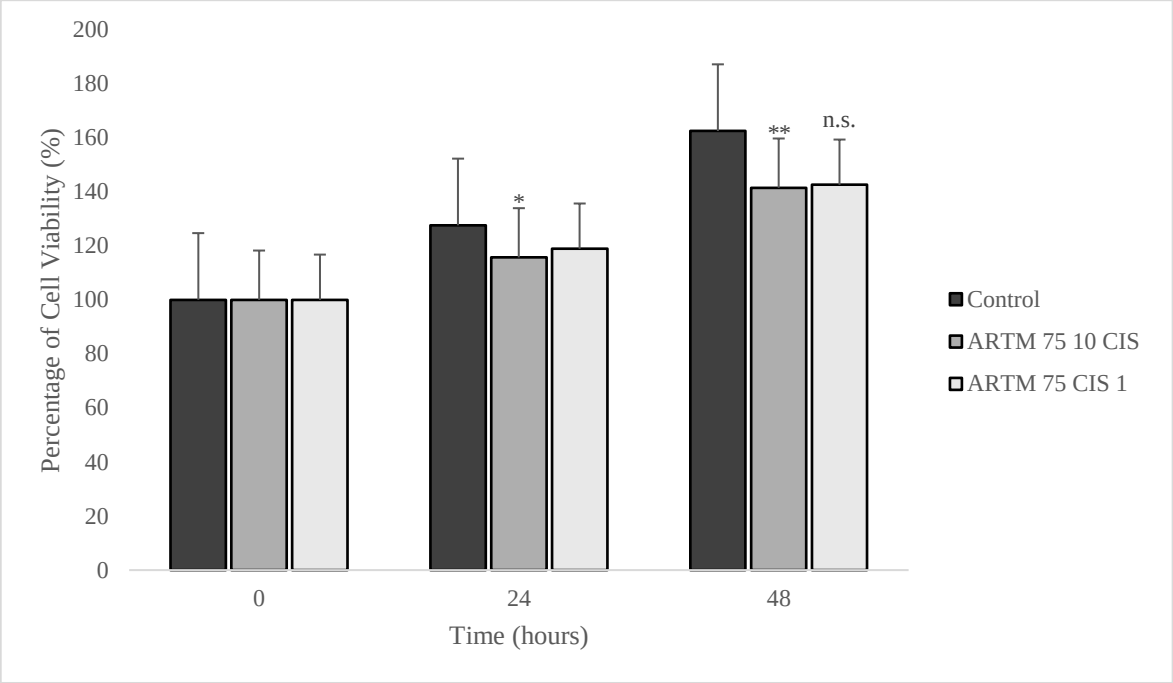

Figure 3.29: Graph representing the percentage of viable HeLa cells treated with ARTM in combination with CIS.

Quantitative graph showing the percentage of viable HeLa cells present post treatment with 75μM ARTM in combination with 10μM and 1μM CIS compared to control treated with 0.1% DMSO.
*Graph was compiled using data generated from 3 independent experiments. Data is displayed as the ± standard deviation with N=3. The statistical significance between the control (treated with 0.1% DMSO) and ARTM + CIS concentrations was evaluated using a two-sample equal variance T-TEST with significance levels *p≤0.05, ** p≤0.01 and ***p≤0.0001.*

ARTM 75μM was tested in combination with 10μM and 1μM CIS, as depicted in Figure 3.28 (A) and 3.28 (C). The quantification of these results, shown in Figure 3.30, highlights that ARTM 75μM combined with 10μM CIS exhibited the most noticeable effect. This combination demonstrated statistically significant effects with p values of less than 0.05 at 24 hours and less than 0.01 at 48 hours, as represented in the graph in Figure 3.29.

3.6.3 Effect of 50µM, 100µM ART in Combination with CIS on HeLa Cell Viability

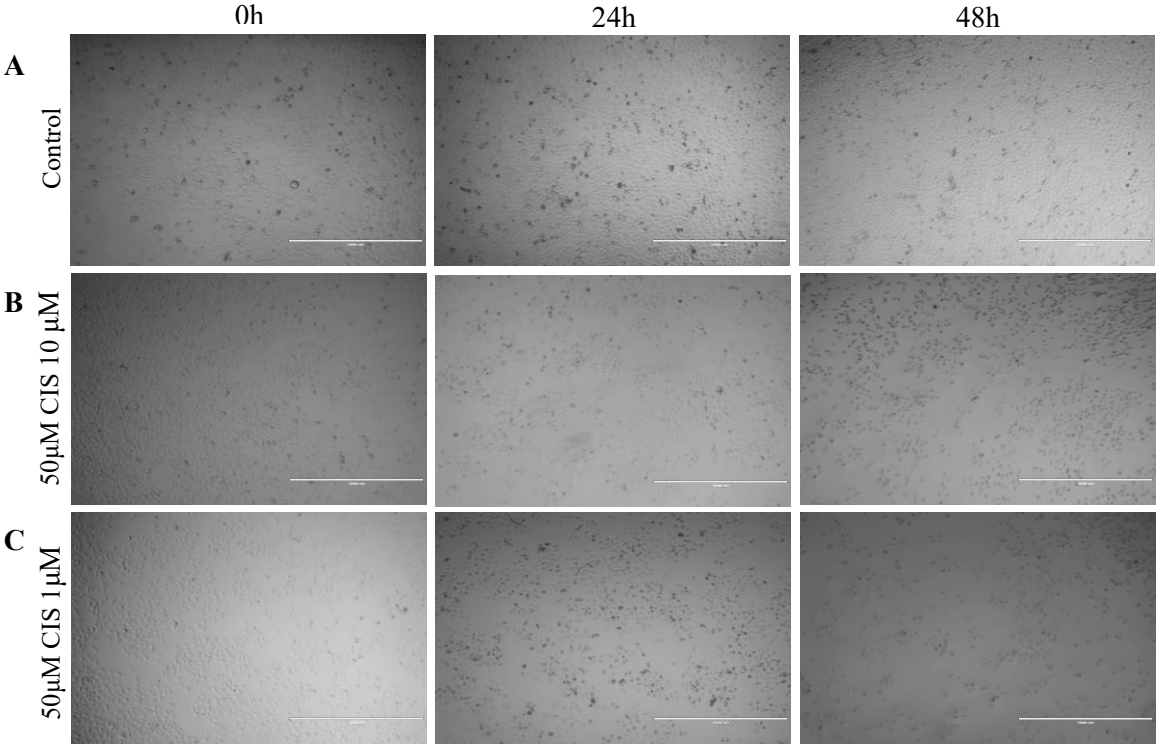

Figure 3.30: Cell viability analysis of HeLa cells treated with ART in combination with CIS.

Brightfield images representing cells at 0-, 24- and 48-hours post treatment with (B) ART 50µM CIS 10µM and (C) ART 50µM CIS 1µM compared to (A) control, treated with 0.1% DMSO. Illustrative images show N=3 experiments. Scale bars represent 1000µm.

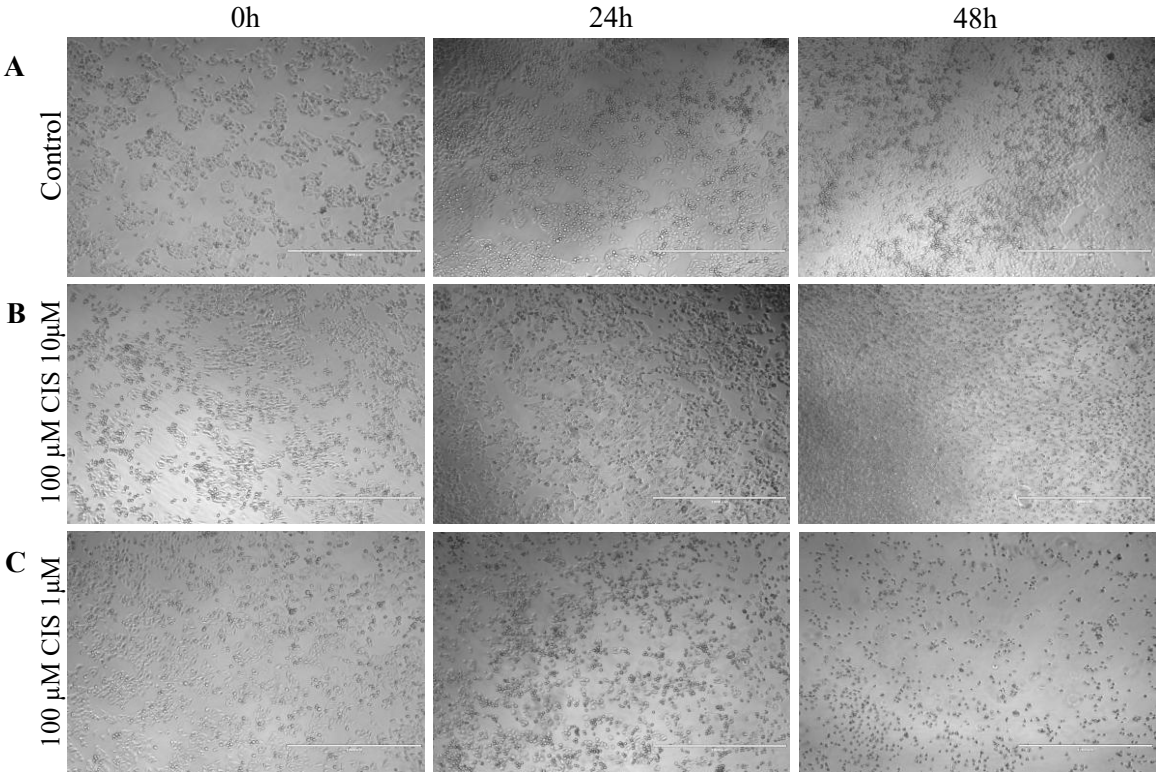

Figure 3.31: Cell viability analysis of HeLa cells treated with ART in combination with CIS.

Brightfield images representing cells at 0-, 24- and 48-hours post treatment with (B) ART 100µM CIS 10µM and (C) ART 100µM CIS 1µM compared to (A) control, treated with 0.1% DMSO. Illustrative images show N=3 experiments. Scale bars represent 1000µm.

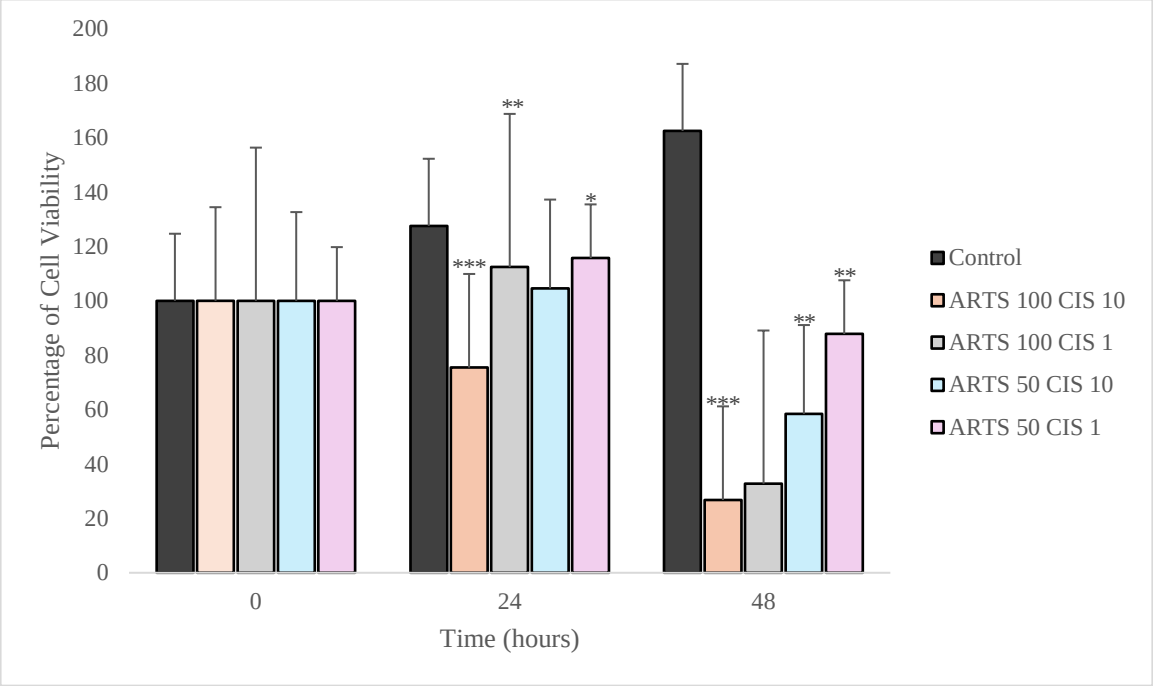

Figure 3.32: Graph representing the percentage of viable HeLa cells treated with ART in combination with CIS.

Quantitative graph showing the percentage of viable HeLa cells present post treatment with 100μM ART in combination with 10μM and 1μM CIS and 50μM ART in combination with 10μM and 1μM CIS compared to control treated with 0.1% DMSO.

*Graph was compiled using data generated from 3 independent experiments. Data is displayed as the ± standard deviation with N=3. The statistical significance between the control (treated with 0.1% DMSO) and ART + CIS concentrations was evaluated using a two-sample equal variance T-TEST with significance levels *p≤0.05, ** p≤0.01 and ***p≤0.0001.*

ART was also evaluated in combination with CIS to assess the effectiveness of this combination therapy. Two concentrations of ART 50μM and 100μM, were tested alongside two CIS concentrations: the optimum dose of 10μM and a lower dose of 1μM. These results are illustrated in Figure 3.30 and Figure 3.31.

Figure 3.34 provides a quantification of the effects at different concentrations. The combination of 100μM and 10μM CIS yielded the most significant results, with p-values below 0.001 at both 24- and 48-hours post-treatment. However, the combination of 100μM ART with 1μM CIS did not demonstrate notable significance. As shown in the graph, this combination achieved statistical significance only at the 24-hour time point, with a p-value of 0.001 but no significance was observed at 48 hours.

The combination of 50μM ART and 10μM CIS exhibited significant effects at 48 hours, as depicted in Figure 3.32. Similarly, the combination of 50μM ART and 1μM CIS showed significance at both 24 and 48 hours according to the corresponding graph.

3.6.4 Effect of 75µM ARTM in Combination with CIS on HeLa Cell Migration

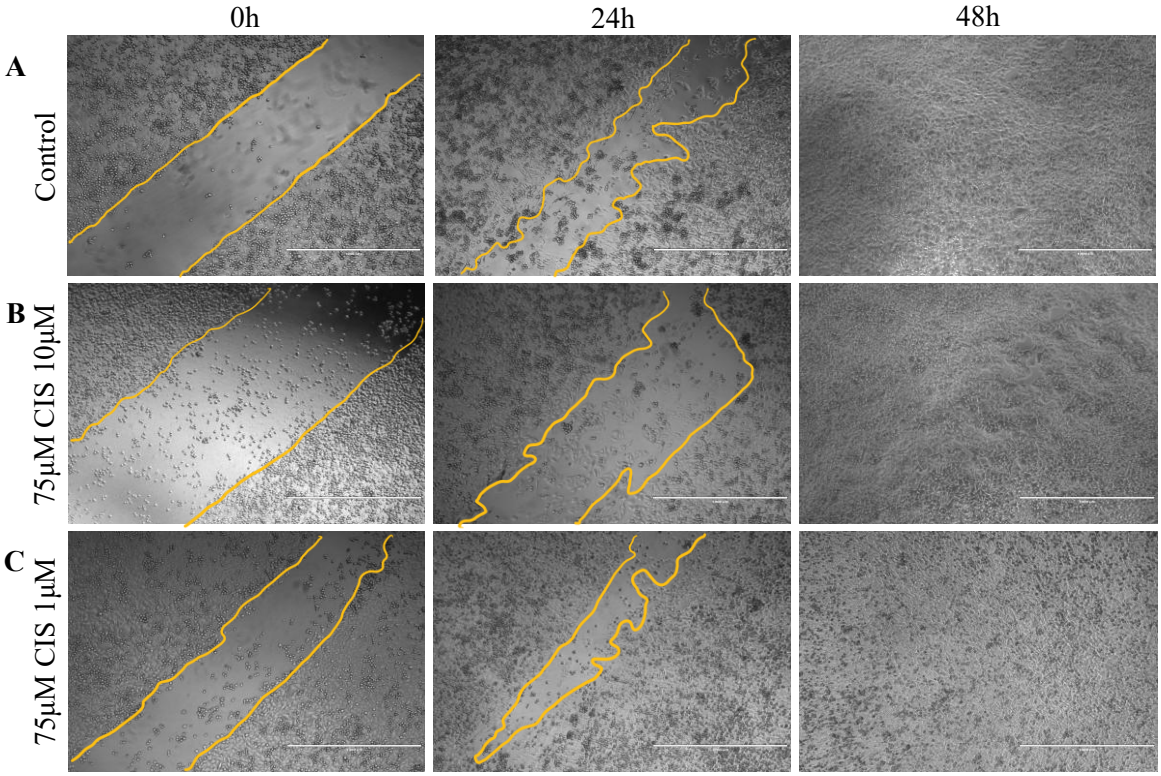

Figure 3.33: Scratch wound analysis of HeLa cells treated with ARTM in combination with CIS.

Brightfield images representing scratch wound closure at 0, 24 and 48 hours post treatment with (B) ARTM 75µM CIS 10µM (C) ARTM 75µM CIS 1µM compared to (A) control, treated with 0.1% DMSO. Illustrative images show N=3 experiments. Scale bars represent 1000µm.

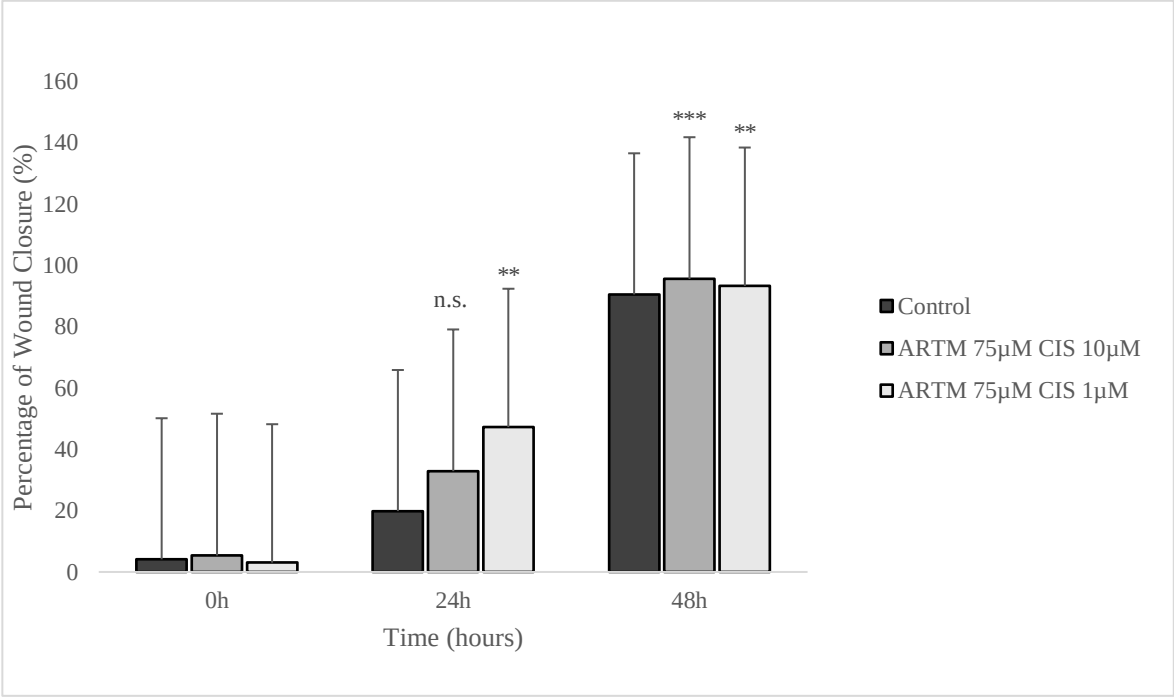

Figure 3.34: Graph representing the percentage closure of scratch wound in HeLa cells treated ARTM in combination with CIS.

Quantitative graph showing the percentage of scratch wound closure present post treatment with 75µM ARTM in combination with 10µM and 1µM CIS compared to control treated with 0.1% DMSO.
*Graph was compiled using data generated from 3 independent experiments. Data is displayed as the ±standard deviation with N=3. The statistical significance between the control (treated with 0.1% DMSO) and ARTM + CIS concentrations was evaluated using a two-sample equal variance T-TEST with significance levels *p≤0.05, ** p≤0.01 and ***p≤0.0001.*

Following the cell viability assay ARTM 75µM in combination with CIS was assessed for its effects on cellular migration as shown in Figure 3.33 (B) and Figure 3.34 (C). The quantification of these results is presented in the graph in Figure 3.35. At 24 hours post-treatment there was no significant difference in wound closure with the combination of 75µM ARTM and 10µM CIS compared to control. However, by 48 hours statistical significance was observed. The alternative combination of 75µM ARTM and 1µM CIS also demonstrated statistical significance at both 24- and 48-hours post-treatment. However, with both sets of combinations as seen in Figure 3.34 (B) and Figure 3.34 (C) almost complete wound closure was evident at 48 hours compared to control. This outcome appears to contradict the statistical significance levels presented in the corresponding graph, suggesting that while the data show measurable differences, the extent of wound closure at later time points visually similar across conditions.

3.6.5 Effect of 50µM, 100µM ART in Combination with CIS on HeLa Cell Migration

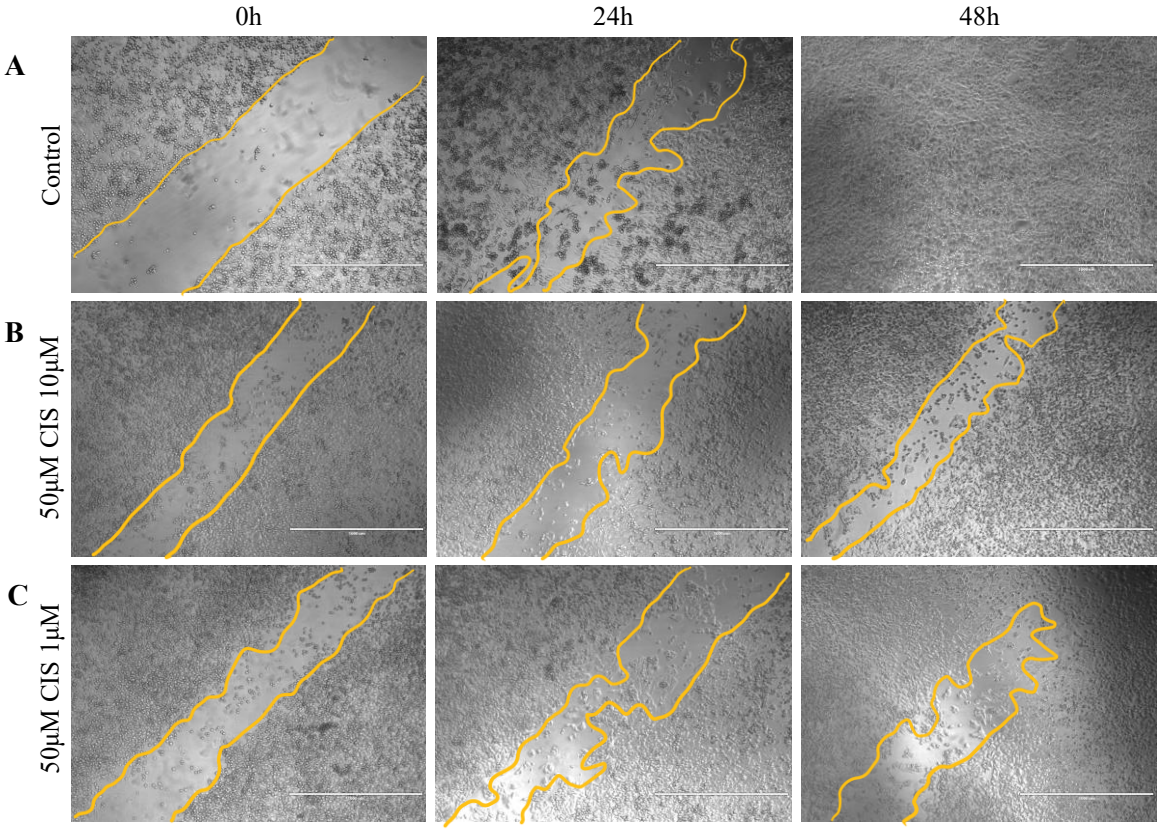

Figure 3.35: Scratch wound analysis of HeLa cells treated with ART in combination with CIS.

Brightfield images representing scratch wound closure at 0, 24 and 48 hours post treatment with (B) ART 50µM CIS 10µM (C) ART 50µM CIS 1µM compared to (A) control, treated with 0.1% DMSO. Illustrative images show N=3 experiments. Scale bars represent 1000µm.

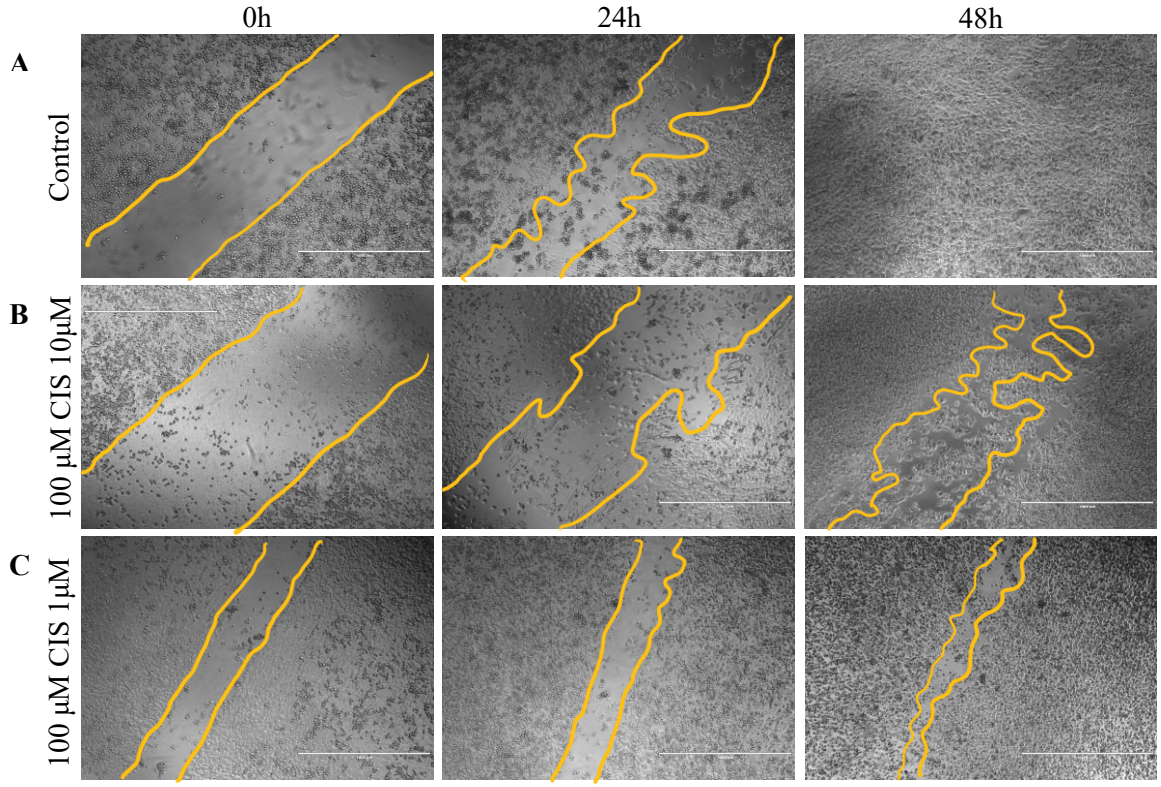

Figure 3.36: Scratch wound analysis of HeLa cells treated with ART in combination with CIS.

Brightfield images representing scratch wound closure at 0, 24 and 48 hours post treatment with (B) ART 100µM CIS 10µM (C) ART 100µM CIS 1µM compared to (A) control, treated with 0.1% DMSO. Illustrative images show N=3 experiments. Scale bars represent 1000µm.

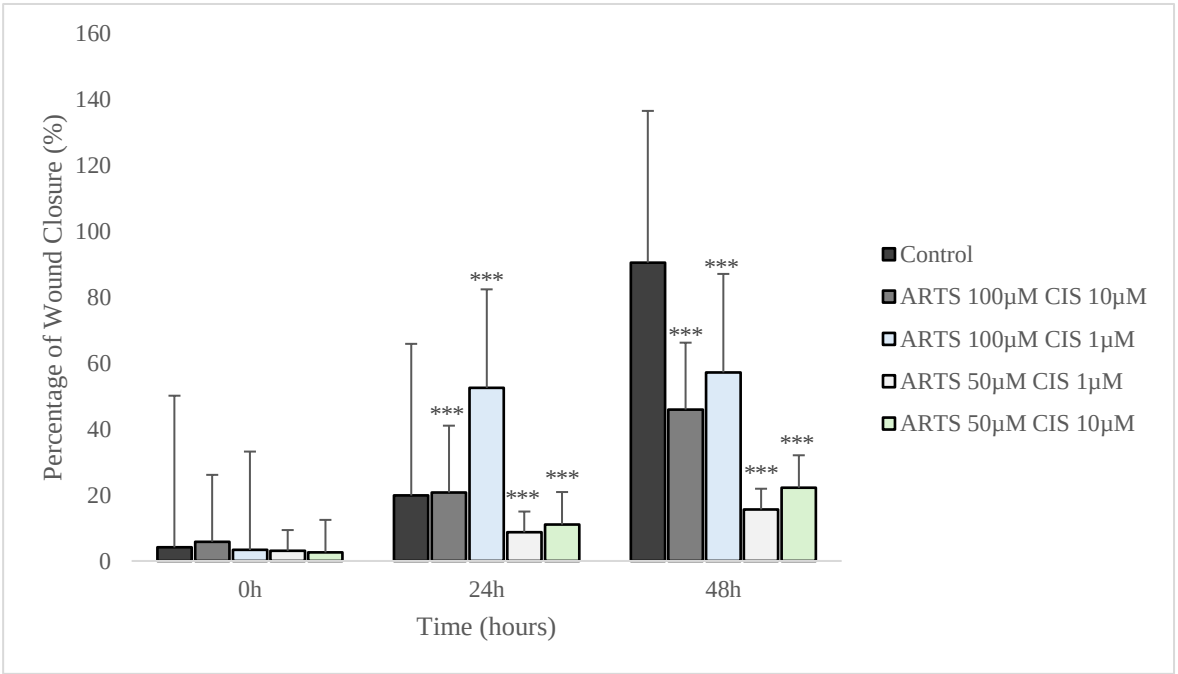

Figure 3.37: Graph representing the percentage closure of scratch wound in HeLa cells treated ART in combination with CIS.

Quantitative graph showing the percentage of scratch wound closure present post treatment with 50µM and 100µM ART and in combination with 10µM and 1µM CIS compared to control treated with 0.1% DMSO.
*Graph was compiled using data generated from 3 independent experiments. Data is displayed as the ±standard deviation with N=3. The statistical significance between the control (treated with 0.1% DMSO) and ART + CIS concentrations was evaluated using a two-sample equal variance T-TEST with significance levels *p≤0.05, ** p≤0.01 and ***p≤0.0001.*

Cell migration was further evaluated in combination with ART, as depicted in Figure 3.35 and Figure 3.36, with the results quantified in the graph presented in Figure 3.37 The quantification demonstrates that all tested combinations exhibited statistical significance at both 24- and 48-hours post-treatment. Combinations of 100µM ART with both 10µM and 1µM CIS as well as 50µM ART with 10µM and 1µM CIS, all produced p-values below 0.001, indicating highly significant effects on cell migration.

3.6.6 Effect of 75µM ARTM in Combination with CIS on HeLa Cell Proliferation utilising MTT Assay

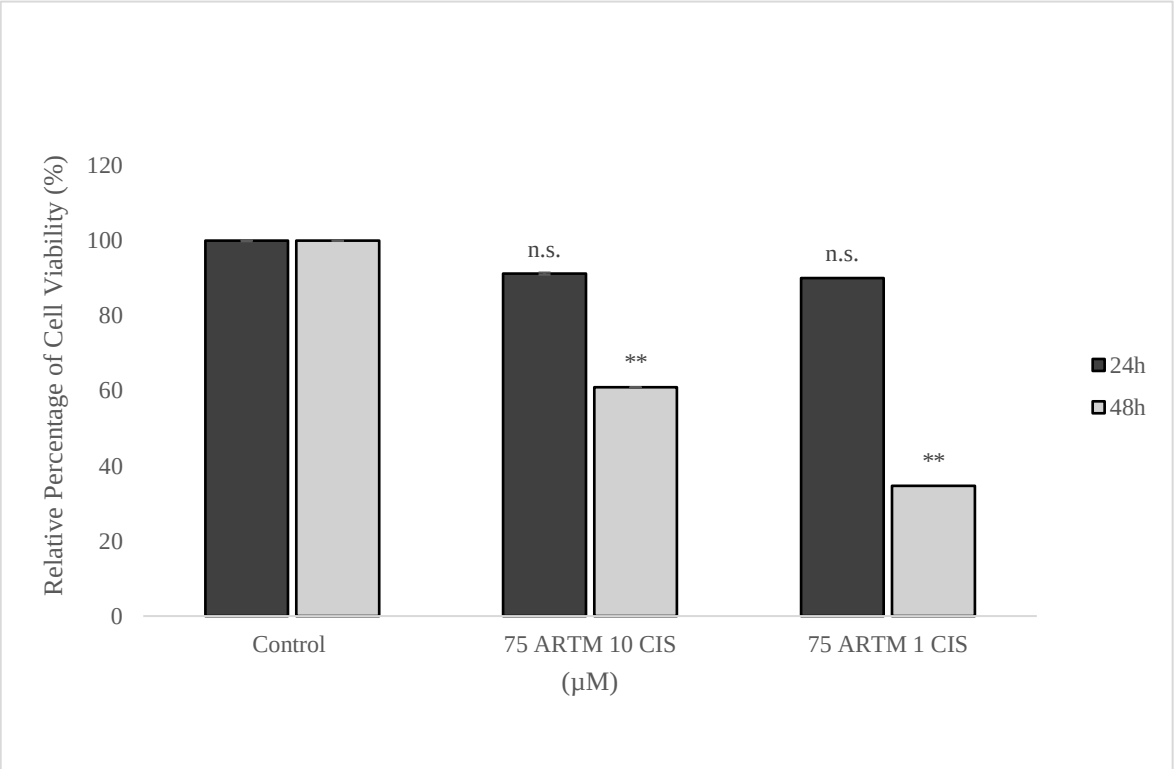

Figure 3.38: Graph representing the percentage of viable cells with ARTM in combination with CIS.

Quantitative graph showing the percentage of cell viability post treatment with 75µM ARTM in combination with 10µM and 1µM CIS compared to control treated with 0.1% DMSO.
*Graph was compiled using data generated from 2 independent experiments with 4 replicates. Data is displayed as the ± standard deviation with N=3. The statistical significance between the control (treated with 0.1% DMSO) and ARTM + CIS concentrations was evaluated using a two-sample equal variance T-TEST with significance levels *p≤0.05, ** p≤0.01 and ***p≤0.0001. No significance is represented as n.s.*

Following the cell viability analysis, an MTT assay was conducted using the same concentrations to validate proliferation effects. As shown in the graph in Figure 3.38, the combination of 75µM ARTM and 10µM CIS did not exhibit statistical significance at 24 hours but did show significance at 48 hours post treatment. Similarly, the combination of

75μM ARTM and 1μM CIS also showed no significance at 24 hours but became statistically significant at 48 hours post-treatment.

3.6.7 Effect of 50μM ART in Combination with CIS on HeLa Cell Proliferation utilising MTT Assay

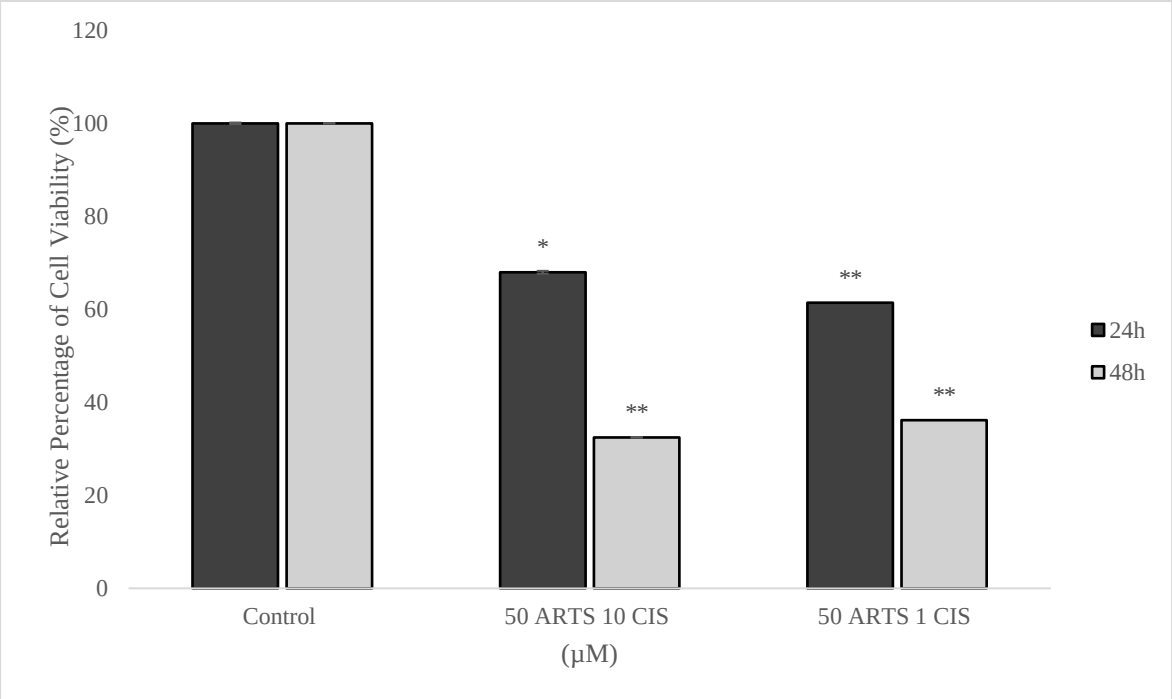

Figure 3.39: Graph representing the percentage of viable cells with ART in combination with CIS.

Quantitative graph showing the percentage of cell viability post treatment with 50μM ARTM in combination with 10μM and 1μM CIS compared to control treated with 0.1% DMSO.
*Graph was compiled using data generated from 2 independent experiments with 4 replicates. Data is displayed as the ± standard deviation with N=3. The statistical significance between the control (treated with 0.1% DMSO) and ART + CIS concentrations was evaluated using a two-sample equal variance T-TEST with significance levels *p≤0.05, ** p≤0.01 and ***p≤0.0001. No significance is represented as n.s.*

When ART was evaluated using MTT assay, both sets of combinations demonstrated statistical significance. Notably, the combination of 50μM ART and 1μM CIS showed statistically significant effects at both 24 and 48 hours, with p-values less than 0.01. Similarly, the combination of 50μM ART 10μM CIS exhibited significant effects at 48 hours with p-values less than 0.01 post-treatment. These findings are illustrated in Figure 3.39.

CHAPTER 4

Effect of Artemisinin and Artesunate on the Hippo Signalling Pathway in Cervical Cancer

4.1 Translocation of YAP upon ARTM, ART and CIS Treatment

Confluent and sparse HeLa cells were treated with specific concentrations of ARTM, ART and CIS to investigate the translocation of YAP. YAP is regulated by the HSP, which when active phosphorylates YAP, causing its cytoplasmic retention and degradation. When inactive, YAP translocates to the nucleus, interacting with co-activators like TEAD to drive genes involved in proliferation, metastasis and drug resistance (Hsu *et al.,* 2020). YAP is more nuclear at low cell densities, where limited cell-cell contact reduces Hippo activation, while in confluent cells, YAP is phosphorylated and retained in the cytoplasm (Gumbiner and Kin, 2014). To explore these dynamics, HeLa cells were seeded at different densities and treated with ARTM, ART and CIS. Following treatment, cells were fixed, stained (as detailed in chapter 2), imaged with a Zeiss Laser Scanning Microscope and analysed using ImageJ software.

4.1.1 Effect of ARTM on YAP Translocation in HeLa cells

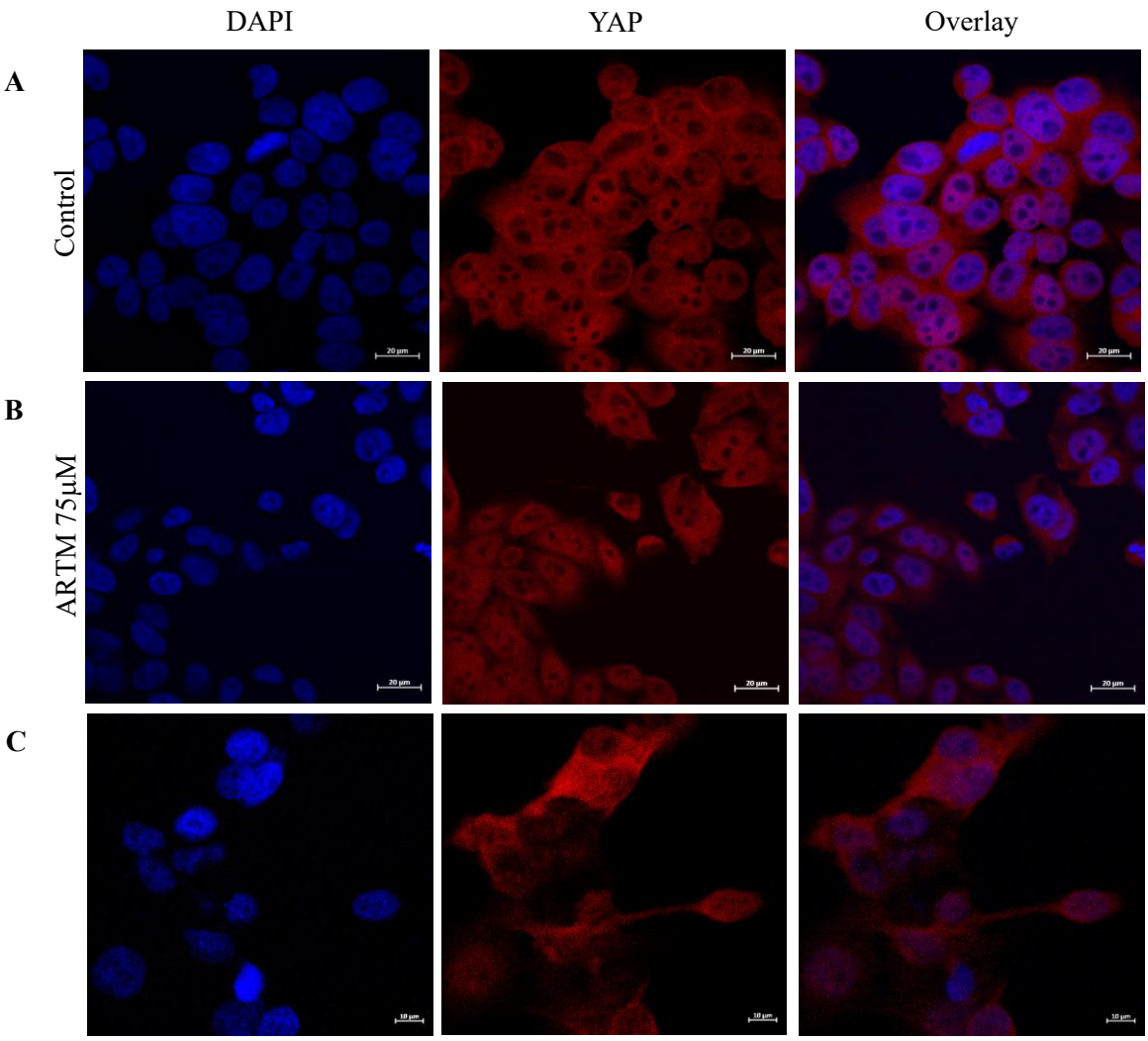

Figure 4.1: The nuclear localisation of YAP upon treatment with ARTM determined by immunofluorescence staining in HeLa cells.

(A) Images represent control treated with 0.1% DMSO stained with DAPI (nuclear staining) and CY3 (staining for YAP) (B) Images represent mid confluent HeLa cells treated with 75µM ARTM stained with DAPI and CY3 (C) Images represent sparse HeLa cells treated with 75µM ARTM stained with DAPI and CY3. Images were taken using a Zeiss Laser Scanning Microscope. Illustrative images show N=3 experiments.

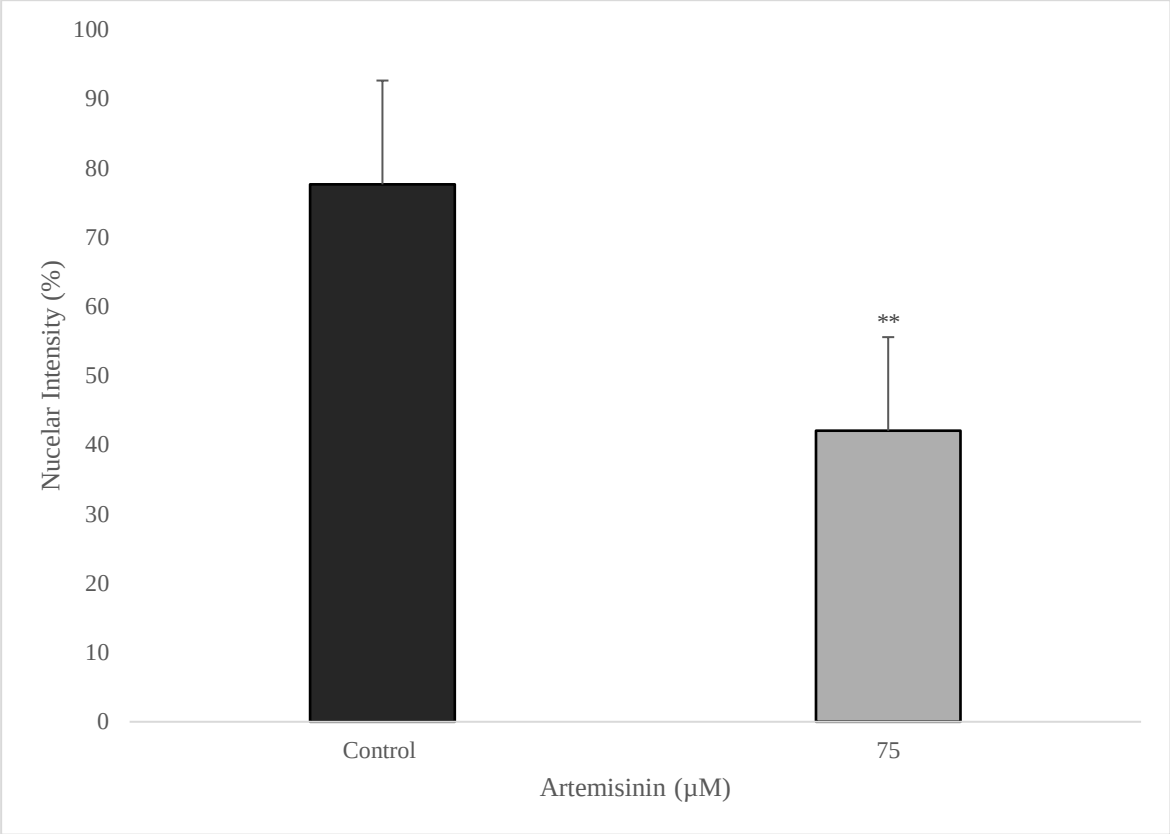

Figure 4.2: Graph representing the mean fluorescent intensity in HeLa Cells with 75µm of ARTM.

Quantitative graph showing the nuclear intensity of HeLa cells treated with 75µM ARTM compared to control treated with 0.1% DMSO.
*Graph was compiled using data generated from 3 independent experiments. Data is displayed as the ±standard deviation with N=3. The statistical significance between the control (treated with 0.1% DMSO) and ARTM concentrations was evaluated using a two-sample equal variance T-TEST with significance levels *p≤0.05, ** p≤0.01 and ***p≤0.0001. No significance is represented as n.s.*

Immunofluorescence staining was performed to detect nuclear intensity following treatment with the drug. In both mid-confluent (Figure 4.1B) and sparse cell images (Figure 4.1C), a lower intensity was observed compared to the control, as shown in Figure 4.1. This reduction in nuclear intensity is further supported by the graph in Figure 4.2, which confirms a statistically significant difference in nuclear intensity between the treated cells and the control.

4.1.2 Effect of ART on YAP Translocation in HeLa cells

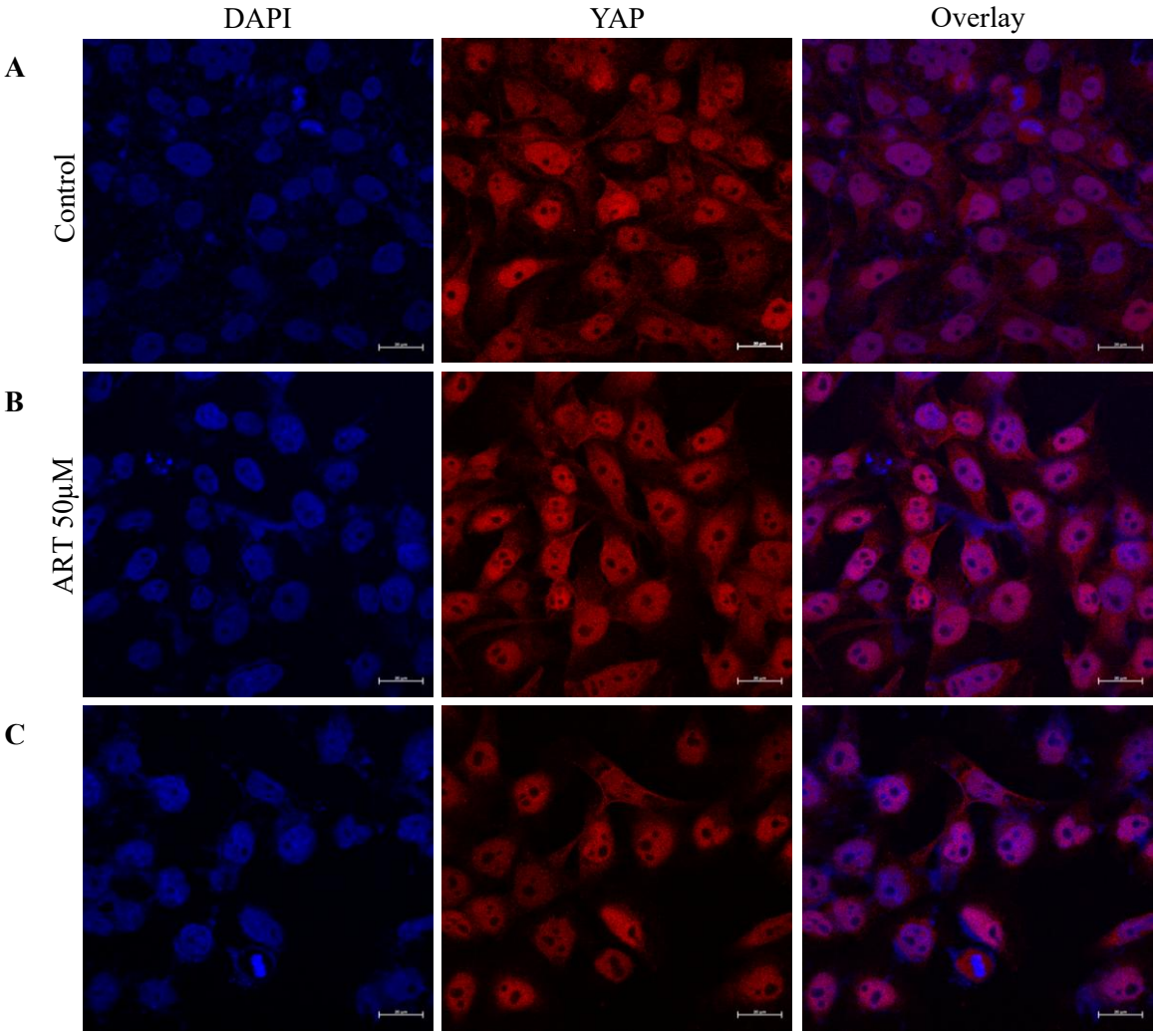

Figure 4.3: The nuclear localisation of YAP upon treatment with ART determined by immunofluorescence staining in HeLa cells.

(A) Images represent control treated with 0.1% DMSO stained with DAPI (nuclear staining), and CY3 (staining for YAP) (B) Images represent mid confluent HeLa cells treated with 50μM ART stained with DAPI and CY3 (C) Images represent sparse HeLa cells treated with 50μM ART stained with DAPI and CY3. Images were taken using a Zeiss Laser Scanning Microscope. Illustrative images show N=3 experiments.

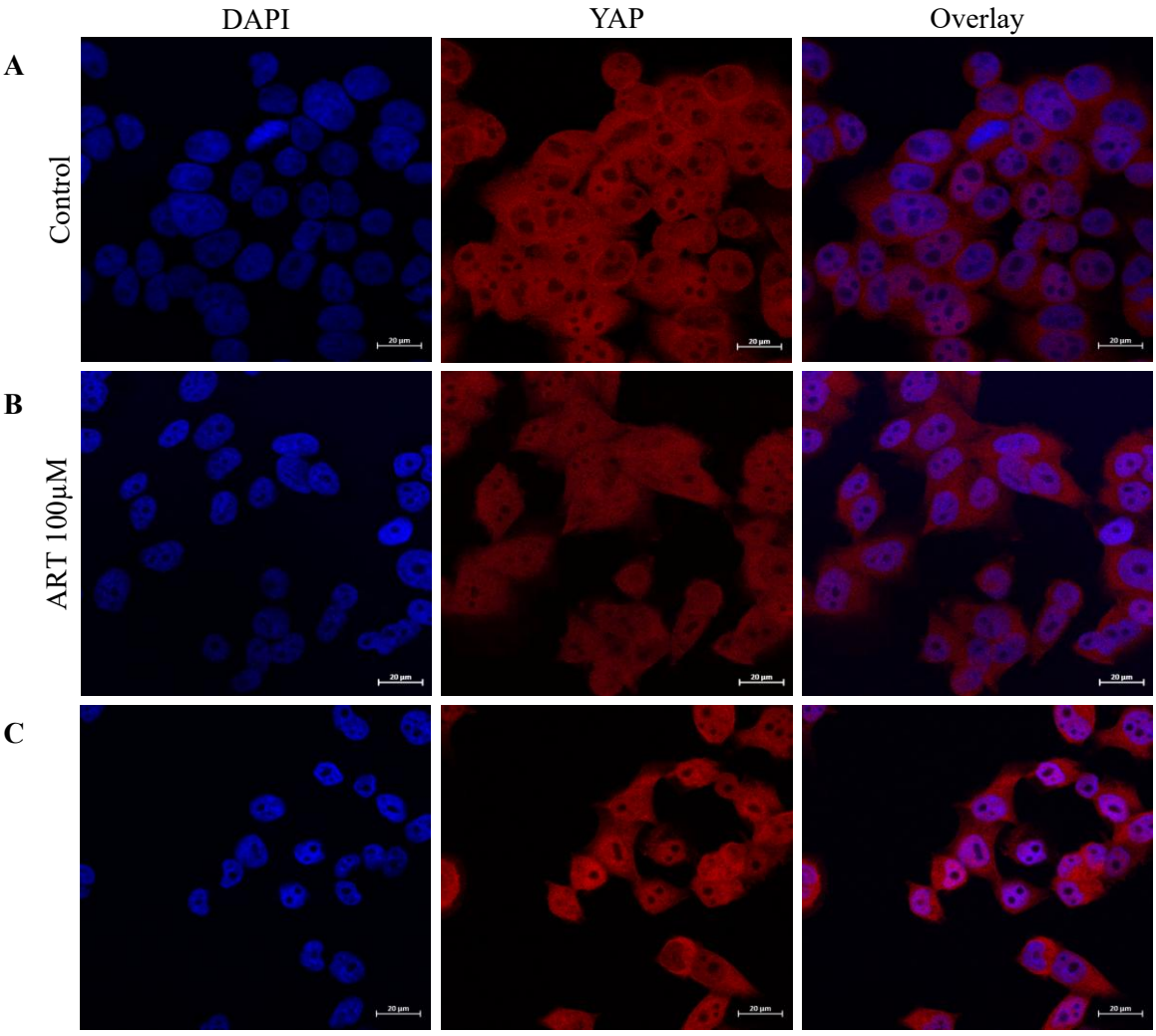

Figure 4.4: The nuclear localisation of YAP upon treatment with ART determined by immunofluorescence staining in HeLa cells.

(A) Images represent control treated with 0.1% DMSO stained with DAPI (nuclear staining), and CY3 (staining for YAP) (B) Images represent mid confluent HeLa cells treated with 100µM ART stained with DAPI and CY3 (C) Images represent sparse HeLa cells treated with 100µM ART stained with DAPI and CY3. Images were taken using a Zeiss Laser Scanning Microscope. Illustrative images show N=3 experiments.

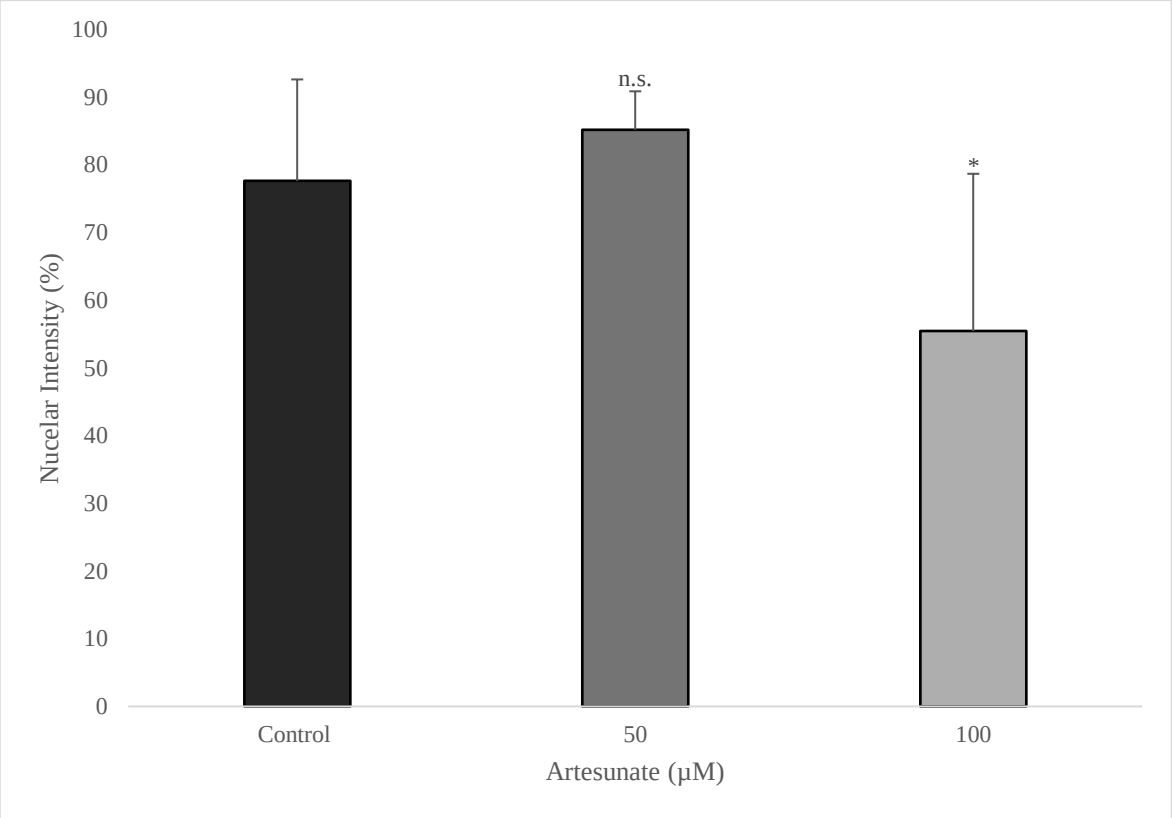

Figure 4.5: Graph representing the mean fluorescent intensity in HeLa cells with 50µm and 100µm of ART.

Quantitative graph showing the nuclear intensity of HeLa cells treated with 50µM and 100µM ART compared to control treated with 0.1% DMSO.
*Graph was compiled using data generated from 3 independent experiments. Data is displayed as the ± standard deviation with N=3. The statistical significance between the control (treated with 0.1% DMSO) and ART concentrations was evaluated using a two-sample equal variance T-TEST with significance levels *p≤0.05, ** p≤0.01 and ***p≤0.0001. No significance is represented as n.s.*

Figure 4.3 displays HeLa cells treated with 50µM of ART at mid (Figure 4.3B) and sparse (Figure 4.3C) confluency, while Figure 4.4 shows HeLa cells treated with 100µM of ART at mid (Figure 4.4B) and sparse (Figure 4.4C) confluency. The quantification of nuclear intensity from these treatments is represented in the graph in Figure 4.5, where it is evident that cells treated with 50µM ART had no statistical significance. In contrast, cells treated with 100µM ART show lower nuclear intensity, which is statistically significant.

4.1.3 Effect of CIS on YAP Translocation in HeLa cells

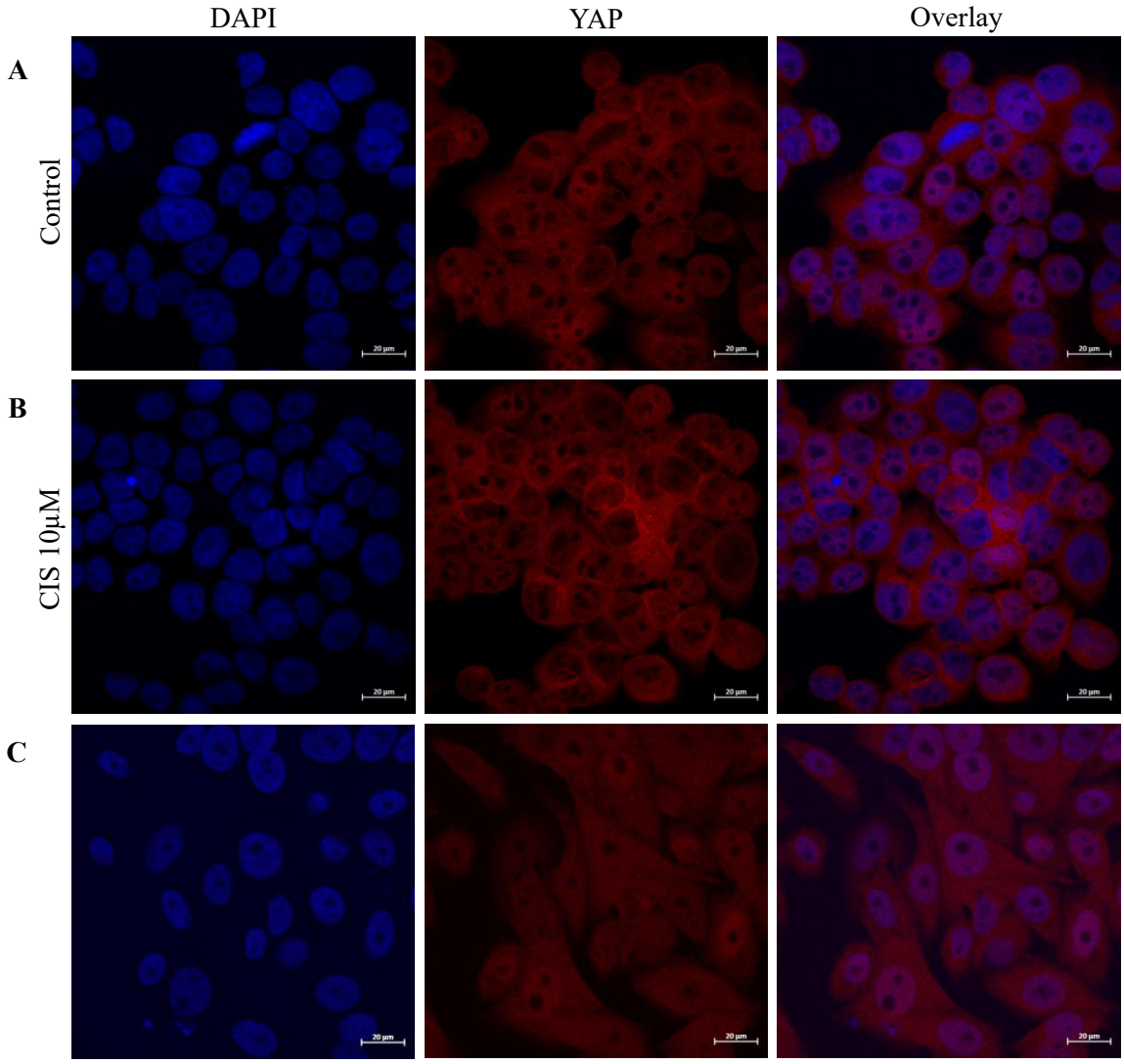

Figure 4.6: The nuclear localisation of YAP upon treatment with CIS determined by immunofluorescence staining in HeLa cells.

(A) Images represent control treated with 0.1% DMSO stained with DAPI (nuclear staining) and CY3 (staining for YAP) (B) Images represent mid confluent HeLa cells treated with 10μM CIS stained with DAPI and CY3 (C) Images represent sparse HeLa cells treated with 10μM CIS stained with DAPI and CY3. Images were taken using a Zeiss Laser Scanning Microscope. Illustrative images show N=3 experiments.

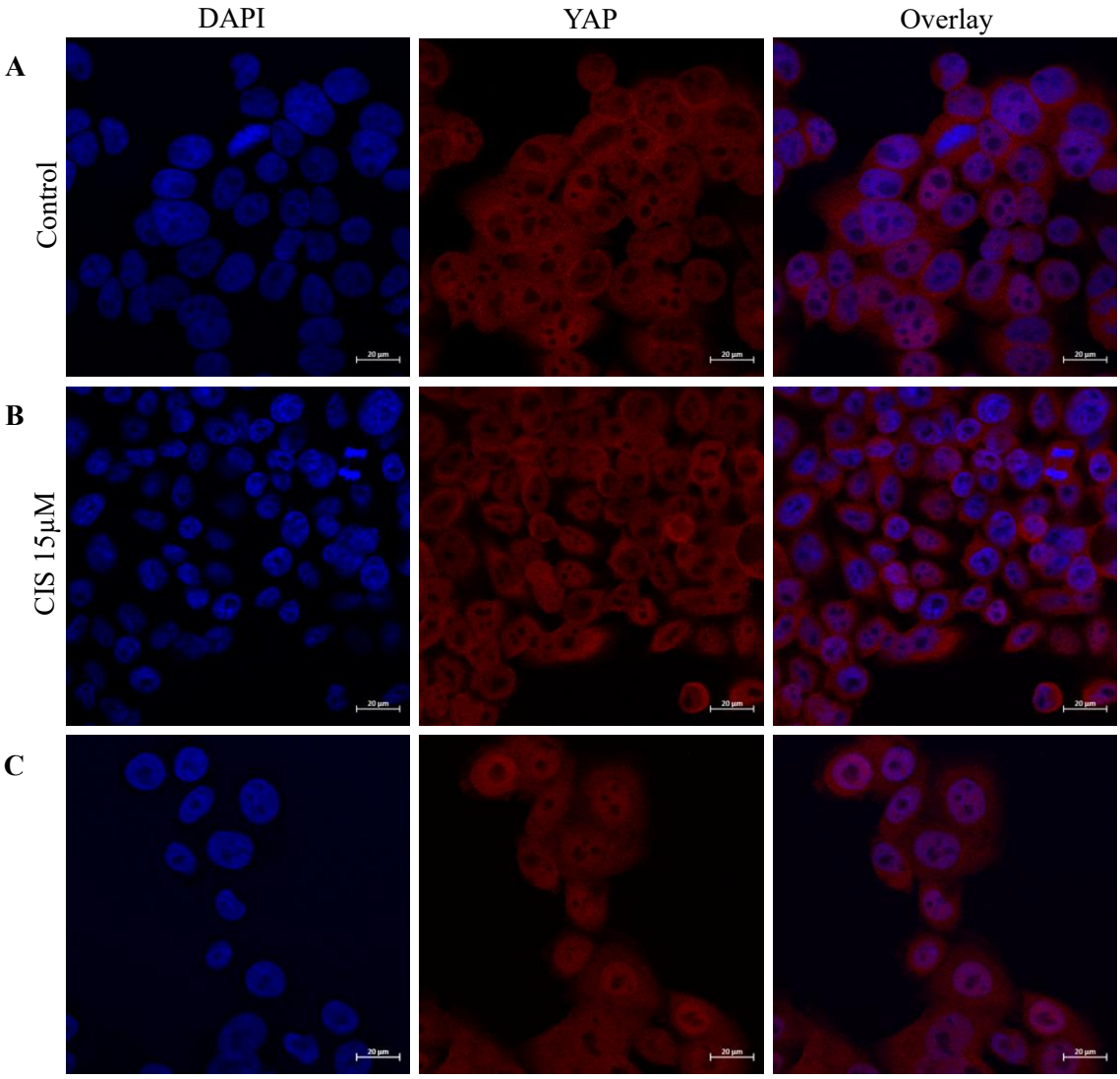

Figure 4.7: The nuclear localisation of YAP upon treatment with CIS determined by immunofluorescence staining in HeLa cells.

(A) Images represent control treated with 0.1% DMSO stained with DAPI (nuclear staining) and CY3 (staining for YAP) (B) Images represent mid confluent HeLa cells treated with 15µM CIS stained with DAPI and CY3 (C) Images represent sparse HeLa cells treated with 15µM CIS stained with DAPI and CY3. Images were taken using a Zeiss Laser Scanning Microscope. Illustrative images show N=3 experiments.14

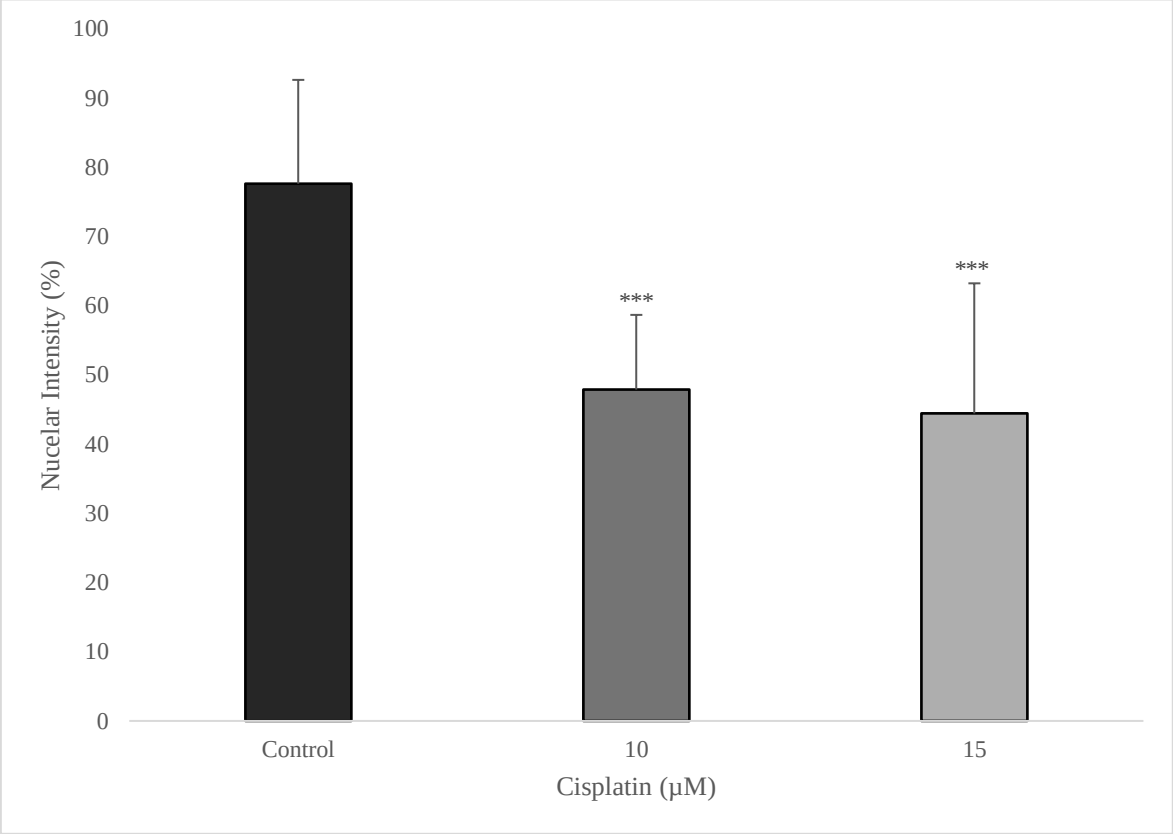

Figure 4.8: Graph representing the mean fluorescent intensity in HeLa Cells with 10µm and 15µm of CIS.

Quantitative graph showing the nuclear intensity of HeLa cells treated with 10µM and 15µM CIS compared to control treated with 0.1% DMSO.
*Graph was compiled using data generated from 3 independent experiments. Data is displayed as the ±standard deviation with N=3. The statistical significance between the control (treated with 0.1% DMSO) and CIS concentrations was evaluated using a two-sample equal variance T-TEST with significance levels *p≤0.05, ** p≤0.01 and ***p≤0.0001. No significance is represented as n.s.*

HeLa cells were treated with 10µM and 15µM of CIS to assess YAP localisation, as depicted in Figure 4.6and Figure *4.7* for both mid-confluent and sparse cells. The quantified data from the staining is shown in the graph in Figure 4.8, which indicates that both concentrations of CIS resulted in lower nuclear intensity compared to the control, with both being statistically significant. Interestingly, as expected, the lower concentration of 10µM exhibited slightly higher nuclear intensity than 15µM, though still lower than the control.

4.2 Effect of ARTM, ART and CIS Treatment on YAP Phosphorylation in HeLa Cells.

Following the IF staining that looked at nuclear intensity to check for nuclear YAP, the same concentrations were subjected to western blot analysis to check for YAP phosphorylation levels at serine 127 as this site is a key regulatory point for YAP's activity in the HSP. When YAP is phosphorylated at S127 by the Hippo kinases, it is sequestered in the cytoplasm by binding to 14-3-3 proteins, preventing its nuclear translocation. While YAP can be phosphorylated at to other sites, S127 binding site directly controls YAP localisation, therefore, its transcriptional activity (Zhao *et al.,* 2007).

4.2.1 Effect of ARTM on YAP Phosphorylation in HeLa Cells

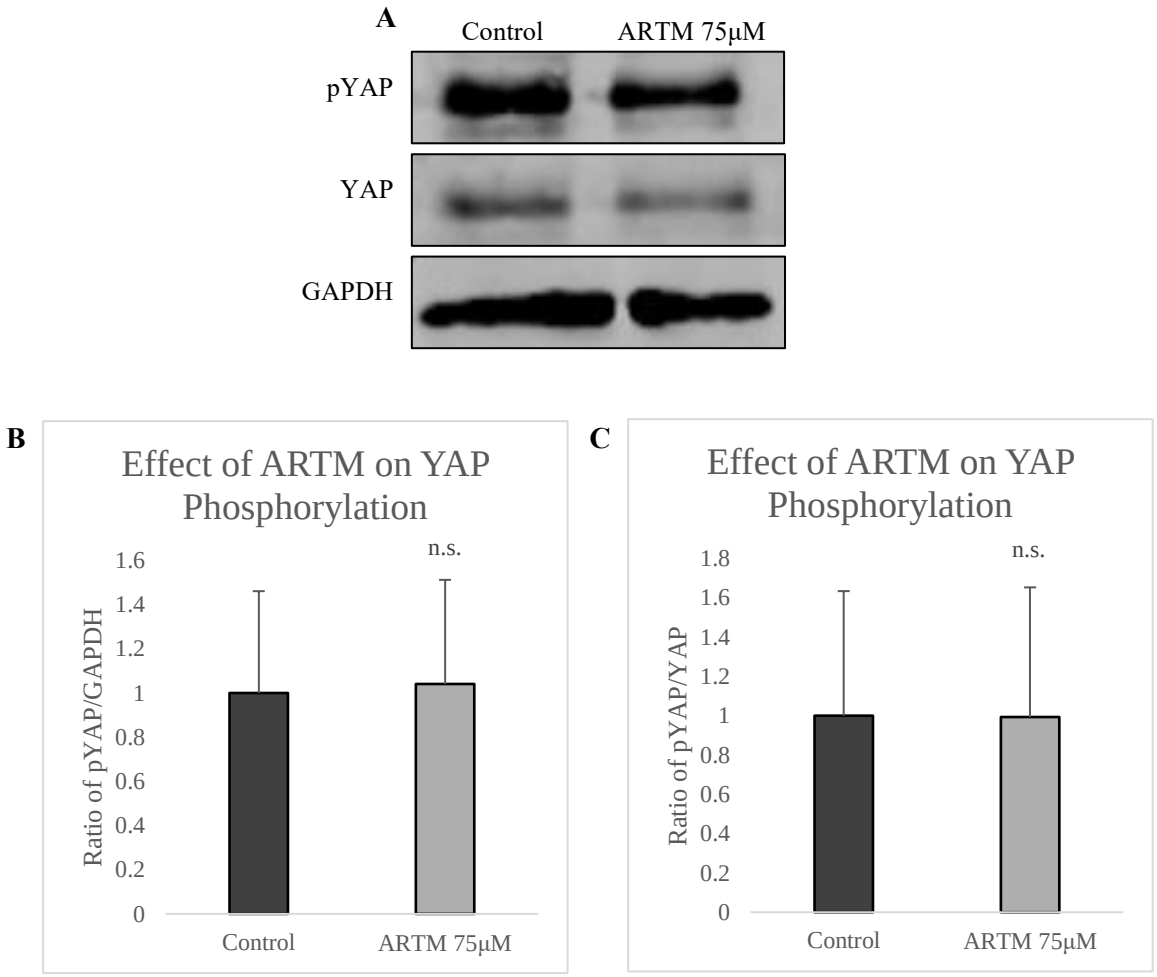

Figure 4.9: The phosphorylation levels of YAP upon treatment with ARTM determined by western blot analysis in HeLa cells.

*(A) Images represent representative western blots treated with pYAP, YAP and GAPDH for ARTM 75µM (B) Graph represents the ratio of total YAP and GAPDH in treated compared to control (C) Graph represents the ratio of total YAP and phophoYAP in treated compared to control. Blots were visualised using a LI-COR Odyssey CLx. Representative blots show results two repeats from 3 individual experiments. Data is displayed as the ± standard deviation with statistical significance between the control (treated with 0.1% DMSO) and ARTM concentration evaluated using a two-sample equal variance T-TEST with significance levels *p≤0.05, ** p≤0.01 and ***p≤0.0001. No significance is represented as n.s.*

Analysis of ARTM 75µM treatment using Western blotting revealed no significant difference in YAP phosphorylation levels compared to the control, with no statistical significance observed. This contrasts with the lower nuclear intensity of YAP detected through IF staining. These findings are illustrated in the graph in Figure 4.9C, showing that, despite reduced nuclear YAP levels, phosphorylation levels remain unchanged.

4.2.2 Effect of ART on YAP Phosphorylation in HeLa Cells

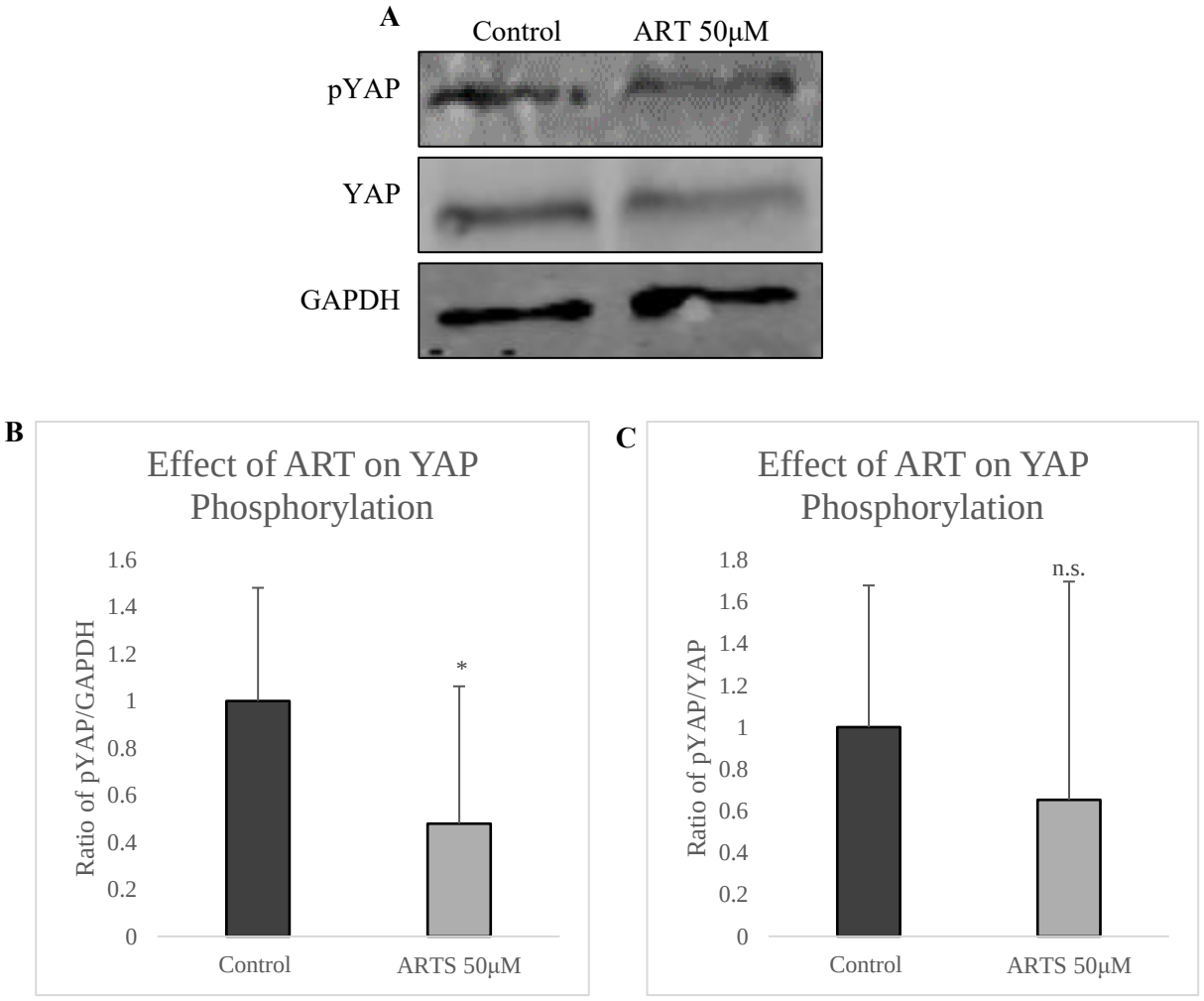

Figure 4.10: The phosphorylation levels of YAP upon treatment with ART determined by western blot analysis in HeLa cells.

*(A) Images represent representative western blots treated with pYAP, YAP and GAPDH for ART 50µM (B) Graph represents the ratio of total YAP and GAPDH in treated compared to control (C) Graph represents the ratio of total YAP and phophoYAP in treated compared to control. Blots were visualised using a LI-COR Odyssey CLx. Representative blots show results two repeats from 3 individual experiments. Data is displayed as the ± standard deviation with statistical significance between the control (treated with 0.1% DMSO) and ART concentration evaluated using a two-sample equal variance T-TEST with significance levels *p≤0.05, ** p≤0.01 and ***p≤0.0001. No significance is represented as n.s.*

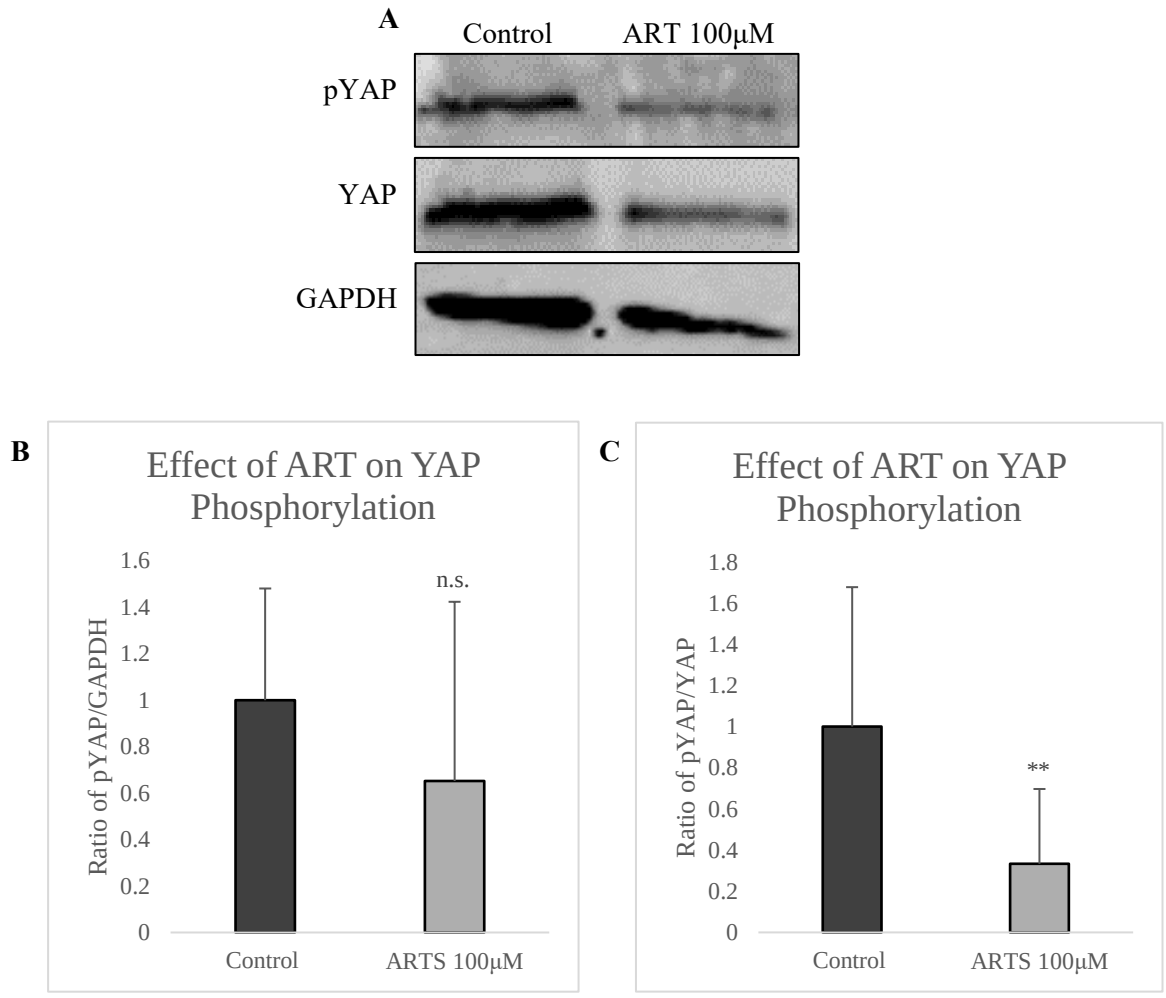

Figure 4.11: The phosphorylation levels of YAP upon treatment with ART determined by western blot analysis in HeLa cells.

*(A) Images represent representative western blots treated with pYAP, YAP and GAPDH for ART 100µM (B) Graph represents the ratio of total YAP and GAPDH in treated compared to control (C) Graph represents the ratio of total YAP and phophoYAP in treated compared to control. Blots were visualised using a LI-COR Odyssey CLx. Representative blots show results two repeats from 3 individual experiments. Data is displayed as the ± standard deviation with statistical significance between the control (treated with 0.1% DMSO) and ART concentration evaluated using a two-sample equal variance T-TEST with significance levels *p≤0.05, ** p≤0.01 and ***p≤0.0001. No significant is represented as n.s.*

The optimum concentration of ART was determined to be 100µM; however, Western blot analysis revealed increased cell death at this concentration, as evidenced by the faint protein bands in Figure 4.11A compared to the control. Despite this, Figure 4.11C shows a statistically significant decrease in YAP phosphorylation in HeLa cells treated with 100µM ART. For comparison, a lower concentration of ART (50µM) was also analysed using Western blot, as shown in Figure 4.9.

Figure 4.10A displays the blot for cells treated with 50µM ART and the corresponding graph in Figure 4.10C indicates YAP phosphorylation levels. The results suggest while the

50μM concentration caused less cell death, it did not significantly affect YAP phosphorylation.

4.2.3 Effect of CIS on YAP Phosphorylation in HeLa Cells

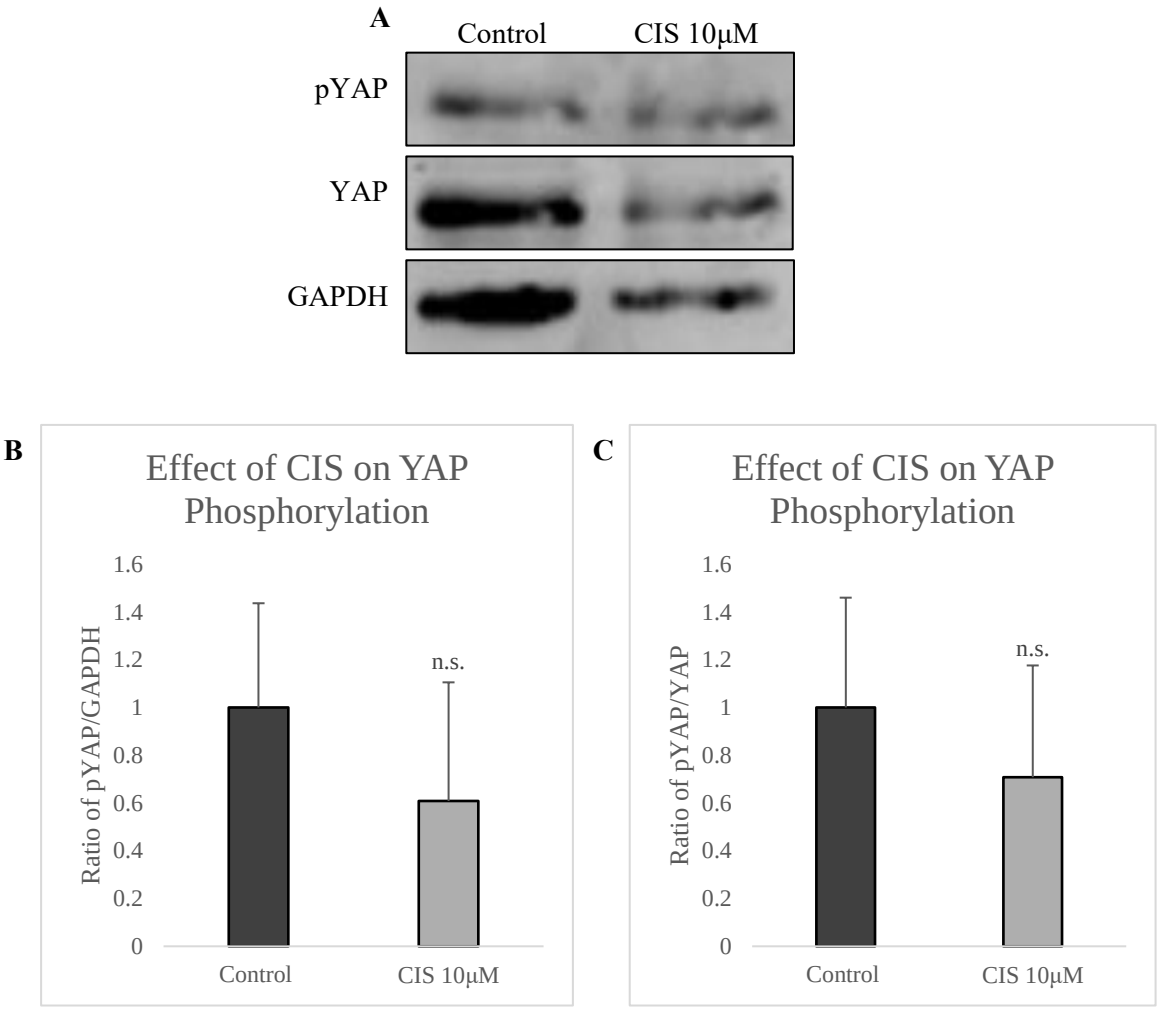

Figure 4.12: The phosphorylation levels of YAP upon treatment with CIS determined by western blot analysis in HeLa cells.

*(A) Images represent representative western blots treated with pYAP, YAP and GAPDH for CIS 10μM (B) Graph represents the ratio of total YAP and GAPDH in treated compared to control (C) Graph represents the ratio of total YAP and phophoYAP in treated compared to control. Blots were visualised using a LI-COR Odyssey CLx. Representative blots show results two repeats from 3 individual experiments. Data is displayed as the ± standard deviation with statistical significance between the control (treated with 0.1% DMSO) and CIS concentration evaluated using a two-sample equal variance T-TEST with significance levels *p≤0.05, ** p≤0.01 and ***p≤0.0001. No significance is represented as n.s.*

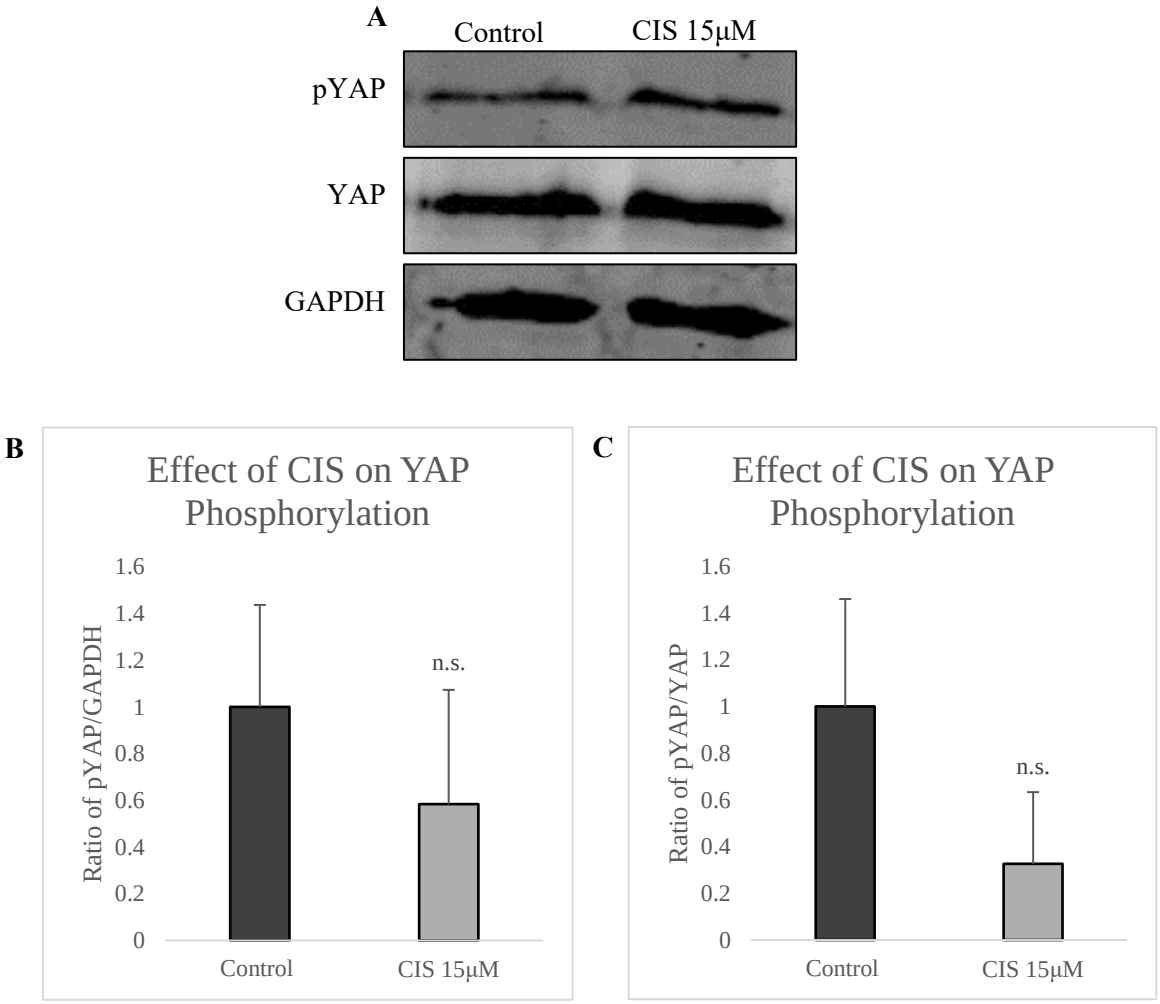

Figure 4.13: The phosphorylation levels of YAP upon treatment with ART determined by western blot analysis in HeLa cells.

*(A) Images represent representative western blots treated with pYAP, YAP and GAPDH for CIS 15µM (B) Graph represents the ratio of total YAP and GAPDH in treated compared to control (C) Graph represents the ratio of total YAP and phophoYAP in treated compared to control. Blots were visualised using a LI-COR Odyssey CLx. Representative blots show results two repeats from 3 individual experiments. Data is displayed as the ± standard deviation with statistical significance between the control (treated with 0.1% DMSO) and CIS concentration evaluated using a two-sample equal variance T-TEST with significance levels *p≤0.05, ** p≤0.01 and ***p≤0.0001. No significance is represented as n.s.*

CIS at concentrations of 10µM and 15µM was also subjected to Western blot analysis following IF staining. Although both concentrations had a significant effect on YAP translocation to the nucleus through IF analysis, Western blot analysis revealed no significant impact on YAP phosphorylation at either concentration, as shown in the graphs in Figure 4.12C and Figure ***4.13***C. This suggests that while CIS affects YAP localisation, it does not significantly alter levels of YAP phosphorylation.

4.3 Effect of ARTM and ART on Gene Expression Levels of CTGF, CYR61 and c-Myc

CFTG, CYR61 and c-Myc are frequently regulated by signalling pathways, particularly the HSP. These genes play roles in various cellular processes. CTGF functions as a growth factor, involved in cell proliferation and tissue remodelling. CYR61 serves as a matricellular protein with angiogenic properties, contributing to processes like cell adhesion and vascular development. c-Myc, an oncogene, is a transcription factor that drives cell cycle progression and is often implicated in cancer due to its role in promoting uncontrolled cell growth and proliferation.

Therefore, the effect of ARTM and ART on the expression levels of CTGF, CYR61 and c-Myc was analysed in HeLa cells using qRT-PCR. This assay was performed to assess how treatment with these drugs influences the expression of these key genes involved in growth factor signalling, angiogenesis and oncogenesis.

4.3.1 Effect of ARTM on CTGF, CYR61 and c-Myc Expression Levels in HeLa Cells

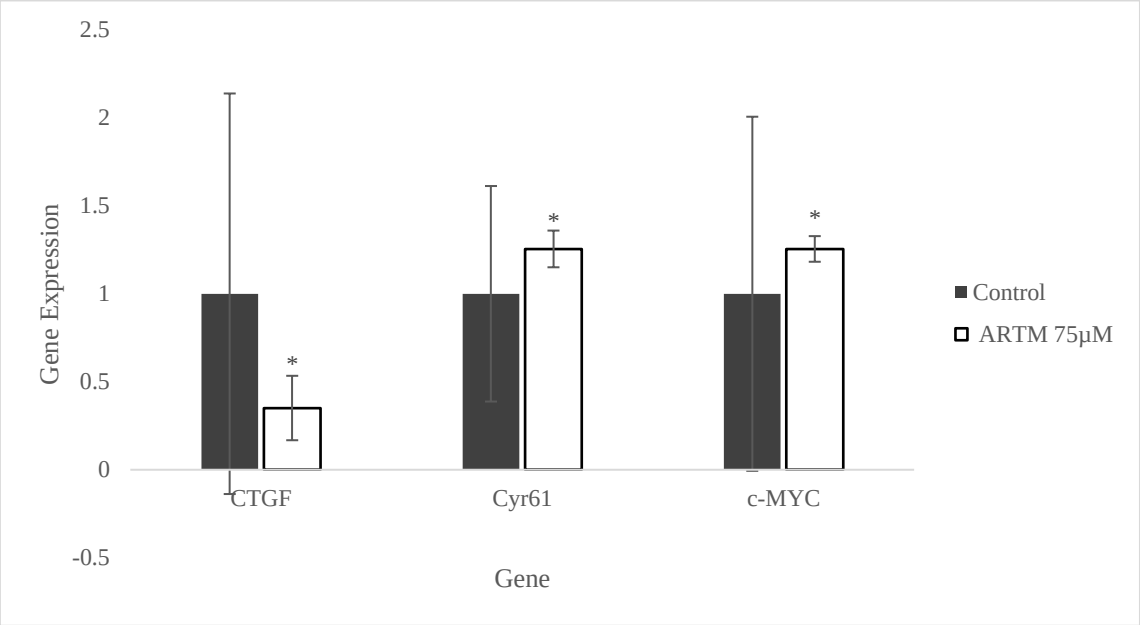

Figure 4.14: The gene expression levels of CTGF, CYR61 and c-Myc upon treatment with ARTM determined by qRT-PCR analysis in HeLa cells.

*The graph illustrates the gene expression levels of CTGF, CYR61 and c-Myc in HeLa cells treated with 75µM ARTM, compared to untreated control cells. The expression levels were normalised using GAPDH as the housekeeping gene to ensure accurate quantification. Data is displayed as the ± standard deviation with statistical significance between the control (treated with 0.1% DMSO) and CIS concentration evaluated using a two-sample equal variance T-TEST with significance levels *$p \leq 0.05$, ** $p \leq 0.01$ and ***$p \leq 0.0001$. No significance is represented as n.s.*

Following Western blot analysis, ARTM 75µM was subjected to qRT-PCR to assess the expression levels of key genes associated with the HSP. Quantification of the data revealed that ARTM treatment at 75µM resulted in a substantial decrease in CTGF gene expression, with levels reduced by more than half compared to the control as seen in Figure 4.14. However, Cyr61, and c-Myc expression were significantly upregulated.

Although all results are statistically significant, the upregulation of Cyr61 and c-Myc contrasted with the desired downregulation observed in CTGF.

4.3.2 Effect of ART on CTGF, CYR61 and c-Myc Expression Levels in HeLa Cells

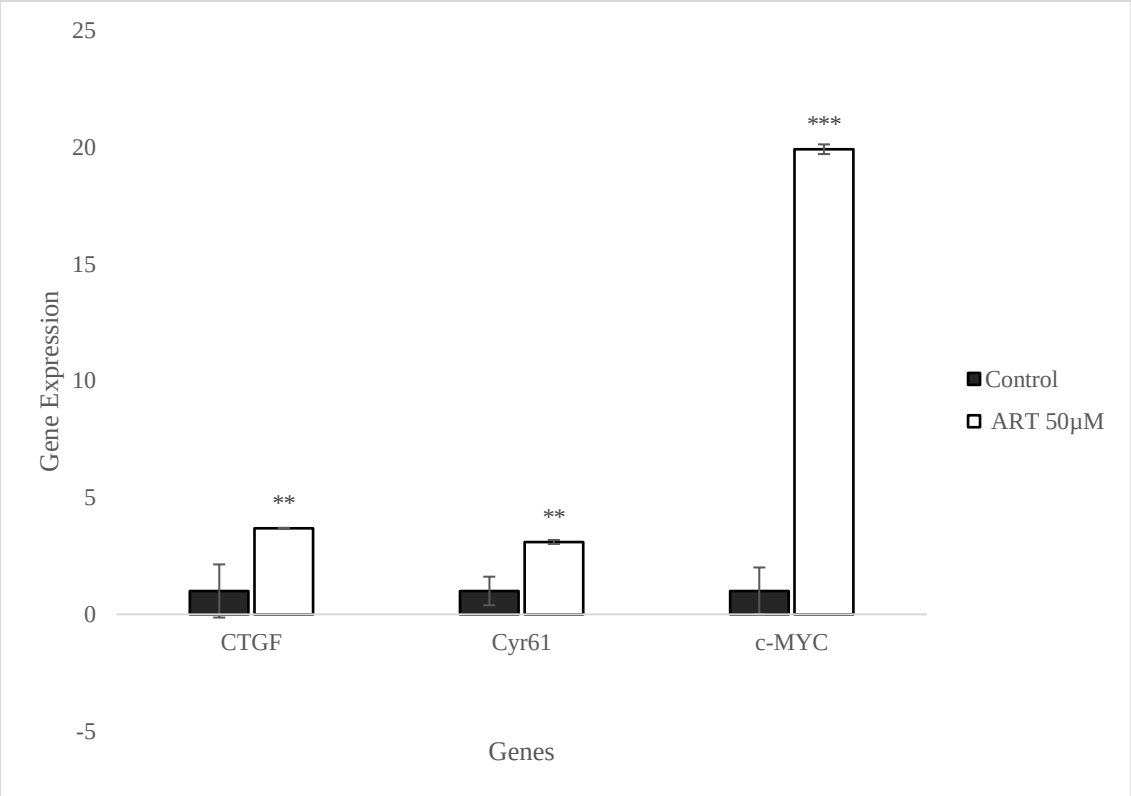

Figure 4.15: The gene expression levels of CTGF, CYR61 and c-Myc upon treatment with ART determined by qRT-PCR analysis in HeLa cells.

*The graph illustrates the gene expression levels of CTGF, CYR61 and c-Myc in HeLa cells treated with 50µM ART, compared to untreated control cells. The expression levels were normalised using GAPDH as the housekeeping gene to ensure accurate quantification. Data is displayed as the ± standard deviation with statistical significance between the control (treated with 0.1% DMSO) and CIS concentration evaluated using a two-sample equal variance T-TEST with significance levels *p≤0.05, ** p≤0.01 and ***p≤0.0001. No significance is represented as n.s.*

Despite the lack of significant effect of ART 50µM in the Western blot analysis for YAP phosphorylation, both ARTµM and 100µM were further tested via qRT-PCR to evaluate their impact on the expression levels of the same genes analysed with ARTM 75µM. The data quantification revealed that neither concentration led to the downregulation of CTGF, Cyr61 or c-Myc. Instead, both 50µM and 100µM ART treatments resulted in a significant upregulation of all these genes. Although the results are statistically significant, this outcome was contrary to the desired downregulation of gene expression. These findings are depicted in Figure 4.15 (50µM) and Figure 4.16 (100µM). With the weal effect on downstream genes of the HSP, it was important to assess further signalling pathways to see if the drugs had an effect on such pathways as well.

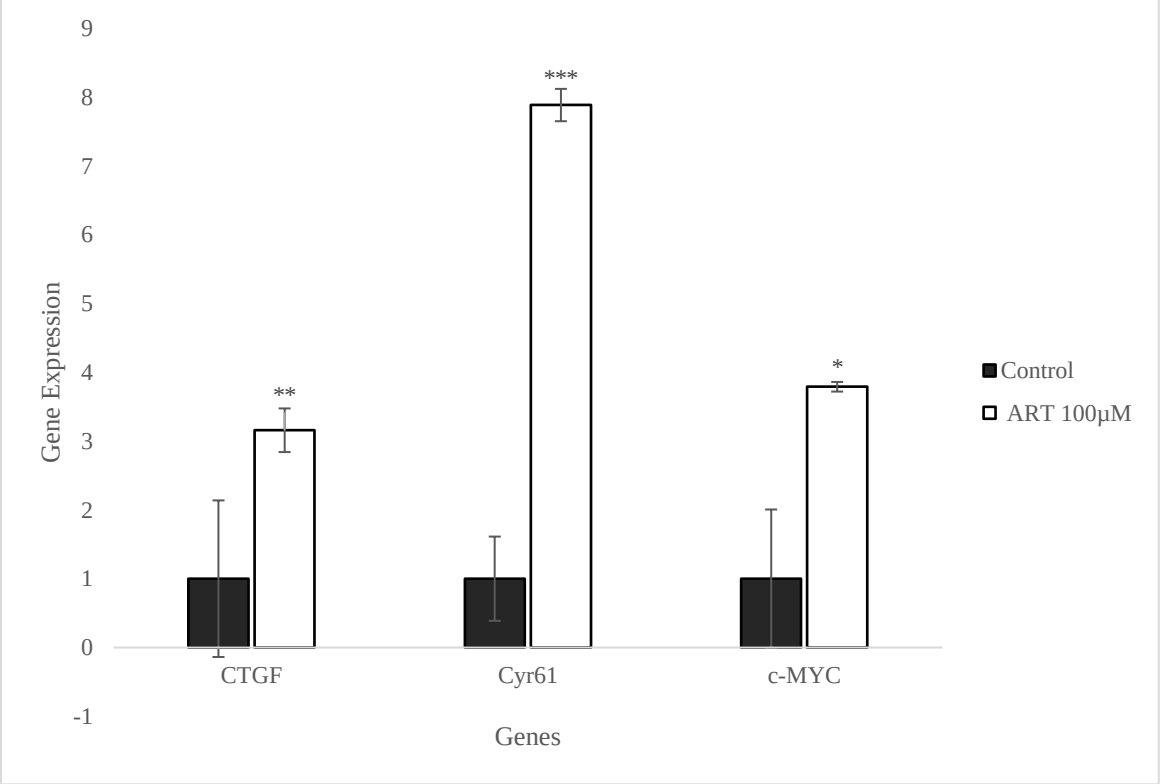

Figure 4.16: The gene expression levels of CTGF, CYR61 and c-Myc upon treatment with ART determined by qRT-PCR analysis in HeLa cells.

*The graph illustrates the gene expression levels of CTGF, CYR61 and c-Myc in HeLa cells treated with 100µM ART, compared to untreated control cells. The expression levels were normalised using GAPDH as the housekeeping gene to ensure accurate quantification. Data is displayed as the ± standard deviation with statistical significance between the control (treated with 0.1% DMSO) and CIS concentration evaluated using a two-sample equal variance T-TEST with significance levels *p≤0.05, ** p≤0.01 and ***p≤0.0001. No significance is represented as n.s.*

4.4 Effect of ARTM and ART on B-cat, p53, mTOR and Wnt-1 Expression Levels in HeLa Cells

qRT-PCR analysis revealed that ARTM and ART treatment did not significantly affect the expression of CTGF, CYR61 and c-Myc, as most gene expression levels were upregulated. As mentioned, on 75µM ARTM- treated cells exhibited downregulation of CTGF. As a result, we further investigated the same concentrations (75µM ARTM, 50µM ART and 100µM ART) by assessing gene expression levels related to the Wnt/β-catenin pathway, including β-catenin, p53, mTOR and Wnt-1, to explore potential effects on this signalling pathway.

4.4.1 Effect of ARTM on B-cat, p53, mTOR and Wnt-1 Expression Levels in HeLa Cells

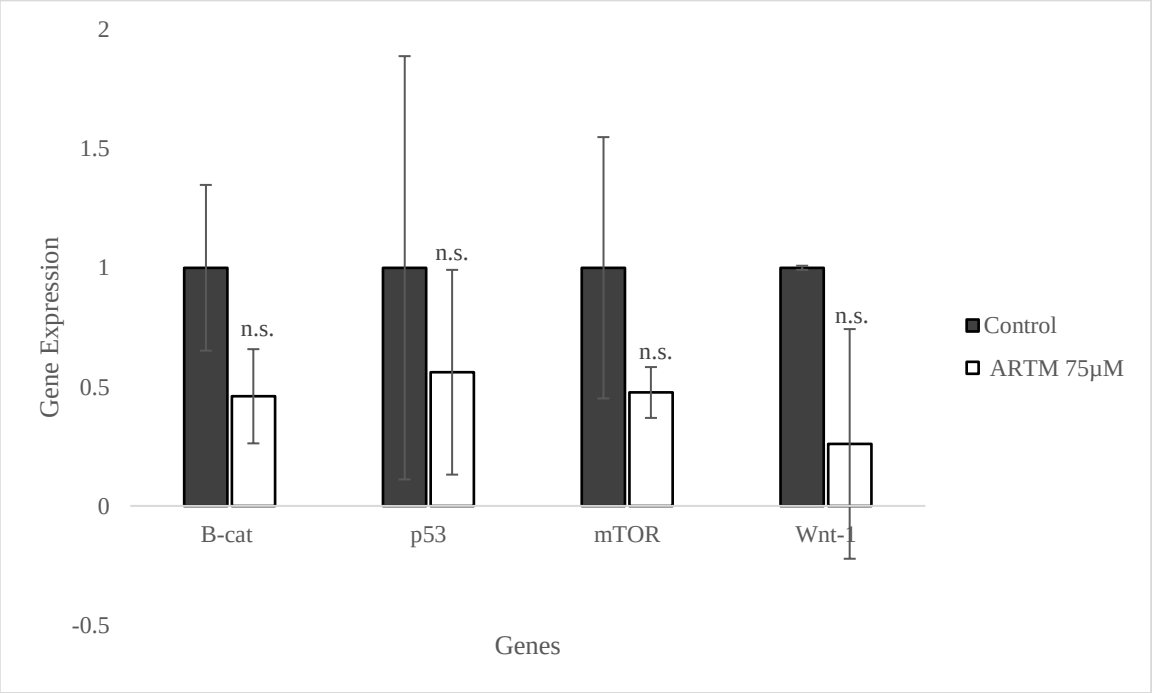

Figure 4.17: The gene expression levels of B-cat, p53, mTOR and Wnt-1 upon treatment with ARTM determined by qRT-PCR analysis in HeLa cells.

*The graph illustrates the gene expression levels of B-cat, p53, mTOR and Wnt-1 in HeLa cells treated with 75µM ARTM, compared to untreated control cells. The expression levels were normalised using GAPDH as the housekeeping gene to ensure accurate quantification. Data is displayed as the ± standard deviation with statistical significance between the control (treated with 0.1% DMSO) and CIS concentration evaluated using a two-sample equal variance T-TEST with significance levels *p≤0.05, ** p≤0.01 and ***p≤0.0001. No significance is represented as n.s.*

The lack of significant effects on gene expression levels of HSP related genes prompted a brief investigation into the potential influence of ARTM on genes associated with the Wnt/β-catenin pathway.

Although the results did not reach statistical significance, as all values were lower than the control, ARTM 75µM did lead to the downregulation of all genes tested within the Wnt/β-catenin pathway, as shown in Figure 4.17. Notably, there was a significant downregulation in the expression levels of Wnt-1. Similarly, though not as pronounced, ARTM 75µM also resulted in the downregulation of β-catenin, mTOR and p53, further supporting the potential impact of this drug on Wnt/β-catenin, as represented in Figure 4.17.

4.4.2 Effect of ART on B-cat, p53, mTOR and Wnt-1 Expression Levels in HeLa Cells

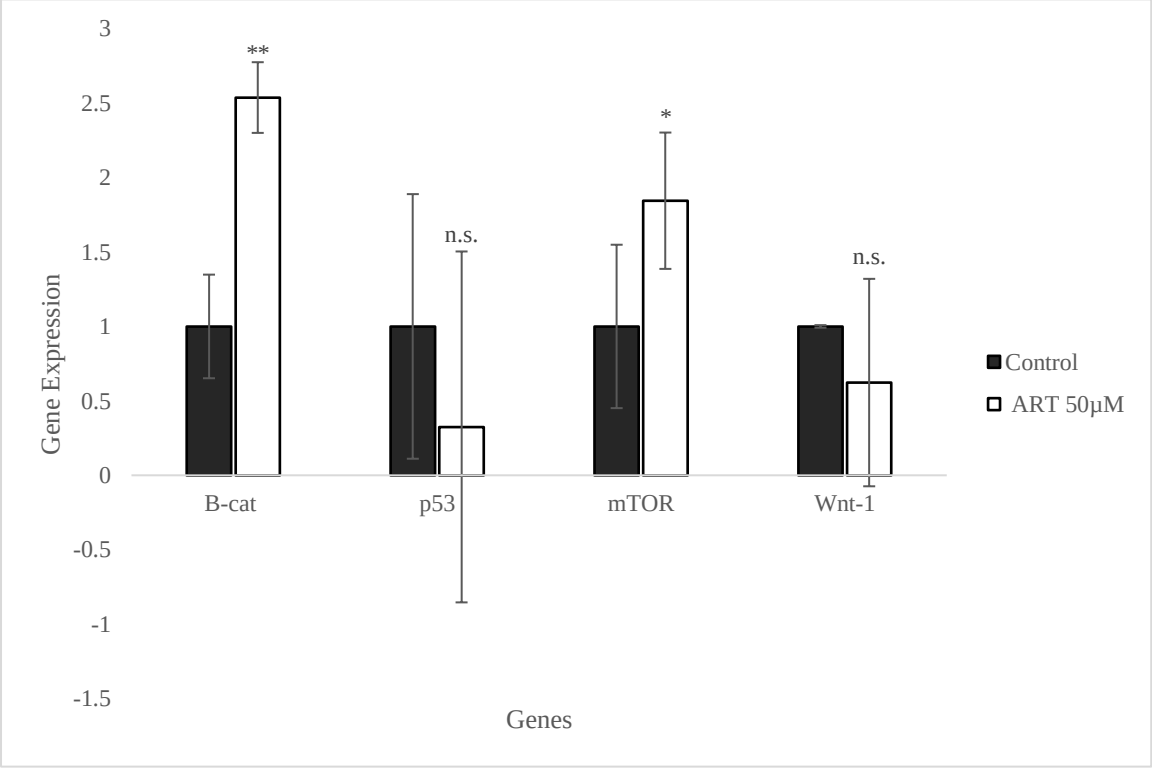

Figure 4.18: The gene expression levels of B-cat, p53, mTOR and Wnt-1 upon treatment with ART determined by qRT-PCR analysis in HeLa cells.

*The graph illustrates the gene expression levels of B-cat, p53, mTOR and Wnt-1 in HeLa cells treated with 50µM ART, compared to untreated control cells. The expression levels were normalised using GAPDH as the housekeeping gene to ensure accurate quantification. Data is displayed as the ± standard deviation with statistical significance between the control (treated with 0.1% DMSO) and CIS concentration evaluated using a two-sample equal variance T-TEST with significance levels *p≤0.05, ** p≤0.01 and ***p≤0.0001. No significance is represented as n.s.*

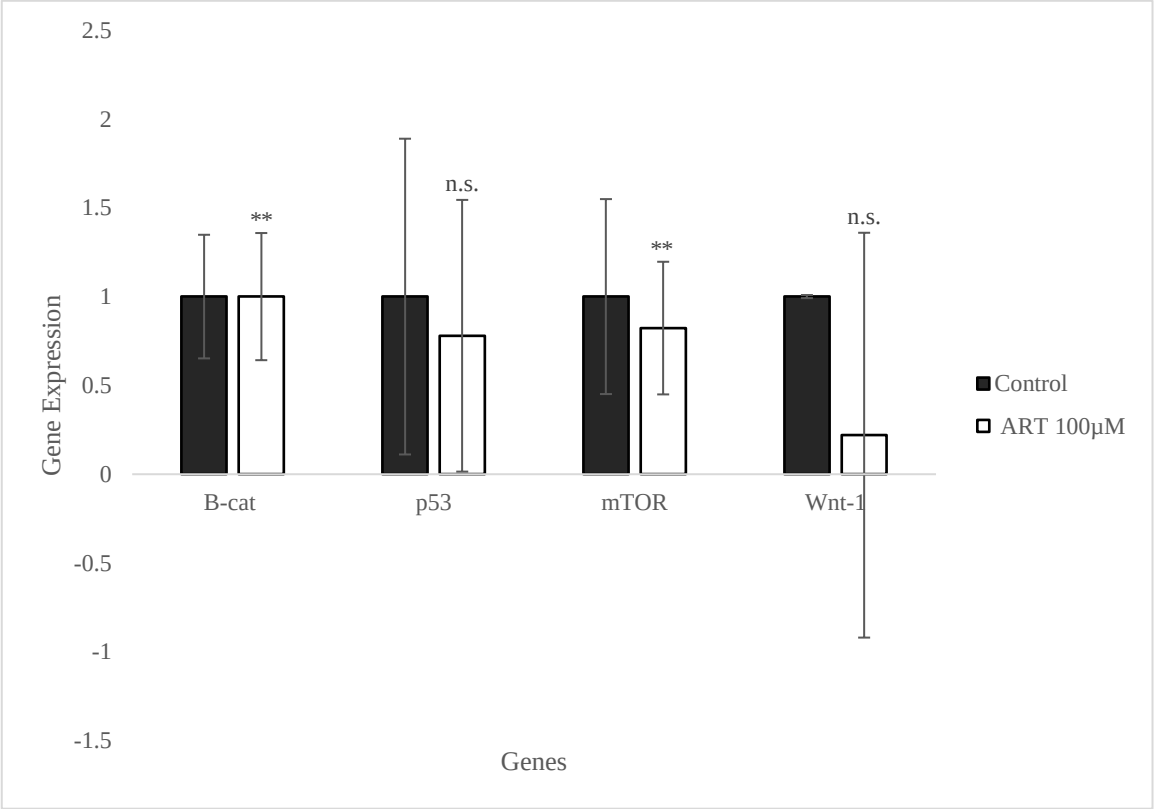

Figure 4.19: ***The gene expression levels of B-cat, p53, mTOR and Wnt-1 upon treatment with ART determined by qRT-PCR analysis in HeLa cells.***

*The graph illustrates the gene expression levels of B-cat, p53, mTOR and Wnt-1 in HeLa cells treated with 100µM ART, compared to untreated control cells. The expression levels were normalised using GAPDH as the housekeeping gene to ensure accurate quantification. Data is displayed as the ± standard deviation with statistical significance between the control (treated with 0.1% DMSO) and CIS concentration evaluated using a two-sample equal variance T-TEST with significance levels *p≤0.05, ** p≤0.01 and ***p≤0.0001. No significance is represented as n.s.*

Similar, to the findings with CTGF, Cyr61 and c-Myc, both concentrations of ART (50µM and 100µM) did not show a significant effect on Wnt-associated genes when compared to ARTM. However, there were notable differences between the two concentrations of ART when the results were quantified (Figure 4.18 and Figure 4.19).

At 50µM, ART led to a significant upregulation of β-catenin and mTOR whereas p53 and Wnt-1 were downregulated, although not statistically significant. In contrast, 100µM ART did not result in any upregulation but showed downregulation in p53, mTOR and Wnt-1, with a significant decrease in Wnt-1 gene expression levels. However, β-catenin expression remained similar to that of the untreated control.

4.5 Effect of Combination Therapy on the Hippo Signalling Pathway

4.5.1 Effect of Combination Therapy with 75µM ARTM and CIS on YAP Translocation in HeLa cells

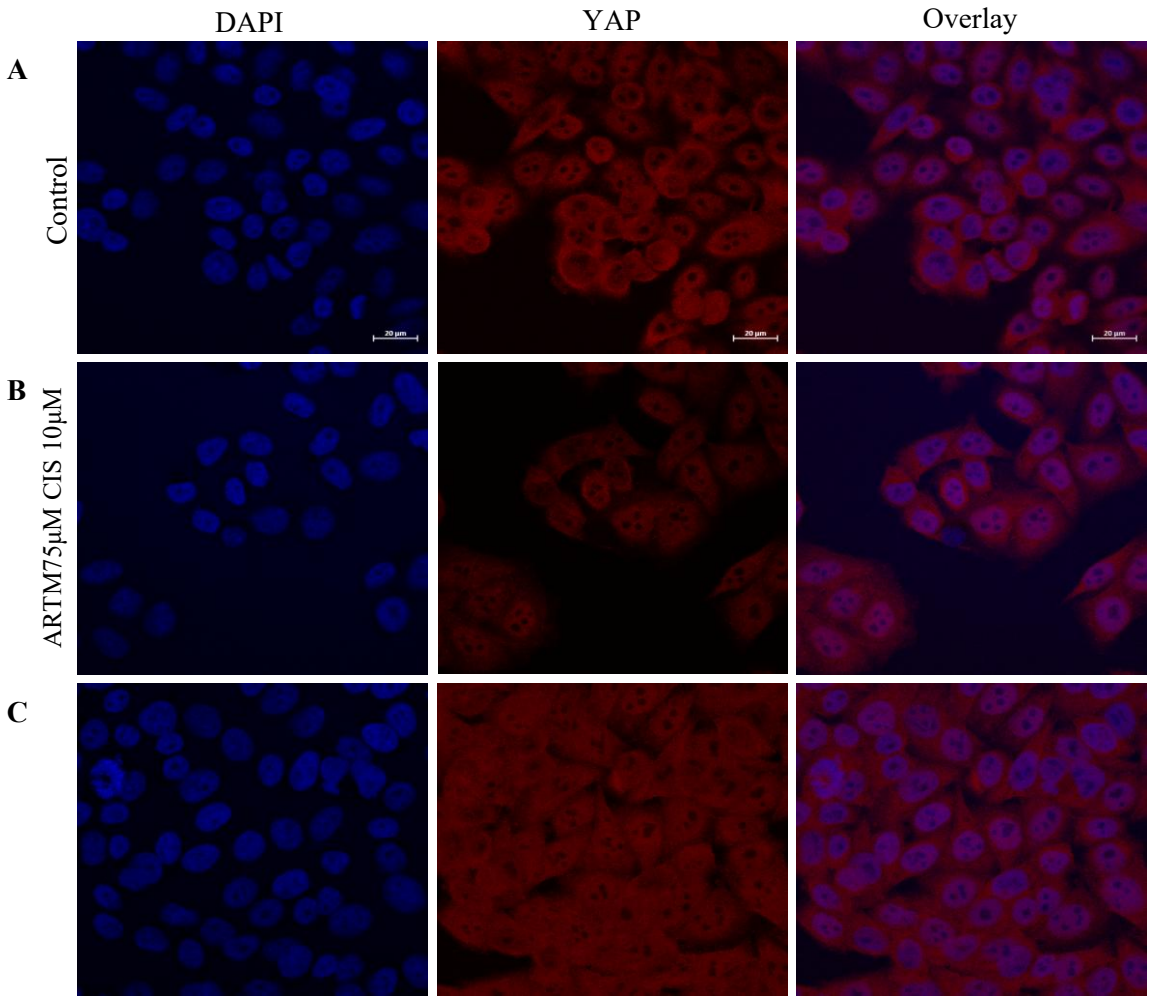

Figure 4.20: The nuclear localisation of YAP upon treatment with ARTM in combination with CIS determined by immunofluorescence staining in HeLa cells.

(A) Images represent control treated with 0.1% DMSO stained with DAPI (nuclear staining) and CY3 (staining for YAP) (B) Images represent mid confluent HeLa cells treated with 75µM ARTM 10µM CIS stained with DAPI and CY3 (C) Images represent sparse HeLa cells treated with 75µM ARTM 10µM CIS stained with DAPI and CY3. Images were taken using a Zeiss Laser Scanning Microscope. Illustrative images show N=3 experiments.

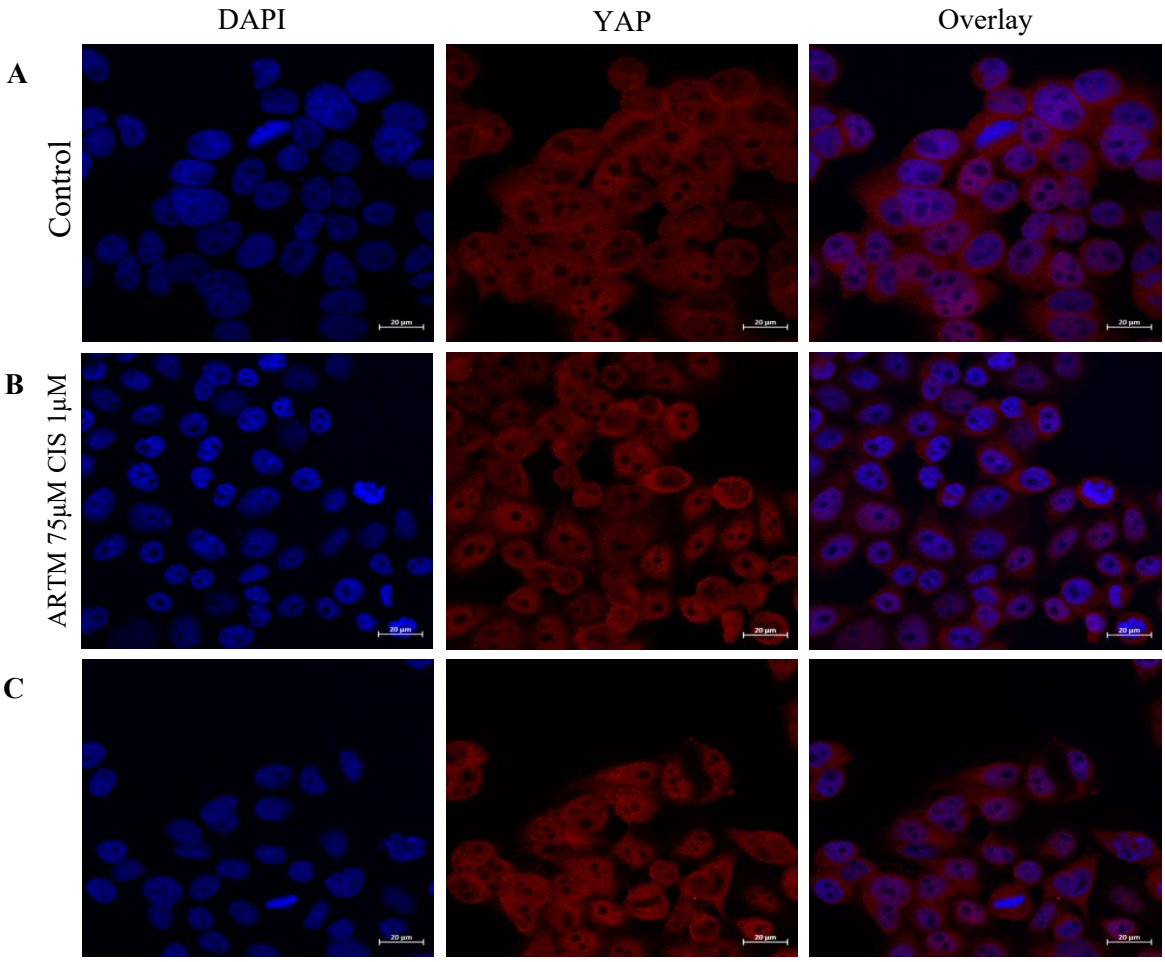

Figure 4.21: The nuclear localisation of YAP upon treatment with ARTM in combination with CIS determined by immunofluorescence staining in HeLa cells.

(A) Images represent control treated with 0.1% DMSO stained with DAPI (nuclear staining) and CY3 (staining for YAP) (B) Images represent mid confluent HeLa cells treated with 75µM ARTM 1µM CIS stained with DAPI and CY3 (C) Images represent sparse HeLa cells treated with 75µM ARTM 1µM CIS stained with DAPI and CY3. Images were taken using a Zeiss Laser Scanning Microscope. Illustrative images show N=3 experiments.

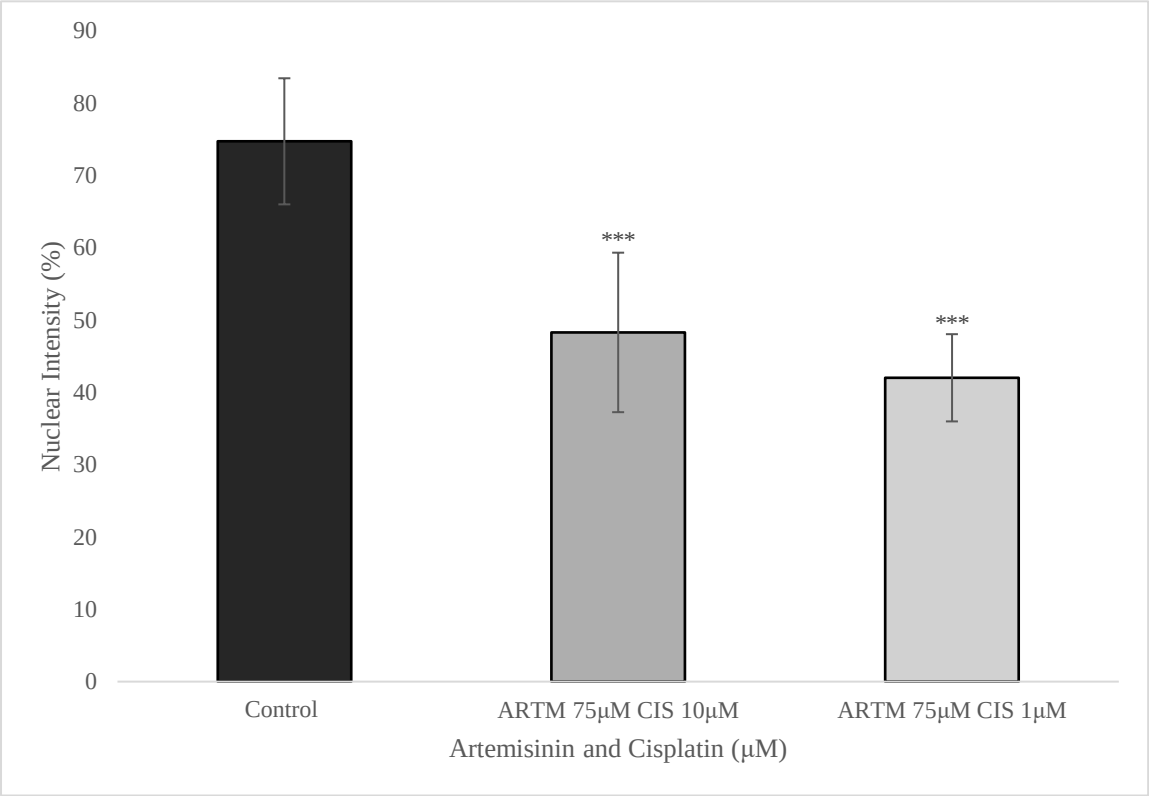

Figure 4.22: Graph representing the mean fluorescent intensity in HeLa Cells with ARTM in combination with CIS

Quantitative graph showing the nuclear intensity of HeLa cells treated with ARTM 75µM in combination with CIS 10µM and CIS 1µM compared to control treated with 0.1% DMSO.
*Graph was compiled using data generated from 3 independent experiments. Data is displayed as the ± standard deviation with N=3. The statistical significance between the control (treated with 0.1% DMSO) and ARTM + CIS concentrations was evaluated using a two-sample equal variance T-TEST with significance levels *p≤0.05, ** p≤0.01 and ***p≤0.0001. Not significant data is represented as n.s.*

ARTM 75µM, combined with both 10µM and 1µM CIS, was further evaluated through immunofluorescence staining to examine YAP localisation, as illustrated in Figure 4.20 and Figure 4.21. The quantification of these results is provided in Figure 4.22. Both treatment combinations resulted in a significant reduction in nuclear YAP intensity compared to the control group. This reduction was statistically significant, with p-values less than 0.0001, indicating a noticeable impact on YAP nuclear localisation.

4.5.2 Effect of Combination Therapy with 50µM, 100µM ART and CIS on YAP Translocation in HeLa cells

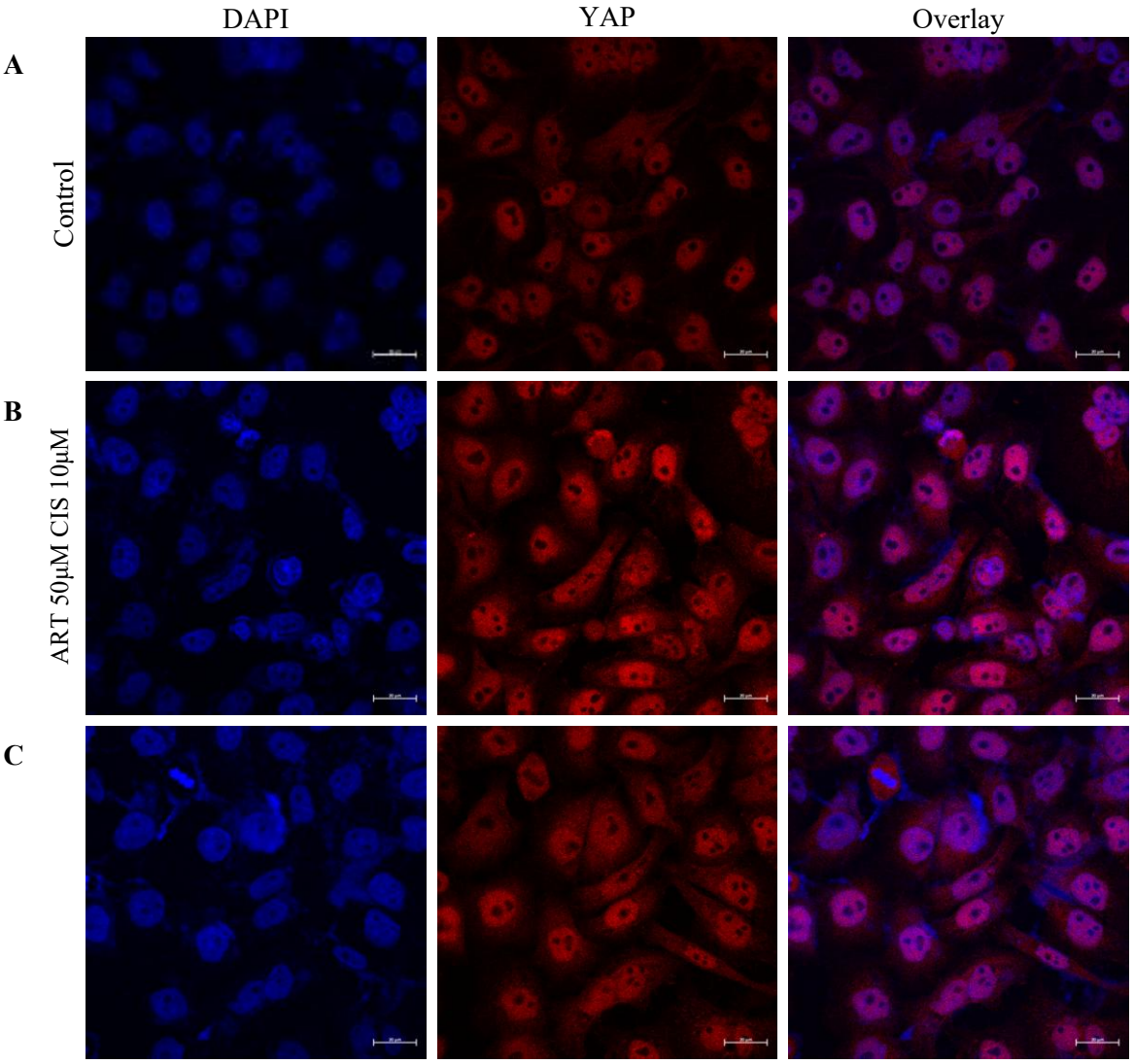

Figure 4.23: The nuclear localisation of YAP upon treatment with ART in combination with CIS determined by immunofluorescence staining in HeLa cells.

(A) Images represent control treated with 0.1% DMSO stained with DAPI (nuclear staining) and CY3 (staining for YAP) (B) Images represent mid confluent HeLa cells treated with 50µM ART 10µM CIS stained with DAPI and CY3 (C) Images represent sparse HeLa cells treated with 50µM ART 10µM CIS stained with DAPI and CY3. Images were taken using a Zeiss Laser Scanning Microscope. Illustrative images show N=3 experiments.

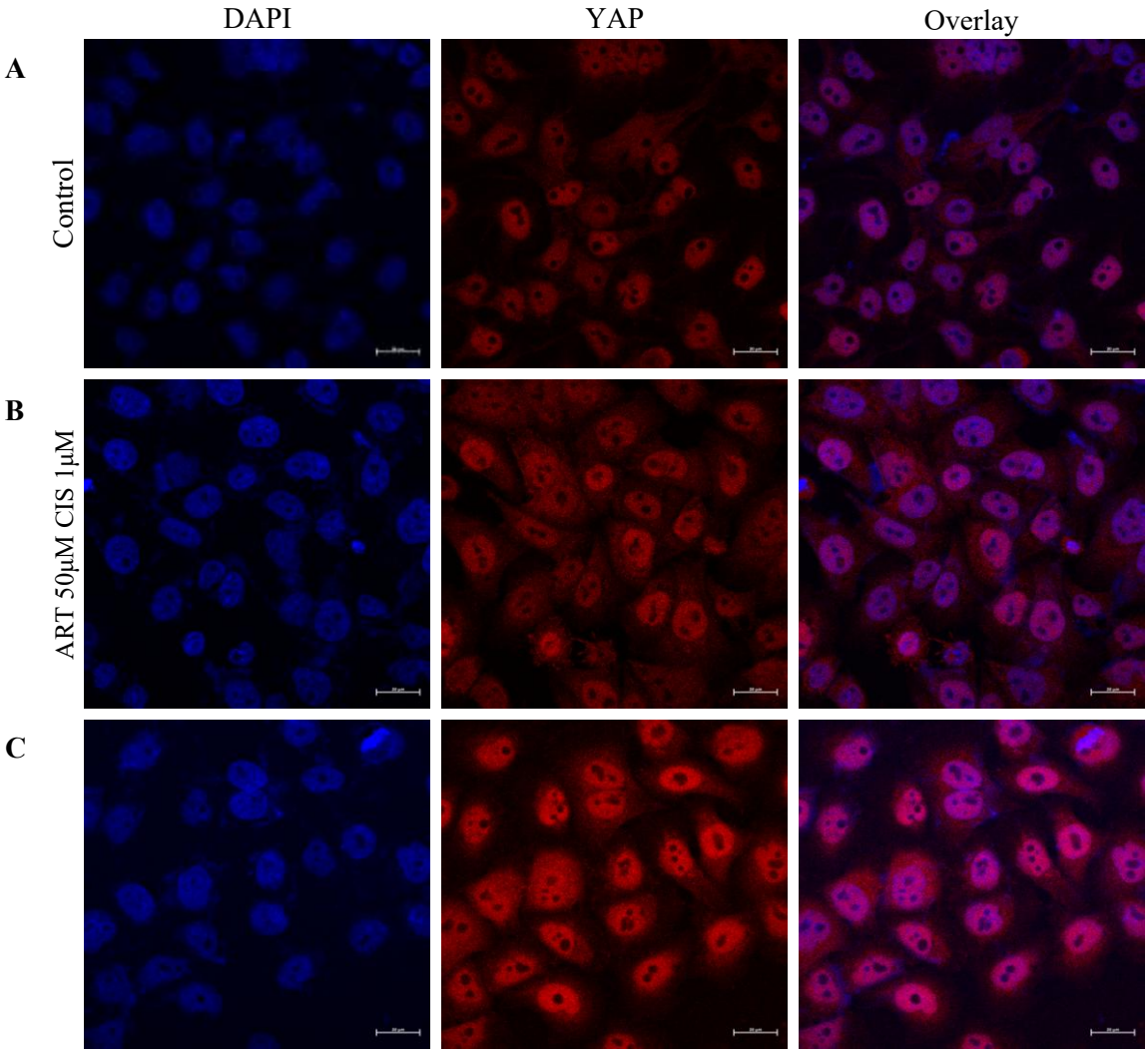

Figure 4.24: The nuclear localisation of YAP upon treatment with ART in combination with CIS determined by immunofluorescence staining in HeLa cells.

(A) Images represent control treated with 0.1% DMSO stained with DAPI (nuclear staining) and CY3 (staining for YAP) (B) Images represent mid confluent HeLa cells treated with 50μM ART 1μM CIS stained with DAPI and CY3 (C) Images represent sparse HeLa cells treated with 50μM ART 1μM CIS stained with DAPI and CY3. Images were taken using a Zeiss Laser Scanning Microscope. Illustrative images show N=3 experiments.

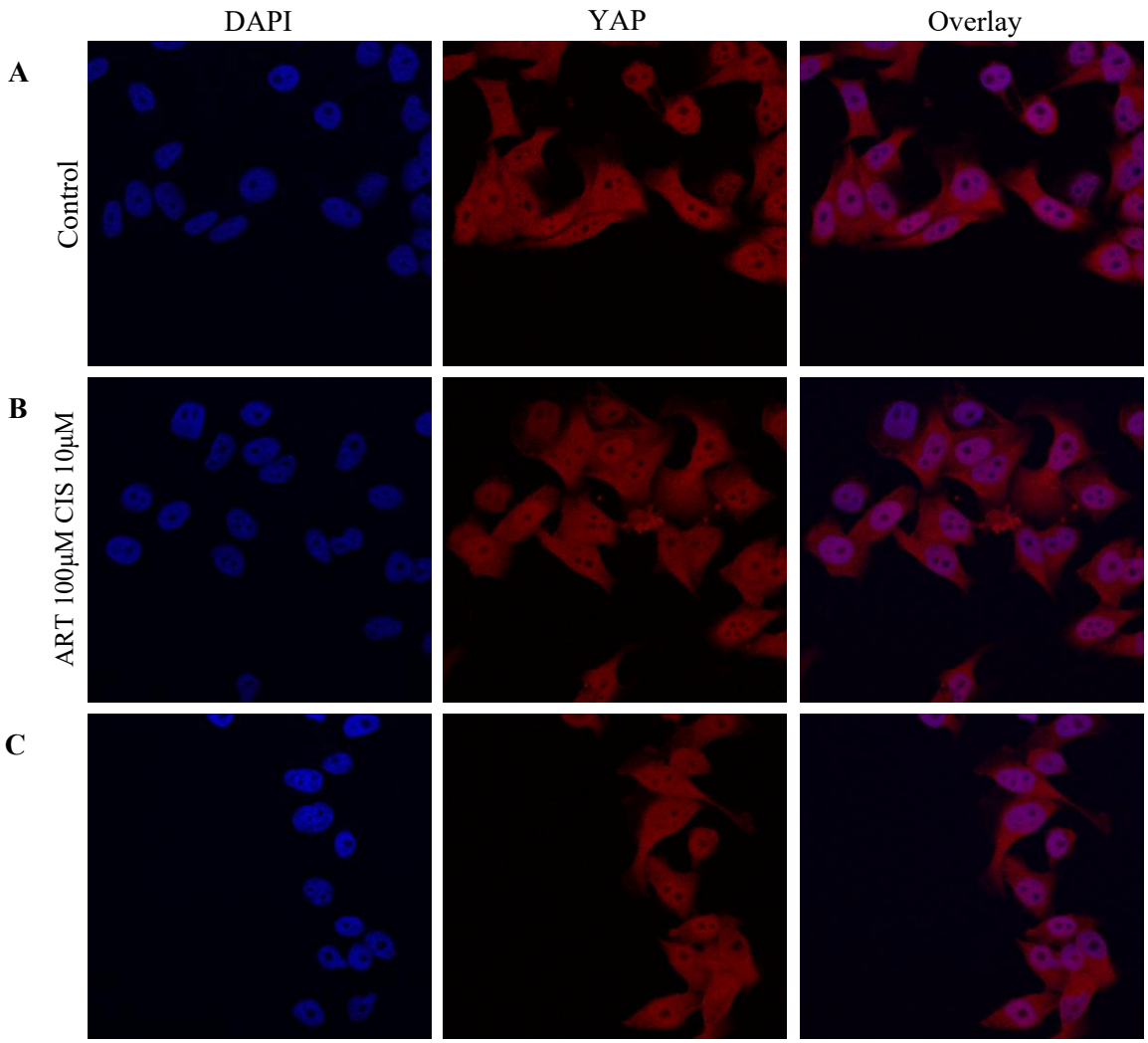

Figure 4.25: The nuclear localisation of YAP upon treatment with ART in combination with CIS determined by immunofluorescence staining in HeLa cells.

(A) Images represent control treated with 0.1% DMSO stained with DAPI (nuclear staining) and CY3 (staining for YAP) (B) Images represent mid confluent HeLa cells treated with 100μM ART 10μM CIS stained with DAPI and CY3 (C) Images represent sparse HeLa cells treated with 100μM ART 10μM CIS stained with DAPI and CY3. Images were taken using a Zeiss Laser Scanning Microscope. Illustrative images show N=3

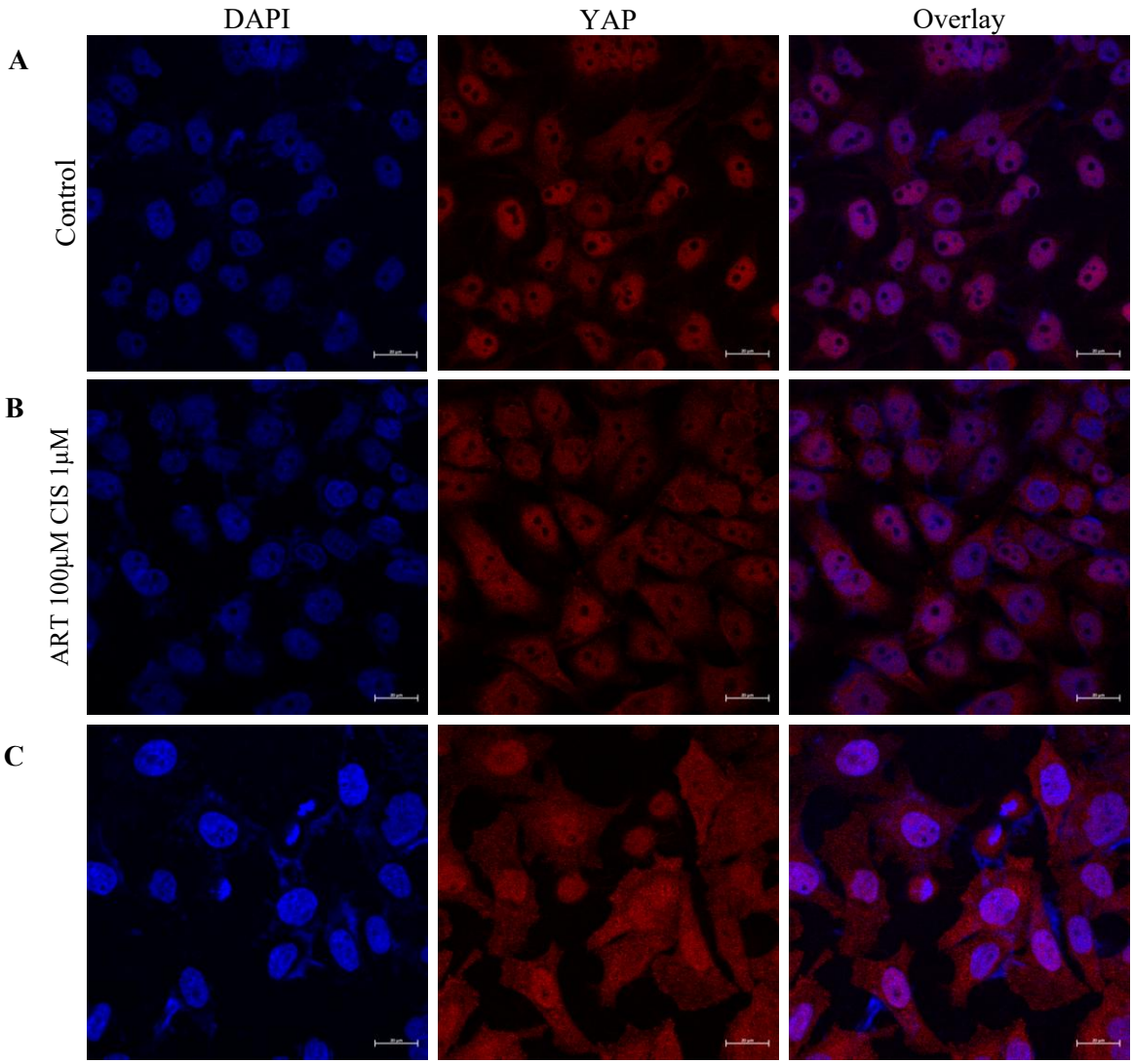

Figure 4.26: The nuclear localisation of YAP upon treatment with ART in combination with CIS determined by immunofluorescence staining in HeLa cells.

(A) Images represent control treated with 0.1% DMSO stained with DAPI (nuclear staining) and CY3 (staining for YAP) (B) Images represent mid confluent HeLa cells treated with 100μM ART 1μM CIS stained with DAPI and CY3 (C) Images represent sparse HeLa cells treated with 100μM ART 1μM CIS stained with DAPI and CY3. Images were taken using a Zeiss Laser Scanning Microscope. Illustrative images show N=3 experiments.

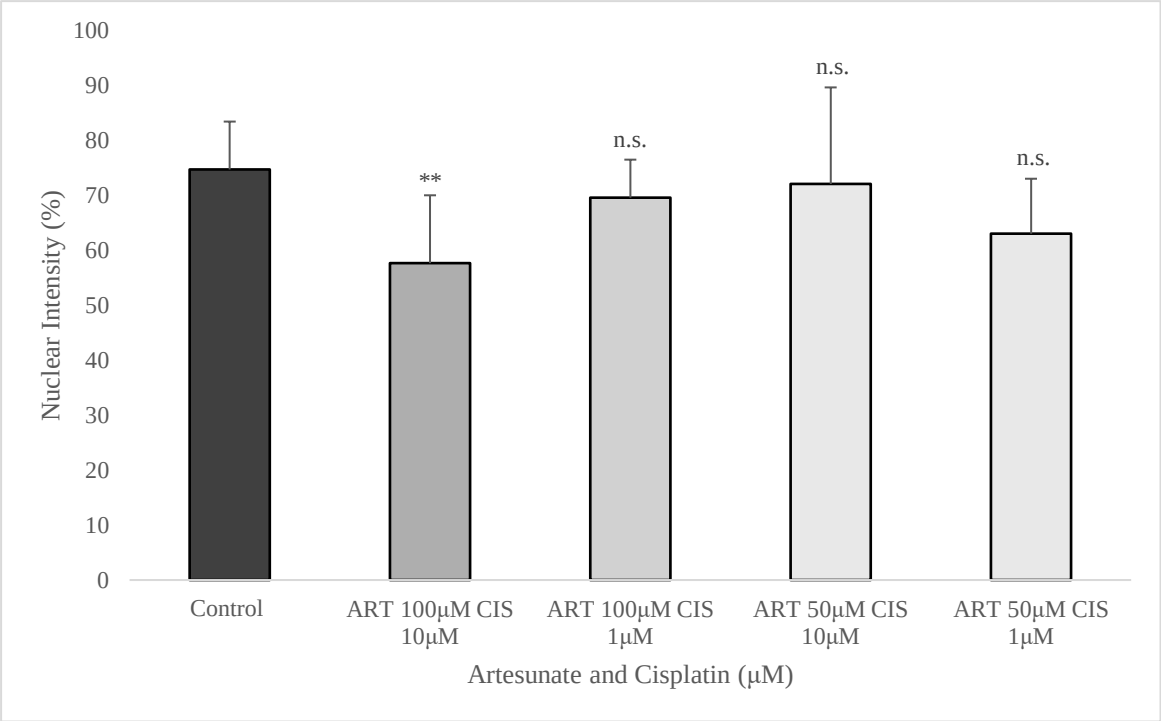

Figure 4.27: Graph representing the mean fluorescent intensity in HeLa Cells with ART in combination with CIS.

*Quantitative graph showing the nuclear intensity of HeLa cells treated with ART 100µM in combination with CIS 10µM and CIS 1µM and ART 50µM in combination with CIS 10µM and CIS 1µM compared to control treated with 0.1% DMSO. Graph was compiled using data generated from 3 independent experiments. Data is displayed as the ± standard deviation with N=3. The statistical significance between the control (treated with 0.1% DMSO) and ART + CIS concentrations was evaluated using a two-sample equal variance T-TEST with significance levels *p≤0.05, ** p≤0.01 and ***p≤0.0001. No significance is represented as n.s.*

Figure 4.23 - Figure 4.26 illustrate the results of YAP localisation in various ART and CIS combination treatments. Specifically, ART at 50µM combined with CIS at 10µM and 1µM, as well as ART at 100µM combined with CIS 10µM and 1µM, were quantified in the graph presented in Figure 4.27.

According to the statistical analysis shown in Figure 4.27, only the combination of 100µM ART with 10µM CIS exhibited a statistically significant reduction in nuclear YAP intensity. Despite other combinations demonstrating lower nuclear YAP intensity compared to the control, none of these differences were statistically significant.

4.5.3 Effect of Combination Therapy with 75µM ARTM and CIS on YAP Phosphorylation in HeLa Cells.

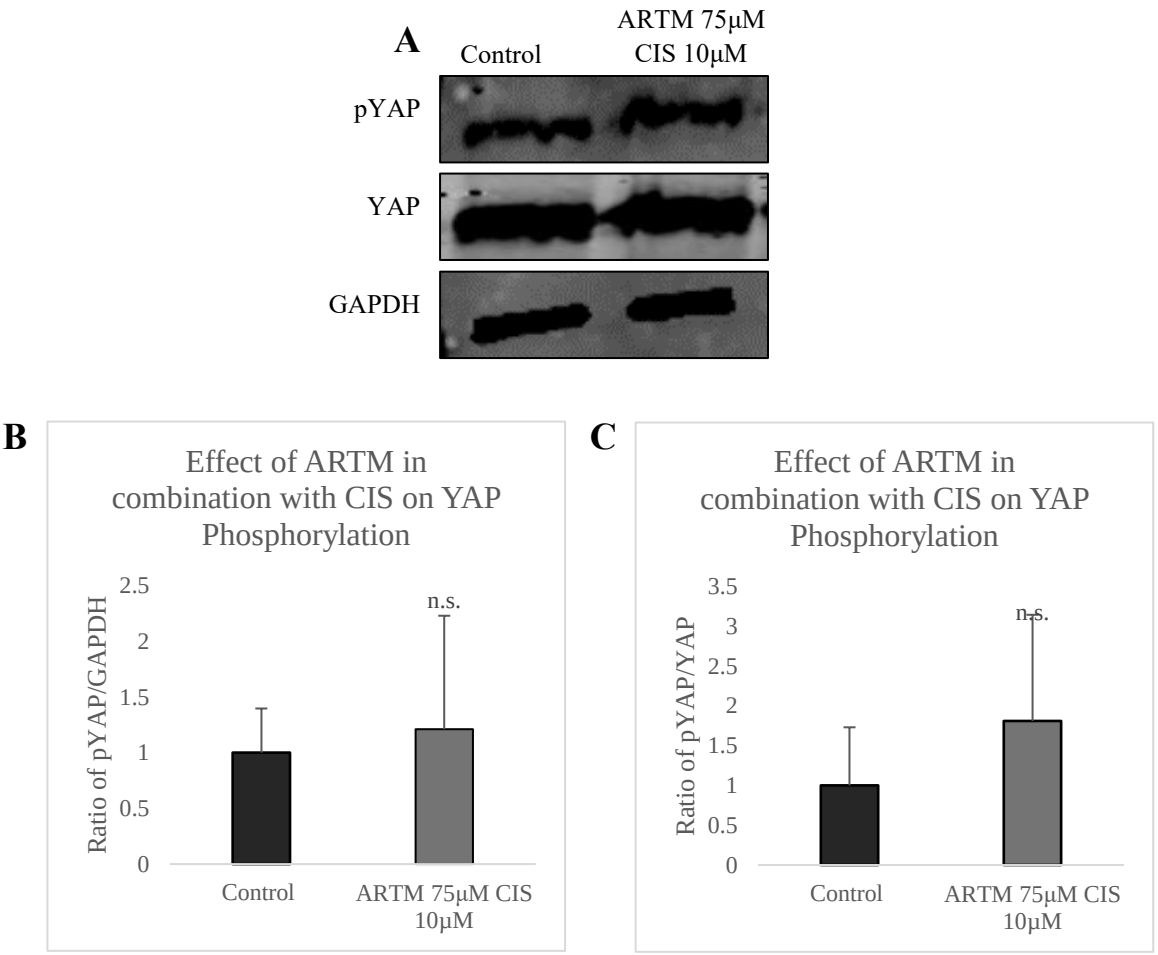

Figure 4.28: The phosphorylation levels of YAP upon treatment with ARTM in combination with CIS determined by western blot analysis in HeLa cells.

*(A) Images represent representative western blots treated with pYAP, YAP and GAPDH for ARTM 75µM CIS 10µM (B) Graph represents the ratio of total YAP and GAPDH in treated compared to control (C) Graph represents the ratio of total YAP and phophoYAP in treated compared to control. Blots were visualised using a LI-COR Odyssey CLx. Representative blots show results two repeats from 3 individual experiments. Data is displayed as the ± standard deviation with statistical significance between the control (treated with 0.1% DMSO) and ARTM + CIS concentration evaluated using a two-sample equal variance T-TEST with significance levels *p≤0.05, ** p≤0.01 and ***p≤0.0001. No significance is represented as n.s.*

IF analysis of ARTM in combination with CIS demonstrated a significant reduction in nuclear intensity compared to the control group. As a result, ARTM 75µM in combination with CIS 10µM was further subjected to Western blot analysis to assess phosphorylation levels. The data presented in Figure 4.28 indicate an increase in YAP phosphorylation following treatment with this combination. However, upon statistical evaluation, the increase was not found to be significant, as the observed difference in phosphorylation levels compared to the control is seen to be minimal as shown in Figure 4.28B and C.

4.5.4 Effect of Combination Therapy with 50µM, 100µM ART and CIS on YAP Phosphorylation in HeLa Cells.

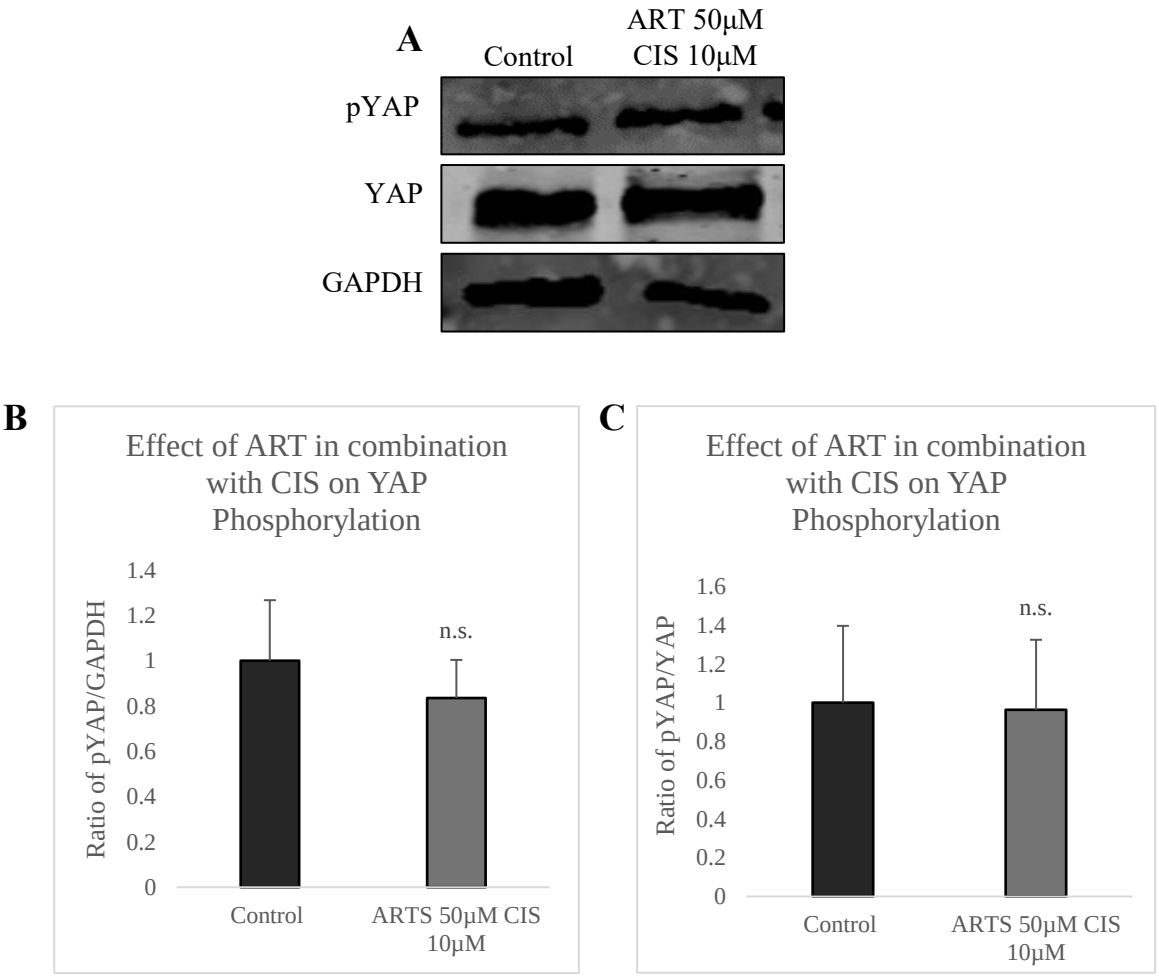

Figure 4.29: The phosphorylation levels of YAP upon treatment with ART in combination with CIS determined by western blot analysis in HeLa cells.

*(A) Images represent representative western blots treated with pYAP, YAP and GAPDH for ART 50µM CIS 10µM (B) Graph represents the ratio of total YAP and GAPDH in treated compared to control (C) Graph represents the ratio of total YAP and phophoYAP in treated compared to control. Blots were visualised using a LI-COR Odyssey CLx. Representative blots show results two repeats from 3 individual experiments. Data is displayed as the ± standard deviation with statistical significance between the control (treated with 0.1% DMSO) and ART + CIS concentration evaluated using a two-sample equal variance T-TEST with significance levels *p≤0.05, ** p≤0.01 and ***p≤0.0001. No significance is represented as n.s.*

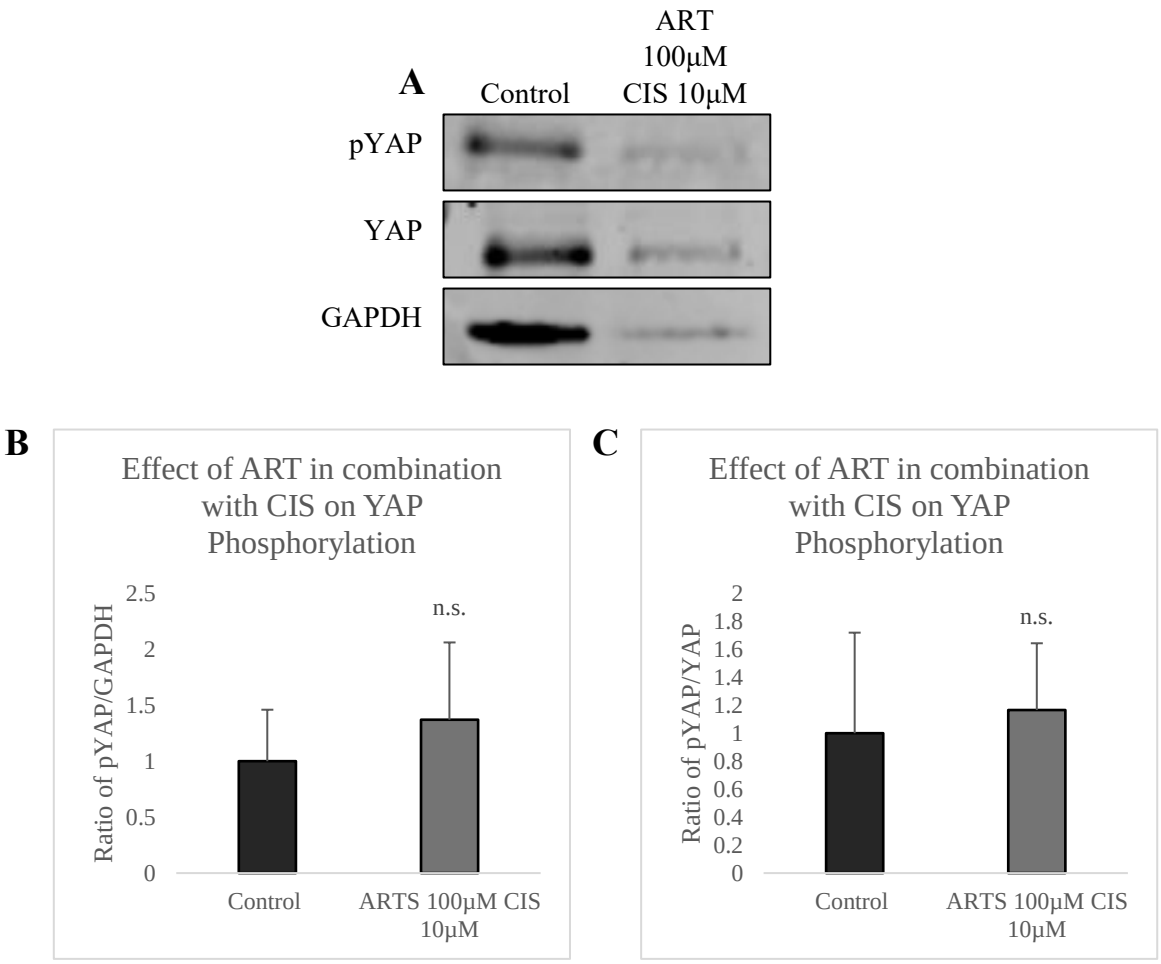

Figure 4.30: The phosphorylation levels of YAP upon treatment with ART in combination with CIS determined by western blot analysis in HeLa cells.

*(A) Images represent representative western blots treated with pYAP, YAP and GAPDH for ART 100µM CIS 10µM (B) Graph represents the ratio of total YAP and GAPDH in treated compared to control (C) Graph represents the ratio of total YAP and phophoYAP in treated compared to control. Blots were visualised using a LI-COR Odyssey CLx. Representative blots show results two repeats from 3 individual experiments. Data is displayed as the ± standard deviation with statistical significance between the control (treated with 0.1% DMSO) and ART + CIS concentration evaluated using a two-sample equal variance T-TEST with significance levels *p≤0.05, ** p≤0.01 and ***p≤0.0001. No significance is represented as n.s.*

Similarly, as shown in Figure 4.29 and Figure ***4.30***, ART in combination with CIS was analysed by Western blot to assess YAP phosphorylation levels. As previously noted, IF analysis of ART combined with CIS did not show statistical significance in reducing nuclear intensity compared to the control, except for one combination: ART 100µM with CIS 10µM.

This combination, along with ART 50µM and CIS 10µM, was subjected to further Western blot analysis, as depicted in Figure 4.29 and Figure ***4.30***. The ART 50µM and CIS 10µM combination did not show significant changes as YAP phosphorylation levels appeared

lower than in the control. In contrast, the other combination of ART 100μM CIS 10μM, while not statistically significant, exhibited increased YAP phosphorylation levels.

CHAPTER 5

Effect of Mass Spectroscopy to Determine Novel Protein Interactions of Specific Genes in the Hippo Signalling Pathway

5.1 Mass Spectrometry Analysis of HeLa cells treated with ARTM and ART

Control	ARTM 75	ART 50	ART 100	Accession Number	Protein	Gene
				P04264	*Keratin, type II cytoskeletal 1*	**KRT10**
				P11021	*Endoplasmic reticulum chaperone BiP*	**HSPA5**
				O94875	*Sorbin and SH3 domain-containing protein 2*	**SORBS2**
				P13645	*Keratin, type I cytoskeletal 10*	**KRT10**
				P11142	*Heatshock cognate 71kDa protein*	**HSPA8**
				P35908	*Keratin, type II cytoskeletal 2*	**KRT2**
				P12956	*X-ray repair cross-complementing protein 6*	**XRCC6**
				Q8N3R9	*MAGUK p55 subfamily member 5*	**MPP5**
				P05186	*Alkaline phosphatase, tissue non specific isozyme*	**ALPL**
				P09923	*Intestinal-type alkaline phosphatase*	**ALPI**
				Q9UHB6	*LIM domain and actin-binding protein 1*	**LIMA1**
				Q16891	*MICSO complex subunit MIC60*	**IMMT**
				P14923	*Junction plakoglobin*	**JUP**
				Q8IVT2	*Mitotic interactor and substrate of PLK1*	**MISP**
				P35527	*Keratin, type I cytoskeletal 9*	**KRT9**
				P40939	*Trifunctional enzyme subunit alpha, mitochondrial*	**HADHA**
				P02768	*Serum albumin*	**ALB**
				P08238	*Heatshock protein HSP 90-beta*	**HSP90AB1**
				P12814	*Alpha-actinin-1*	**ACTN1**
				P0DMV9	*Heatshock 70kDa protein 1B*	**HSPA1B**
				O43707	*Alpha-actinin-4*	**ACTN4**
				P38646	*Stress-70 protein, mitochondrial*	**HSPA9**
				Q9H0H5	*Rac GTPase-activating protein 1*	**RACGAP1**
				P02545	*Prelamin-A/C*	**LMNA**
				P02538	*Keratin, type II cytoskeletal 6A*	**KRT6A**
				P13647	*Keratin, type II cytoskeletal 5*	**KRT5**
				P13010	*X-ray repair cross-complementing protein 5*	**XRCC5**

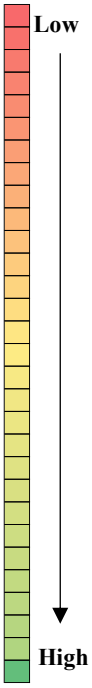

Figure 5.1: Mass spectrometry analysis of protein interactions with YAP upon ARTM75μM, ART 50μM and 100μM treatment.

The heat map illustrates the protein interactions relative to the control (with YAP), with green indicating higher levels of interaction and red representing lower levels.

Mass spectroscopy, a widely recognised method for analysing protein-protein interactions was employed following treatment with ARTM 75μM**,** ART 50μM and ART 100μM through co-immunoprecipitation with YAP using the method outlined in Chapter 2.

The results indicated that ARTM 75μM exhibited significantly reduced interactions with MAGUK p55 member 5, YAP1, heatshock cognate 71kDA and endoplasmic reticulum chaperon BiP, while showing moderately lower interactions with Sorbin.

The two concentrations of ART exhibited distinct patterns. ART 50μM caused a notable downregulation of keratin type II cytoskeletal protein, along with slight reductions in x-ray repair cross-complementing protein 6, MISCO complex subunit MIC60 and alpha actinin. On the other hand, ART 100μM significantly decreased interactions with MAGUK p55 reflecting a trend similar to that of ARTM 75μM, YAP1, Rac GTPase-activating protein 1 and keratin type II.

As depicted in Figure 5.1, all other protein interactions in the treated conditions were either upregulated or remained unchanged compared to the control.

CHAPTER 6

Discussion

6.1 Effect on Cervical Cancer (HeLa Cell Line)

Cervical cancer, the fourth most common malignancy found globally, is primarily driven by persistent infection with high-risk strains of human papillomavirus (HPV). Despite its widespread prevalence, cervical cancer is regarded as one of the most preventable cancers, particularly when diagnosed at an early stage. This prevention is largely due to effective vaccination against HPV and advanced screening programs both of which have significantly reduced cervical cancer incidence in high-income countries. However, in low-income regions, the situation is remarkably different. Limited access to healthcare resources, coupled with insufficient vaccination and screening initiatives mean the disease often progresses unchecked, leading to higher morbidity and mortality rates (Burmeister *et al.,* 2022).

This study aimed to investigate the effect of widely used antimalarial drugs ARTM and ART on cervical cancer alone and in combination with a commonly used chemotherapeutic agent CIS. The initial hypothesis predicted that these drugs would have a significant impact on cervical cancer cells and the experimental results confirm this demonstrating positive outcomes across various assays.

As presented in Chapter 3, ARTM and ART exhibited a significant impact on both cell viability and migration, which were assessed using cell viability, MTT and scratch wound assays, with notable effects observed at concentrations of 75μM and 100μM for ARTM and ART, respectively (as shown in Figures 3.2, 3.4, 3.12 and 3.18). These findings align with numerous studies. For example, research on the lung adenocarcinoma cells A549 demonstrated that artemisinin-based drugs induced dose-dependent cytotoxicity (Li *et al.,* 2018). Similarly, a study involving human neuroblastoma cells concluded that ARTM noticeably inhibited cell proliferation, though in that case, a concentration of 300μM was required to observe a remarkable effect, as opposed to the 75μM ARTM concentration used in the present study. This discrepancy may be attributed to the differences in the cell line

used in the respective experiments (Gong *et al.,* 2012; Zhu *et al.,*2014). Moreover, ART has been shown in another study to suppress the proliferation of lymphoma cells corroborating the findings of the present study (Yuan-Ce *et al.,* 2023).

In the context of uveal melanoma (UM), one of the most common primary ocular neoplasms, ARTM was found to inhibit both migration and invasion of UM cells (Farhan *et al.,* 2021). This parallels the results of the current study, which demonstrated that ARTM significantly reduced cell migration in cervical cancer cells, as outlined in Chapter 3 Figure 3.12 (Zhu *et al.,* 2014). An alternative study found ART to inhibit migration and invasion of oesophageal squamous cell carcinoma cells (KYSE-150). This effect was attributed to ART's ability to suppress cell elasticity while simultaneously increasing cell adhesion. These findings suggest that ART not only impairs the mobility of cancer cells but also strengthens its attachment to the substrate, which may reduce their invasive potential and ability to metastasise (Shi *et al.,* 2015).

Additionally, the present study examined the activity of caspase-3, a critical protease involved in programmed cell death (apoptosis), in HeLa cells treated with ARTM and ART at specific concentrations. The quantified data revealed a significant effect in caspase-3 activity in ARTM and ART at both 75μM and 100μM concentrations (as shown in Figures 3.25 and 3.26). This finding is consistent with prior research, where ARTM and ART induced dose-dependent caspase-3 cleavage in human hepatocellular carcinoma (HepG2) cells, further supporting the apoptotic effect observed in this study (Hsu *et al*., 2023). In studies conducted on melanoma, breast, ovarian, prostate and renal cancer cell line, ARTM derivatives, including ARTM dimers and trimers demonstrated significant antitumor effects. These compounds were observed to induce apoptosis through a caspase-3 dependent mechanism, highlighting their potential in targeting cancer cells via programmed cell death. Furthermore, in prostate cancer cells, ARTM dimers exhibited dual

effects by promoting apoptosis while also inducing cell growth arrest, suggesting a variable approach to inhibiting tumour progression in this particular cancer type (Nam *et al.,* 2006).

CIS, a key first line chemotherapeutic agent for cervical cancer, was also used on HeLa cells in this study to determine an optimum concentration for combination therapy. Both cell viability and proliferation assay's (MTT), revealed that concentrations between 10μM and 15μM had the most pronounced effects on reducing cell viability and proliferation (as shown in Figures 3.7 and 3.24). These findings align with a similar study that demonstrated a significant decrease in HeLa cell viability at concentrations of 10μM or higher, corroborating the results observed in the present research. (Liu *et al.,* 2019). Additionally, when cell migration was evaluated at these higher concentrations, the most significant reduction in cell migration was observed at 10μM and 15μM (Figure 3.21), this observation is consistent with previous research that investigated CIS's effect on cervical cancer cell lines, including HeLa cells, where it was shown to noticeably inhibit both cell migration and invasion (Cheng *et al.,* 2017).

Following the identification of the most effective concentrations for each drug in terms of cell viability, migration and apoptosis both ARTM and ART were tested in combination with CIS. Specifically, ARTM 75μM and ART 100μM were combined with10μM CIS, the highest effective concentration and 1μM CIS, the lowest concentration (as shown in Figures 3.29, 3.32, 3.34 and 3.37). Although 1μM of CIS did not indicate significant effects on its own, it was included in the combination to evaluate whether it could enhance the efficacy of ARTM and ART without requiring a higher dose of CIS. The rationale behind this approach was to investigate minimising the dose of CIS in combination therapy, in attempt to alleviate its associated side effects in corresponding cervical cancer patients.

In prior research, ART combined with doxorubicin in various cell lines, including HeLa, MCF-7, OVCAR-3 and A549, demonstrated that doxorubicin's efficacy was enhanced in all cell lines. Similarly, the current study explored the combination of CIS with ART and

observed significant effects on cell viability as confirmed by MTT and cell viability assays (Sheng-Wu *et al.,* 2013). These findings suggest that CIS when combined with another drug, specifically ART, it exhibits enhanced therapeutic effects. This combined interaction mirrors findings from other studies, where dihydroartemisinin (DHA) combined with CIS significantly enhanced CIS activity in resistant ovarian cancer cell lines (SKOV3 and DDP) by inhibiting the mTOR pathway and inducing apoptosis (Feng *et al.,* 2014). This suggests that ART, like its active metabolite DHA, may enhance CIS's ability to overcome resistance mechanisms in cancer therapy. Thus, combining the drugs may offer a more effective approach to cancer therapy by maximising the impact of CIS while potentially reducing the required therapeutic dose, keeping it well below its toxic dose.

Furthermore, when CIS was combined with 75μM ARTM at both 10μM and 1μM concentrations, significant effects on cell viability and migration were observed. However, it remains unclear whether CIS at 1μM contributed significantly to these effects, as 75μM ARTM alone also demonstrated significant impacts on cell viability and migration. On the other hand, when ART was tested at a lower concentration of 50μM in combination with both 10μM and 1μM CIS, significant effects on cell viability and migration were noted, even at the 1μM CIS concentration. This suggests that the combination of ART at 50μM with 1μM CIS is effective, indicating that ART can enhance CIS's efficacy at lower concentrations. These results not only validate the assumption that optimum concentrations of ART would show significant effects but also reinforce the idea that ART, like DHA, enhances CIS's antitumour activity, even at low doses.

6.2 Effect of ARTM, ART and CIS on the Hippo Signalling Pathway

After analysing the effects of ART and ARTM on cell viability, migration and apoptosis, the study shifted its focus to the primary aim: investigating the impact of these drugs, both alone and in combination with CIS on a key cancer signalling pathway, the Hippo signalling

pathway and its influence on one of the key transcriptional coactivators and main effector, YAP. The HSP plays a critical role in regulating cell proliferation, apoptosis and organ size. YAP is a major downstream effector whose dysregulation has been linked to cancer progression. When the Hippo pathway is active, it triggers a signalling cascade that results in the phosphorylation of YAP, preventing its nuclear translocation and thereby inhibiting cell proliferation. In contrast, when the Hippo pathway is inactive, YAP remains dephosphorylated, allowing it to enter the nucleus and promote cell proliferation as represented in Figure 6.1 (Boopathy and Hong, 2019). By exploring how ART, ARTM and CIS modulate YAP activity, this study aimed to uncover potential mechanisms through which these treatments may exert their anticancer effects.

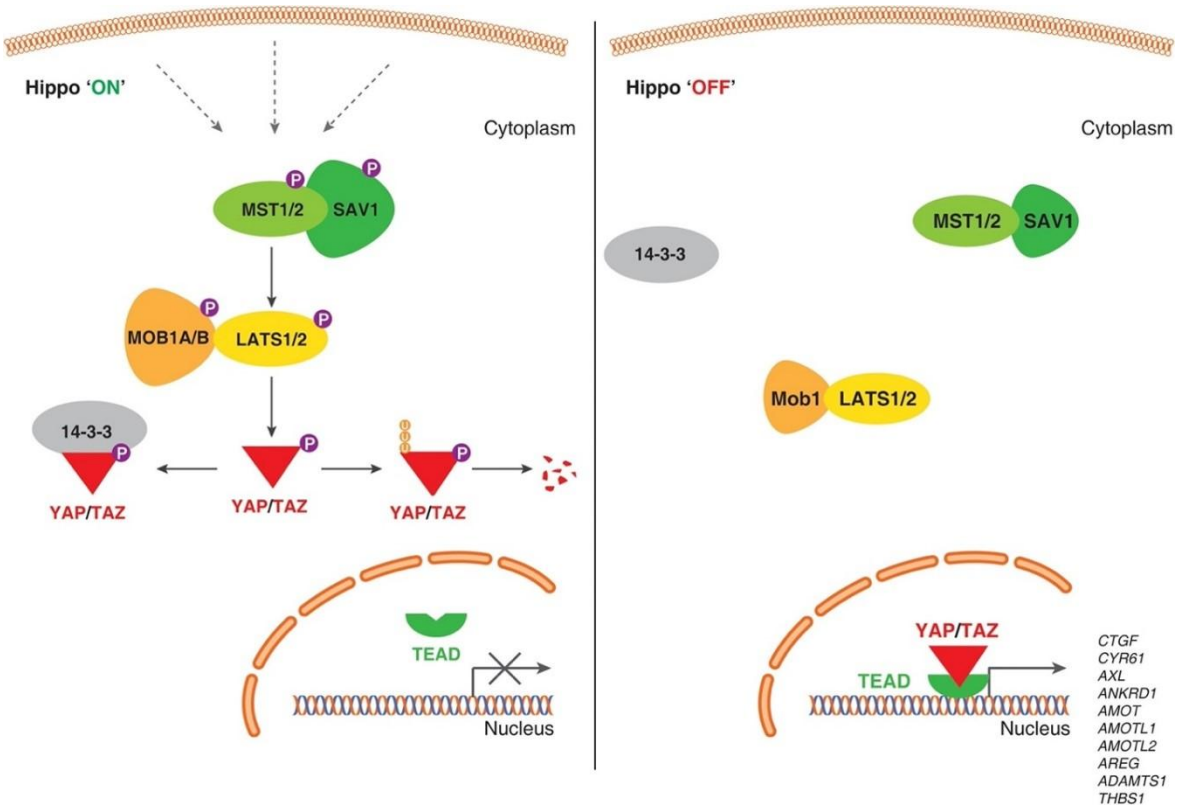

***Figure 6.1**: How the active and inactive state of the Hippo pathway affect YAP (Boopathy and Hong, 2019)*

To assess YAP activity, IF staining was conducted using the concentrations previously identified to have anticancer effects, as detailed in Chapter 3. For all concentrations, both, mid confluent and sparse were looked at to properly localise YAP. In sparse cells, where there is space between cells, YAP is often found in the nucleus. This nuclear localisation is

associated with YAP actively promoting gene expression related to cell growth and proliferation. In contrast, in confluent cell cultures, where cells are densely packed, YAP tends to move to the cytoplasm. This shift in localisation is associated with reduced cell proliferation and a more inactive state, as the cells reach contact inhibition. This dynamic movement of YAP between the nucleus and cytoplasm helps regulate cell growth in response to changes in cell density (Das *et al.,* 2016; Hao *et al.,* 2024).

IF staining was specifically utilised to localise YAP and, in this study, nuclear intensity was quantified to measure nuclear YAP levels. The IF analysis of ARTM at 75μM (Figure 4.1B) revealed a significant reduction in nuclear intensity compared to the control treated with 0.1% DMSO (Figure 4.1A), indicating decreased nuclear localisation of YAP. Similarly, ART at 100μM (Figure 4.3) also resulted in lower nuclear YAP intensity. This finding is critical, as YAP activity is regulated by phosphorylation; when phosphorylated by LATS kinases, YAP is sequestered in the cytoplasm by 14-3-3 proteins, inhibiting its function as a coactivator. Dephosphorylated YAP, however, translocates to the nucleus where it interacts with TEAD transcription factors to promote gene expression that drives cell growth and proliferation (Fu *et al.,* 2022). Moreover, YAP can also be regulated by SRC kinase activity as YAP can be directly phosphorylated at Y341, Y357 and Y394 by SRC. Additionally, SRC can regulate YAP indirectly through the inhibition of LATS ½ (Li *et al.,* 2016).

Consistent with these observations, another study found that ARTM inhibits the nuclear localisation of YAP in HCC (Li *et al.,* 2019). Additionally, research involving ART investigated its effects on MALAT1, an upstream regulator of YAP. MALAT1 binds to the pro-metastatic transcription factor TEAD, blocking its association with YAP. The study demonstrated that ART significantly downregulated MALAT1 mRNA expression in C918 cells, thereby inhibiting YAP's coactivator function and potentially reducing tumour growth and metastasis (Jiu, Liu and Wen, 2021).

Moreover, research suggests that silencing YAP can enhance cell sensitivity to anti-tumour drugs across various cancers, including ovarian, pancreatic, liver and oral squamous cell carcinoma (Nguyen and Yi, 2020). For instance, a study analysing YAP expression in gastric cancer cells revealed that YAP levels were significantly higher in a cancerous tissue compared to normal tissue. This is expected, as YAP promotes cell proliferation, a hallmark of cancer development. In the same study, YAP knockdown in gastric cancer cells led to a notable reduction in cell proliferation. Furthermore, the knockdown of YAP enhanced the cells' sensitivity to CIS, showing a greater response to the drug compared to when YAP was overexpressed. These findings emphasise the potential of targeting YAP to improve the efficacy of chemotherapeutic agents like CIS (Lu, Sun and Zhu, 2018).

In the present study, IF staining was conducted to assess the effect of CIS at concentrations of 10μM (Figure 4.6B) and 15μM (Figure 4.7B) on YAP localisation in HeLa cells. Quantitative analysis demonstrated a significant reduction in nuclear YAP compared to the control. This suggests that CIS effectively reduces YAP nuclear translocation, like impairing its transcriptional activity and its role in promoting cell proliferation. Notably, this reduction occurred without the need for direct YAP knockdown, indicating that CIS exerts its antitumour effects, at least in part by modulating YAP activity and preventing its accumulation in the nucleus.

Similarly, the combinations of ARTM and ART with CIS were also subjected to IF analysis. Both ARTM 75μM with CIS 10μM and CIS 1μM (Figures 4.20 and 4.21) showed statistically significant reduction in nuclear intensity compared to control (Figure 4.22). Moreover, ART 100μM in combination with CIS 10μM (Figure 4.25) also showed significance although when combined with CIS 1μM (Figure 4.26) there was no statistically significant effect despite the nuclear intensity being lower than the control (Figure 4.27).

In addition to the IF analysis, it became evident that directly assessing the effect of the drugs on YAP localisation was challenging as it was difficult to discern the precise impact of each drug on YAP. A key observation was that the absence of YAP in the nucleus could indicate a lack of phosphorylation, which would otherwise enable YAP to activate transcription factors and promote cell growth. To address this, the study employed Western blot analysis to evaluate YAP phosphorylation levels and determine if the drugs influence YAP phosphorylation and subsequent translocation to the cytoplasm. Western blot analysis of ARTM 75μM (Figure 4.9), ART 100μM (Figure 4.11) and CIS 10μM (Figure 4.12) and 15μM (Figure 4.13) revealed distinct results for each treatment. Despite showing reduced nuclear YAP intensity, indicating less YAP in the nucleus, the results suggested that the drugs did not uniformly lead to LATS specific YAP dephosphorylation at the s127 site in the nucleus.

ARTM 75μM did not significantly increase YAP phosphorylation. Similarly, CIS at 10μM and 15μM, as well as ART 100μM, also failed to increase YAP phosphorylation, instead exhibited a decrease compared to the control suggesting that these treatments do not affect YAP phosphorylation levels. A study involving drug repurposing across various cancers found that deoxybouvardin, a natural compound similar to ARTM, decreased YAP levels in HeLa cells but did not significantly impact YAP phosphorylation (Ji *et al.,* 2018). This observation indicates that natural compounds like ARTM may reduce nuclear YAP levels, despite not directly influencing YAP phosphorylation, potentially affecting different signalling pathways. A study on UM cells treated with ARTM revealed inhibition to the PI3K/AKT/mTOR signalling pathways. The HSP, which is known to interact with PI3K/AKT/mTOR pathways, inhibits cell growth by inactivating the mTOR pathway, similarly, HCC treated with ART indicated increased apoptosis by inhibiting PI3K/AKT/mTOR pathway supporting the previous observation (Samji *et al.,* 2021; Tumaneng *et al.,* 2014; Yang *et al.,* 2021). In contrast, a study on MDA-MB-231 breast

cancer cells treated with DHA revealed that the SRC pathway was inhibited (Efferth, 2017). Notably, SRC activates YAP through three key processes: by direct phosphorylation at site Y357 facilitating YAP nuclear translocation; by repression of Hippo kinases via inhibition or the activation of pathways such as MAPK, PI3K and by Hippo-independent mechanisms (Hsu *et al.,* 2020). Literature has shown that nuclear YAP levels decrease when SRC is inhibited or knocked down. Therefore, despite the absence of phosphorylation at the LATS specific S127 site as concluded by the Western blot analysis, the reduction in nuclear YAP suggests that this decrease may not result from Hippo kinase regulation rather SRC inhibition and the non-canonical regulatory pathway (Lamar *et al.,* 2019; Li *et al.,* 2016).

Due to the observation of significant cell death at 100µM ART during Western blot analysis, the study shifted focus to a lower concentration of 50µM ART as a less potent alternative (as shown in Figure 4.10). Although 50 µM ART exhibited some effect on cancer cells (discussed in Chapter 3), it did not show a notable impact on YAP or pYAP levels when assessed through IF staining and Western blot analysis. This suggests that 50µM ART, while less toxic was ineffective in modulating YAP or its phosphorylation status under the conditions tested. Similarly, 50µM ART was subjected to IF as part of combination therapy with both 10µM and 1µM CIS to assess whether combination would impact YAP levels in the nucleus. However, despite a visible reduction in nuclear intensity, neither combination resulted in a statistically significant decrease in nuclear YAP intensity compared to the control. This suggests that, while there may be some effect on YAP localisation, the reduction in YAP nuclear levels was not pronounced enough to reach statistical significance in these experiments.

Furthermore, when 75µM ARTM (Figure 4.28), 50µM (Figure 4.29) and 100µM (Figure 4.30) ART were tested in combination with 10µM CIS, all combinations except for 50µM ART and CIS showed an increase in YAP phosphorylation levels compared to the control. However, the increase in phosphorylation was not significant enough to reach statistical

significance. CIS induces DNA damage and cellular stress, which activates the HSP, leading to enhanced regulation of YAP phosphorylation. This suggests that the stress induced by CIS may sensitise cells to the effects of ARTM and ART, particularly at concentrations of 75µM and 100µM, which explains the results (low nuclear intensity of YAP) observed when HeLa cells were treated with ARTM and ART alone. Indeed, CIS-induced stress may activate pathways such as MAPK, JNK or p38 which can enhance the activity of kinases like LATS½. LATS½ play a crucial role in phosphorylating YAP, leading to its inactivation and cytoplasmic retention. Therefore, the combinations of CIS with ARTM and ART at these concentrations may be driving a stronger activation of these pathways thus contributing to the observed increase in YAP phosphorylation (Lee and Yonehara, 2020; Mo *et al.,* 2015)

While GAPDH is widely recognised as a reliable housekeeping gene for normalising expression levels due its stable expression under many conditions, its use in this study appears valid but nuanced by experimental conditions. The variability noted in Figures 4.12A and 4.30A can be attributed not to the unsuitability of GAPDH itself but to the potent cytotoxic effects of the drug being tested. At the concentrations tested, the drug's cell-killing efficacy likely reduces the overall cell population, leading to altered cellular responses and inconsistencies in GAPDH expression levels in the images. Despite the variability GAPDH remains an appropriate choice for normalisation provided that the experimental design accounts for these effects.

Expanding on this matter, when ARTM and ART were tested on HeLa cells to investigate their effects on common YAP target genes such as CTGF, Cyr61 and c-Myc, the results varied across drug concentrations. ARTM at 75µM showed a significant downregulation of CTGF compared to the control, while Cyr61 and c-Myc were slightly upregulated (as shown in Figure 4.14). Similarly, ART 50µM led to the upregulation of all three genes, with c-Myc showing a particularly strong upregulation compared to the others (as shown in

Figure 4.15). Interestingly, ART at 100μM, despite being the same drug produced a different profile. While all the genes were upregulated, Cyr61 was notably more highly upregulated than the others and the control (as shown in Figure 4.16).

Inhibition of the HSP prevents the phosphorylation of YAP, allowing its translocation into the nucleus. Once in the nucleus, YAP interacts with transcription factors such as TEAD facilitating the transcription of target genes involved in cell proliferation, survival and growth, i.e., CTGF, c-MYC and Cyr61 (Zhao *et al.,* 2021). Therefore, the upregulation from the RT-PCR analysis suggests that the effects of ARTM and ART might involve pathways beyond just YAP signalling. To further investigate this, the expression levels of β-catenin, mTOR, p53 and Wnt-1 (genes that interact with YAP/Hippo) were examined. Interestingly, despite ARTM 75μM not showing downregulation of all YAP target genes, it significantly downregulated β-catenin, p53, mTOR and Wnt-1 (as shown in Figure 4.17). This could align with studies suggesting that the HSP interact with the Wnt signalling cascade, potentially involving a non-canonical pathway which suppresses the canonical Wnt cascade (Park *et al.,* 2016). Furthermore, other research has indicated that YAP can serve as a transcriptional coactivator of β-catenin, which may explain the downregulation of β-catenin noticed when treated with ARTM 75μM (Azzolin *et al.,* 2014). ARTM has been observed to inactivate the Wnt/β-catenin signalling pathway in A549 and H1299 cells. These findings align with the present study, which demonstrated the downregulation of both Wnt and β-catenin when treated with ARTM (Tong *et al.,* 2016). ART, on the other hand exhibited distinct effects across different concentrations. At 50μM, ART led to the significant downregulation of p53 and Wnt-1, while upregulating β-catenin and mTOR (as shown in Figure 4.18). Contrary to ART at 100μM downregulated p53, mTOR and Wnt-1 but had no noticeable effect on β-catenin compared to the control (as shown in Figure 4.19).

The drugs in this study influence the expression of p53, a critical tumour suppressor involved in cell cycle arrest, DNA repair and apoptosis (Rivlin *et al.,* 2011). This

observation contradicts the idea that ARTM and ART exert anti-cancer effects. However, literature indicates that HeLa cells lack detectable levels of functional p53 protein, although they have active p53 mRNA. HeLa cells contain a mutant form of p53, which is dysfunctional and unable to carry out the typical tumour-suppressing functions. Therefore, the downregulation of p53 observed with these drugs could be a response to the mutant form, contributing to their anti-cancer activity by targeting and reducing the activity of this defective protein (May, Jenkins and May, 1991; Hoppe-Seyler and Butz, 1993)

6.3 ARTM and ART treatment on Novel Protein Interactions with the Hippo Signalling Pathway

After evaluating the effects of the drugs on YAP and the HSP, specific drug concentrations were subjected to mass spectroscopy analysis. The results shown in Figure 5.1 revealed significant interactions between YAP and various proteins, although a lack of variation was noted between the control and treatments. Regardless, all three drug treatments – ARTM 75µM, ART 50µM and ART 100µM – demonstrated increased interactions with LIMA1 (LIM domain and actin-binding protein 1) compared to the untreated control. LIMA 1 is crucial for regulating the actin cytoskeleton by binding to actin filaments and controlling their polymerisation. It is known to be downregulated in cancers and research indicated that its knockdown significantly enhances cancer cell invasion (Ohashi *et al.,* 2017). Although there is limited literature directly linking YAP and LIMA1 the observed increased interaction of LIMA1 with YAP1 in the presence of the drugs suggests that LIMA1 may function as a regulator of YAP1, influencing its activity and localisation in response to mechanical signals. IF analysis further supports this idea, showing that ARTM and ART treatments result exhibited low nuclear YAP levels, helping retain YAP in the cytoplasm and thereby modulating its nuclear translocation and downstream signalling (Zhang *et al.,* 2011).

The observed reduction in the association between MPP5 and YAP upon treatment with ARTM 75μM and ART 100μM may be attributable to the modulation of YAP activity by MPP5, potentially through influencing upstream Hippo pathway components or mechanical sensing at cell junctions. Notably, a previous study employing mass spectroscopy to investigate cell contact-related interactions found strong interactions between MPP5 and YAP (Varelas *et al.,* 2010). The present study's data, which shown decrease association between MPP5 and YAP following ARTM and ART treatment, suggest that these treatments might affect cell proliferation by altering the regulatory dynamics between MPP5 and YAP (Sterling *et al.,* 2020).

Additionally, the analysis of YAP interactions in cells treated with ART 50μM showed minor differences compared to control. This aligns with the findings from Chapter 5, which indicated minimal impact of ART on the HSP. This lack of effect at lower concentrations may be due to ART needing to reach a higher threshold to significantly alter protein interactions. A study on colorectal cancer supports this, showing that ART's ability to promote apoptosis and inhibit proliferation is dose-dependent, requiring higher concentrations to achieve notable changes in protein interactions (Yang *et al.,* 2021).

In conclusion, the experiments conducted on HeLa cells suggest that ARTM and ART do impact cancer-related processes. Although the primary focus of this study was to investigate the drugs' effect on the HSP, the findings indicate that these drugs may not significantly influence this pathway. However, they do appear to affect the localisation of YAP, a crucial factor in cancer management, as maintaining phosphorylated YAP outside the nucleus is important for controlling cell proliferation. Despite this, Western blot analysis revealed that the drugs did not alter YAP phosphorylation levels at S127, suggesting that the drugs may retain YAP in the cytoplasm by inhibiting the SRC pathway rather than the Hippo pathway. This is likely due to integrin-activated SRC crosstalk, which represses Hippo kinases like LATS1, thereby influencing YAP activation. Further analysis

of downstream regulatory genes of the HSP revealed the downregulation of genes associated with a different signalling pathway such as Wnt. Therefore, it can be concluded that while these drugs impact cancer-related signalling pathways, their effects may not be specifically linked to the Hippo pathway.

6.4 Future Work

RNA sequencing could provide valuable insights into how ARTM and ART affect gene expression, particularly after mass spectrometry has identified the proteins of interest. By analysing RNA-sequencing data, it can be determined whether these drugs upregulate or downregulate specific genes, offering a more comprehensive understanding of their impact on cellular pathways.

Additionally, incorporating multiple non-cancerous cell lines including cervical cell line into the study would allow for a comparison of the drugs' effects on both cancerous and non-cancerous cells and validate findings. This approach would help to assess the specificity and potential cytotoxicity of the drugs, providing a clearer picture of their therapeutic potential and side effects.

Furthermore, animal models could be incorporated to evaluate the efficacy and safety of ARTM and ART in a more complex biological system which will provide important details on the pharmacokinetics and pharmacodynamics of the drugs.

BIBLIOGRAPHY

Abdel-Aziz, A. K. *et al.* (2022) 'A Critical Review of Chloroquine and Hydroxychloroquine as Potential Adjuvant Agents for Treating People with Cancer', *Future Pharmacology,* 2(4), pp. 431-443. Available at: https://doi.org/10.3390/futurepharmacol2040028

Abraham, J. and Staffurth, J. (2020) 'Hormonal therapy for cancer', *Medicine,* 48(2), pp. 103-107. Available at: https://doi.org/10.1016/j.mpmed.2019.11.007

Agalakova, N. I. (2024) 'Chloroquine and Chemotherapeutic Compounds in Experimental Cancer Treatment', *International Journal of Molecular Sciences,* 25(2), p. 945. Available at: https://doi.org/10.3390/ijms25020945

Akashdeep, B. *et al.* (2020) 'Incidence and severity of self-reported chemotherapy side-effects in patients with hematolymphoid malignancies' *Cancer Research, Statistics and Treatment,* 3(4), pp. 736-741. Available at: https://doi.org/10/4103/CRST.CRST_87_20

Amjad, M. T., Chidharla, A. and Kasi, A. (2023) *Cancer Chemotherapy*. Available at: https://www.ncbi.nlm.nih.gov/books/NBK564367/ (Accessed: 06 August 2024).

Aprioku, J. S. and Obianime, A. W. (2011) 'Structure-Activity-Relationship (SAR) of Artemisinins on some Biological Systems in Male Guinea Pigs', *Insight Pharmaceutical Sciences,* 1(1), pp. 1-10.

Augustin, Y., Staines, H. M. and Krishna, S. (2020) 'Artemisinins as a novel anti-cancer therapy: Targeting a global cancer pandemic through drug repurposing', *Pharmacology & Therapeutics,* 216, article number 107706. Available at: https://doi.org/10.1016/j.pharmthera.2020.107706

Azzolin, L. *et al.* (2014) 'YAP/TAZ incorporation in the β-catenin destruction complex orchestrates the Wnt response', *Cell,* 158(1), pp. 157 170. Available at: https://doi.org/10.16/j.cell.2014.06.013

Bataouli, A. *et al*. (2014) 'The global cancer divide: Relationships between national healthcare resources and cancer outcomes in high-income vs. middle- and low-income countries', *Journal of Epidemiology and Global Health,* (4)2, pp. 115-124.

Boogard, W. M. C. and Komninos, D. S. J. (2022) 'Chemotherapy Side-Effects: Not All DNA Damage Is Equal', *Cancers,* 14(3), p.627. Available at: https://doi.org/10.3390/cancers14030627

Boopathy, G. T. K. and Hong, W. (2019) 'Role of Hippo Pathway-YAP/TAZ Signaling in Angiongenesis', *Frontiers in Cell and Developmental Biology,* 7. Available at: https://doi.org/10.3389/fcell.2019.00049

Bouvard, V. *et al.* (2021) 'The IARC Perspective on Cervical Cancer Screening', *The New England Journal of Medicine,* 385(20), pp. 1908-1918. Available at: https://doi.org/10.1056/NEJMsr2030640

Burmeister, C. A. *et al.* (2022) 'Cervical cancer therapies: Current challenges and future perspectives', *Tumour Virus Research,* 13, article number: 200238. Available at: https://doi.org/10.1016/j.tvr.2022.200238

Cancer Research UK (2020) *Worldwide cancer statistics.* Available at: https://www.cancerresearchuk.org/health-professional/cancer-statistics/worldwide-cancer#heading-One (Accessed: 01 August 2024)μμ

Chen, X. *et al.* (2017) 'Artesunate Activates the Intrinsic Apoptosis of HCT116 Cells through the suppression of Fatty Acid Synthesis and the NF-κB Pathway', *Molecules,* 22(8), p. 1272. Available at: https://doi.org/10.3390/molecules22081272

Cheng, J. *et al.* (2017) 'Cisplatin inhibits the growth, migration and invasion of cervical cancer cells by down-regulation IL-17E/IL-17RB', *International Journal of Clinical & Experimental Pathology,* 10(9), pp. 9341-9351. Available at: https://www.ncbi.nlm.nih.gov/pmc/articles/PMC6965941/ (Accessed: 02 September 2024).

Chung, M. *et al.* (2012) 'Embryotoxicity and Toxicokinetics of the Antimalarial Artesunate in Rats', *Toxicological Research,* 29(1), pp. 27-34.

Ciarimboli, G. (2012) 'Membrane transporters as mediators of Cisplatin effects and side effects', *Scientifica*. Available at: https://pubmed.ncbi.nlm.nih.gov/24278698/ (Accessed: 20 August 2024).

Cooper, G. M. (2000) *The Cell: A Molecular Approach.* Available at: https://www.ncbi.nlm.nih.gov/books/NBK9963/ (Accessed: 15 August 2024).

Dai, G. *et al.* (2017) 'The synergistic antitumor effect of cinobufagin and cisplatin in human osteosarcoma cell line *in vitro* and *in vivo*', *Oncotarget,* 8(49), pp. 85150-85168. Available at: https://doi.org/10.18632/oncotarget.19554

Das, A. *et al.* (2016) 'YAP Nuclear Localization in the Absence of Cell-Cell Contact Is Mediated by a Filamentous Actin-dependent, Myosin II- and Phopho-YAP-independent Pathway during Extracellular Matrix Mechanosensing', *Journal of Biological Chemistry,* 291(12), pp. 6096-6110. Available at: https://doi.org/10.1074/jbc.M115.708313

Dasari, S *et al. (2022)* 'Pharmacological Effects of Cisplatin Combination with Natural Products in Cancer Chemotherapy', *International Journal of Molecular Science,* 23(3), p. 1532. Available at: https://doi.org/10.3390/ijms23031532

Daugan, M. *et al.* (2016) 'Metformin: AN anti-diabetic drug to fight cancer', *Pharmacological Research,* 113(A), pp. 675-685. Available at: https://doi.org/10.1016/j.phrs.2016.10.006

Debela, D. T. *et al.* (2021) 'New approaches and procedures for cancer treatment: Current perspectives', *SAGE Open Medicine,* 9. Available at: https://doi.org/10.1177/20503121211034366

Dorsey, J. F. *et al*. (2010) 'Modulation of the anti-cancer efficacy of microtubule-targeting agents by cellular growth conditions', *Cancer Biology & Therapy,* 9(10), pp. 809-818. Available at: https://doi.org/10.4161/cbt.9.10.11453

Efferth, T. (2017) 'From ancient herb to modern drug: *Artemisia annua* and artemisinin for cancer therapy' , *Seminars in Cancer Biology,* 46, pp. 65-83.

Elbediwy, A. *et al.* (2016) 'Integrin signalling regulates YAP and TAZ to control skin homeostasis', *Development,* 143(10), pp. 1674-1687.

Farhan, M. *et al.* (2021) 'Artemisinin Inhibits the Migration and Invasion in Uveal Melanoma via inhibition of the PI3K/AKT/mTOR Signaling Pathway', *Oxidative Medicine and Cellular Longevity,* 2021(1), article number 9911537. Available at: https://doi.org/10.1155/2021/9911537

Feng, X. *et al.* (2014) 'Dihydroartemisinin potentiates the anticancer effect of cisplatin via mTOR inhibition in cisplatin-resistant ovarian cancer cells: involvement of apoptosis and autophagy', *Communications,* 3(14), pp. 376-281. Available at: https://doi.org/10.1016/j.bbrc.2014.01.053

Fu, M. *et al.* (2022) 'The Hippo signalling pathway and its implications in human health and diseases', *Signal Transduction and Targeted Therapy,* 7, article number 376. Available at: https://doi.org/10.1038/s41392-022-01191-9

Galluzzi, L. *et al.* (2012) 'Molecular mechanisms of cisplatin resistance', *Oncogene,* 31(15), pp. 1869-1883. Available at: https://doi.org/10.1038/onc.2011.384

Gilbert, D. C., Chalmers, A. J. and El-Khamisy, S. F. (2012) 'Topoisomerase I inhibition in colorectal cancer: biomarkers and therapeutic targets', *British Journal of Cancer,* 106(1), pp. 18-24. Available at: https://doi.org/10.1038/bjc.2011.498

Gold, J. M. and Raja, A. (2023) *Cisplatin.* Available at: https://www.ncbi.nlm.nih.gov/books/NBK547695/ (Accessed: 10 August 2024).

Gong, X. *et al.* (2012) 'Selective radiosensitization of human cervical cancer cells and normal cells by artemisinin through the abrogation of radiation –induced G2 block', *International Journal of Gynecological Cancer',* 22(5), pp. 718-724. Available at: https://doi.org/10.1097/IGC.0b013e31824a67c9

Grimmett, E. *et al.* (2022) 'Cancer vaccines: past, present and future; a review article', *Discover Oncology,* 13, p. 31. Available at: https://doi.org/10.1007/s12672-022-00491-4

Gumbiner, B. M. and Kim, N. (2014) 'The Hippo-YAP signaling pathway and contact inhibition of growth', *Journal of Cell Science,* 127(4), pp. 709-717. Available at: https://doi.org/10.1242/jcs.140103

Haddad, N. *et al.* (2024) 'Drug Repurposing: Exploring Potential Anti-Cancer Strategies by Targeting Cancer Signalling Pathways', *Biology,* 13(6), p. 386.

Hao, S. *et al.* (2024) 'YAP condensates are highly organized hubs', *iScience,* 27(6), article number 109927. Available at: https://doi.org/10.1016/j.isci.2024.109927

He, H. *et al.* (2021) 'Targeting Signaling Pathway Networks in Several Malignant Tumors: Progresses and Challenges', *Frontiers in Pharmacology,* 12, article number 67675. Available at: https://doi.org/10.3389/fphar.2021.675675

Hoppe-Seyer, F. and Butz, K. (1993) 'Repression of endogenous p53 transactivation function in HeLa cervical carcinoma cells by human papillomavirus type 16 E6, human mdm-2, and mutant p53', *Journal of Virology,* 67(6), pp. 3111-3117. Available at: https://doi.org/10.1128/jvi.67.6.3111-3117.1993

Hou, J. *et al.* (2008) 'Experimental therapy of hepatoma with artemisinin and its derivatives: *in vitro* and *in vivo* activity, chemosensitization, and mechanisms of action', *Cancer Therapy: Preclinical,* 14(17), pp. 5519-5530. Available at: https://doi.org/10.1158/1078-0432.CCR-08-0197

Hasu, P. *et al.* (2020) 'The crosstalk between Src and Hippo/YAP Signalinh Pathways in Non-Small Cell Lung Cancer (NSCLC)', *Cancers,* 12(6), p. 1361.

Hsu, Y. *et al.* (2023) 'Anticancer Activity and Molecular Mechanisms of an Ursodeoxycholic Acid Methyl Ester-Dihydroartemisinin Hybrid via a Triazole Linkage in Hepatocellular Carcinoma Cells', *Molecules,* 28(5), article number 2358. Available at: https://doi.org/10.3390/molecules28052358

Hua, Y. *et al.* (2022) 'Drug repositioning: Progress and challenges in drug discovery for various diseases', *European Journal of Medicinal Chemistry,* 243, article number 114239. Available at: https://doi.org/10.1016/j.ejmech.2022.114239

Ismail, M. *et al.* (2018) 'Liposomes of dimeric artesunate phospholipid: A combination of dimerization and self-assembly to combat malaria', *Biomaterials,* 163, pp. 76-87. Available at: https://doi.org/10.1016/j.biomaterials.2018.02.026

Jahan, M. *et al.* (2021) 'Structure-Activity Relationships of the Antimalarial Agent Artemisinin 10. Synthesis and Antimalarial Activity of Enantiomers of *rac*-5β-Hydroxy-D -Secoartemisinin and Analogs: Implications Regarding the Mechanism of Action', *Molecules,* 26(14), p. 4163. Available at: https://doi.org/10.3390/molecules26144163

Ji, X. *et al.* (2018) 'Cyclopeptide RA-V Inhibits Organ Enlargement and Tumorigenesis Induced by YAP Activation', *Cancers,* 10(11), article number 449. Available at: https://doi.org/10.3390/cancers10110449

Jia, J. *et al.* (2016) 'Artemisinin inhibits gallbladder cancer cell lines through triggering cell cycle arrest and apoptosis', *Molecular Medicine Reports,* 13, pp. 4461-4468. Available at: https://doi.org/10.3892/mmr.2016.5073

Jiang, F. *et al.* (2018) 'Artesunate induces apoptosis and autophagy in HCT116 colon cancer cells, and autophagy inhibition enhances the artesunate-induced apoptosis', *International Journal of Molecular Medicine,* 42(3), pp. 1295-1304. Available at: https://doi.org/10.3892/ijmm.2018.3712

Jiu, X., Liu, Y. and Wen, J. (2021) 'Artesunate combined with verteporfin inhibits uveal melanoma regulation of the *MALAT1/*yes-associated protein signaling', *Oncology Letters,* 22(2), article number 597. Available at: https://doi.org/10.3892/ol.2021.12858

Kaczmarek, M. *et al.* (2023) 'Cancer Vaccine Therapeutics: Limitations and Effectiveness – A Literature Review', *Cells,* 12(17), p. 2159. Available at: https://doi.org/10.3390/cells12172159

Kamat, S. and Kumari, M. (2021) 'Repurposing Chloroquine Against Multiple Diseases With Special Attention to SARS-Cov-2 and Associated Toxicity', *Frontiers of Pharmacology,* 12, article number 576093. Available at: doi: https://doi.org/10.3389/fphar.2021.576093

Kauanova, S., Urazbayev, A. and Vorobjev, I. (2021) 'The Frequent Sampling of Wound Scratch Assay Reveals the "Opportunity" Window for Quantitative Evaluation of Cell Motility-Impeding Drugs', *Frontiers of Cell Developmental Biology,* 9, article number 640972. Available at: https://doi.org/10.3389/fcell.2021.640972

Kiani, B. H. *et al.* (2020) 'Artemisinin and its derivatives: a promising cancer therapy', *Molecular Biology Reports,* 47, pp. 6321-6336. Available at: https://doi.org/10.1007/s11033-020-05669-z

Kimura, T. *et al.* (2013) 'Chloroquine in Cancer Therapy: A Double-Edged Sword of Autophagy', *American Association for Cancer Research,* 73(1), pp. 3-7. Available at: https://doi.org/10.1158/0008-5472.CAN-12-2464

Krishna, S. *et al.* (2008) 'Artemisinins: their growing importance in medicine', *Trends in Pharmacological Sciences,* 29(10), PP. 520-527. Available at: https://doi.org/10.1016/j.tips.2008.07.004

Kulkarni, V. S. *et al.* (2023) 'Drug Repurposing: An Effective Tool in Modern Drug Discovery', *Russian Journal of Bioorganic Chemistry,* 49, pp. 157-166. Available at: https://doi.org/10.1134/S1068162023020139

Lamar, J. M. *et al.* (2019) 'SRC tyrosine kinase activates the YAP/YAZ axis and thereby drives tumour growth and metastasis', *Journal of Biological Chemistry,* 294(7), pp. 2302-2317.

Lee, K. and Yonehara, S. (2012) 'Identification of Mechanism That Couple Multisite Phosphorylation of Yes-associated Protein (YAP) with Transcriptional Coactivation and

Regulation and Apoptosis', *Journal of Biological Chemistry,* 287(12), pp. 9658-9578. Available at: https://doi.org/10.1074/jbc.M111.296954

Li, P. *et al.* (2016) 'αE-catenin inhibits a Src-YAP$_1$ oncogenic module that couples tyrosine kinases and the effector of Hippo signaling pathway', *Genes & Development,* 30, pp. 798-811.

Li, X. *et al.* (2018) 'The selectivity of artemisinin-based drugs on human lung normal and cancer cells', *Environmental Toxicology and Pharmacology,* 57, pp. 86-94. Available at: https://doi.org/10.1016/j.etap.2017.12.004

Li, Y. *et al.* (2019) 'Artemisinin suppresses hepatocellular carcinoma cell growth, migration and invasion by targeting cellular bioenergetics and Hippo-YAP signaling', *Archives of Toxicology,* 93, pp. 3367-3383. Available at: https://doi.org/10.1007/s00204-019-02579-3

Li, Z. *et al.* (2018) 'Loss of the FAT1 Tumor Suppressor Promotes Resistance to CDK4/6 Inhibitors via the Hippo Pathway', *Cancer Cell,* 34(6), pp. 893-905. Available at: https://doi.org/10.1016/j.ccell.2018.11.006

Liang, C. *et al.* (2007) '*In vitro* scratch assay: a convenient and inexpensive method for analysis of cell migration *in vivo', Nature,* 2, pp. 329-333. Available at: https://doi.org/10.1038/nprot.2007.30

Liu, H. *et al.* (2019) 'Effects of genistein on anti-tumor activity of cisplatin in human cervical cancer cell lines', *Obstetrics & Gynecology Science,* 62(5), pp. 322-328. Available at: https://doi.org/10.5468/ogs.2019.62.5.322

Lu, T. *et al.* (2018) 'Yes-associated protein enhances proliferation and attenuates sensitivity to cisplatin in human gastric cancer cells', *Biomedicine & Pharmacotherapy,* 105, pp. 1269-1275. Available at: https://doi.org/10.1016/j.biopha.2018.06.031

Lv, L. and Ziangxiang, Z. (2023) 'Targeting Hippo signaling in cancer: novel perspectives and therapeutic potential', *MedComm,* 4(5), p. e375. Available at: https://doi.org/10.1002/mco2.375

Ma, Z. *et al.* (2021) 'Repurposing Artemisinin and its Derivatives as Anticancer Drugs: A Chance or Challenge', *Frontiers of Pharmacology,* 12, article number 828856. Available at: https://doi.org/10.3389/fphar.2021.828856

Marino, P. *et al.* (2023) 'Potential Role of Natural Antioxidant Products in Oncological Diseases', *Antioxidants,* 12(3), p. 704. Available at: https://doi.org/10.3390/antiox12030704

May, E., Jenkins, J. R. and May, P. (1991) 'Endogenous HeLa p53 proteins are easily detected in HeLa cells transfected with mouse deletion mutant p53 gene', *Oncogene,* 6(8), pp. 1363-1365. Available at: https://pubmed.ncbi.nlm.nih.gov/1886712/#:~:text=Here%20it%20is%20shown%20that,as%20by%20Western%20blotting%20experiments. (Accessed: 10 September 2024)

Mizukami, S. *et al.* (1999) 'Imaging of caspase-3 activation in HeLa cells stimulated with etoposide using a novel fluorescent probe', *FEBS Letters,* 453(2), pp. 356-360. Available at: https://doi.org/10.1016/S0014-5793(99)00755-3

Mo, J. *et al.* (2015) 'Cellular energu stress induces AMPK-mediated regulation of YAP and the Hippo pathway', *Nature Cell Biology,* 17, pp. 500-510. Available at: https://doi.org/10.1038/ncb3111

Mukherjee, P. K. (2019) *Bioassay-Guided Isolation and Evaluation.* Available at: https://www.sciencedirect.com/science/article/abs/pii/B9780128133743000132 (Accessed: 15 September 2024)

Nam, W. *et al.* (2006) 'Effects of artemisinin and its derivatives on growth inhibition and apoptosis of oral cancer cells', *Head & Neck,* 29(4), pp. 335-340. Available at: https://doi.org/10.1002/hed.20524

National Cancer Institute (2023) *What Is Cervical Cancer.* Available at: https://www.cancer.gov/types/cervical (Accessed: 01 January 2025).

Nguyen, C. and Yi, C. (2019) 'YAP/TAZ Signaling and Resistance to Cancer Therapy', *Trends in Cancer,* 5(5), pp. 283-296. Available at: https://doi.org/10.1016/j.trecan.2019.02.010

Ohashi, T. *et al.* (2017) 'p53 mediates the suppression of cancer cell invasion by inducing LIMA1/EPLIN', *Cancer Letters,* 390, pp. 58-66. Available at: https://doi.org/10.1016/j.canlet.2016.12.034

Ooko, E. *et al.* (2015) 'Artemisinin derivatives induce iron-dependent cell death (ferroptosis) in tumor cells', *Phytomedicine,* 22(11), pp. 1045-1054. Available at: https://doi.org/10.1016/j.phymed.2015.08.002

Pan, D. (2011) 'The Hippo Signaling Pathway in Development and Cancer', *Developmental Cell,* 19(4), pp. 491-505. Available at: https://doi.org/10.1016/j.devcel.2010.09.011

Pang, Y. *et al.* (2016) 'Artesunate induces ROS-dependent apoptosis via a Bax-mediated intrinsic pathway in Huh-7 and Hep3B cells', *Experimental Cell Research,* 2(1), pp. 251-260. Available at: https://doi.org/10.1016/j.yexcr.2016.06.012

Park, H. W. *et al.* (2015) 'Alternative Wnt Signaling Activates YAP/TAZ', *Cell,* 162(4), pp. 780-794. Available at: https://doi.org/10.1016/j.cell.2015.07.013

Puhalla, S., Bhattacharya, S. and Davidson, N. E. (2012) 'Hormonal therapy in breast cancer: A model disease for the personalization of cancer care', *Molecular Oncology,* 6(2), pp. 222-236. Available at: https://doi.org/10.1016/j.molonc.2012.02.003

Pushpakom, S. *et al.* (2019) 'Drug repurposing: progress, challenges and recommendations', *Nature Reviews Drug Discovery,* 18, pp. 41-58. Available at: https://doi.org/10.1038/nrd.2018.168

Rao, N. *et al.* (2022) 'Drug Repurposing: a Shortcut to New Biological Entities', *Pharmaceutical Chemistry Journal,* 56, pp. 1203-1214. Available at: https://doi.org/10.1007/s11094-022-02778-w

Rivlin, N. *et al.* (2011) 'Mutations in the p53 Tumor Suppressor Gene', *Genes & Cancer,* 2(4), pp. 466-474. Available at: https://doi.org/10.1177/1947601911408889

Runel, G. *et al*. (2021) 'Biomechanical Properties of Cancer Cells', *Cells,* 10(4), p. 887.

Ruwizhi, N. *et al.* (2022) 'Recent Advances in the Therapeutic Efficacy of Artesunate', *Pharmaceutics,* 14(3), p. 504. Available at: https://doi.org/10.3390/pharmaceutics14030504

Samji, R. *et al.* (2021) 'Regulation of Hippo signalling pathway in cancer: A MicroRNA perspective', *Cellular Signalling,* 78, article number 109858. Available at: https://doi.org/10.1016/j.cellsig.2020.109858

Saraei, P. *et al.* (2019) 'The beneficial effects of metformin on cancer prevention and therapy: a comprehensive review of recent advances', *Cancer Management and Research,* 2019(11), pp. 3925-3313. Available at: https://doi.org/10.2147/CMAR.S200059

Sasaki, H. (2015) 'Position- and polarity- dependent Hippo signaling regulates cell fates in preimplantation mouse embryos', *Seminars in Cell & Developmental Biology,* 47-48, pp. 80-87. Available at: https://doi.org/10.1016/j.semcdb.2015.05.003

Schiavoni, G. *et al.* (2024) 'Role of Hippo pathway dysregulation from gastrointestinal premalignant lesions to cancer', *Journal of Translational Medicine,* 22, article number 213. Available at: https://doi.org/10.1186/s12967-024-05027-8

Shi, R. *et al.* (2015) 'Artesunate altered cellular mechanical properties leading to deregulation of cell proliferation and migration in esophageal squamous cell carcinoma', *Oncology Letters,* pp. 2249-2255. Available at: https://doi.org/10.3892/ol.2015.2982

Spreckelmeyer, S., Orvig, C. and Casini, A. (2014) 'Cellular transport mechanisms of cytotoxic metallodrugs: an overview beyond cisplatin', *Molecules,* 19(10), pp. 15584-15610. Available at: https://doi.org/10.3390/molecules191015584

Sterling, N. *et al.* (2020) '*De novo* variants in MPP5 cause global developmental delay and behavioural change', *Human Molecular Genetics,* 29(20), pp. 3388-3401. Available at: https://doi.org/10.1093/hmg/ddaa224

Strik, H., Efferth, T. and Kaina, B. (2024) 'Artesunate in glioblastoma therapy: Case reports and review of clinical studies', *Phytomedicine,* 123, article number 155274. Available at: https://doi.org/10.1016/j.phymed.2023.155274

Tilsed, C. M. *et al.* (2022) 'Cancer chemotherapy: insights into cellular and tumor microenvironmental mechanisms of action', *Frontiers in Oncology,* 12, article number 960317, Available at: https://doi.org/10.3389/fonc.2022.960317

Tong, Y. *et al.* (2016) 'Artemisinin and its derivatives can significantly inhibit lung tumorigenesis and tumor metastasis through Wnt/β-catenin signaling', *Oncotarget,* 7(21), pp. 31413-31428. Available at: https://doi.org/10.18632/oncotarget.8920

Tumaneng, K. *et al.* (2014) 'YAP medicates crosstalk between the Hippo and PI3K-TOR pathways by suppressing PTEN via miR-29', *Nature Cell Biology,* 14, pp. 1322-1329. Available at: https://doi.org/10.1038/ncb2615

Upadhyay, A. (2021) 'Cancer: An unknown territory; rethinking before going ahead', *Genes & Diseases,* 8(5), pp. 655-661.

Varelas, X. *et al.* (2010) 'The Crumbs Complex Couples Cell Density Sensing to Hippo-Dependent Control of the TGF-β-SMAD Pathway', *Developmental Cell,* 19(6), pp. 831-844. Available at: https://doi.org/10.1016/j.devcel.2010.11.012

Wang, L. and Baker, N. E. (2019) 'Salvador-Warts-Hippo pathway regulates sensory organ development via caspase-dependent nonapoptotic signaling', *Cell Death & Disease,* 10, article number 669, Available at: https://doi.org/10.1038/s41419-019-1924-3

World Health Organization (2024) *Cervical Cancer.* Available at: https://www.who.int/news-room/fact-sheets/detail/cervical-cancer (Accessed: 29 December 2024).

Willoughby, J. A. *et al.* (2009) 'Artemisinin Blocks Prostate Cancer Growth and Cell Cycle Progression by Disrupting Sp1 Interactions with the Cyclin-dependent Kinase-4 (CDK_4) Promoter and Inhibiting CDK_4 Gene Expression', *Journal of Biological Chemistry,* 284(4), pp. 2203-2213. Available at: https://doi.org/10.1074/jbc.M804491200

Wong, Y. K. *et al.* (2017) 'Artemisinin as an anticancer drug: Recent advances in target profiling and mechanisms of action', *Medicinal Research Reviews,* 37(6), pp. 1492-1517. Available at: https://doi.org/10.1002/med.21446

Wu, G. *et al.* (2013) 'Synergistic anti-cancer activity of the combination of dihydroartemisinin and doxorubicin in breast cancer cells', *Pharmacological Reports,* 65, pp. 453-459.

Xiao, Y. and Dong, J. (2021) 'The Hippo Signalling Pathway in Cancer: A Cell Cycle Perspective', *Cancers,* 13(24), p. 6214. Available at: https://doi.org/10.3390/cancers13246214

Xu, C. *et al.* (2020) 'Artemisinins as Anticancer Drugs: Novel Therapeutic Approaches, Molecular Mechanisms, and Clinical Trials', *Frontiers of Pharmacology,* 11, article number 529881. Available at: https://doi.org/10.3389/fphar.2020.529881

Xu, N. *et al*. (2015) 'Artesunate Induces SKM-1 Cells Apoptosis by Inhibiting Hyperactive β-catenin Signalling Pathway', *International Journal of Medical Sciences,* 12(6), pp. 524-529. Available at: https://doi.org/10.7150/ijms.11352

Yang, X. *et al.* (2021) 'Progress on the study of the anticancer effects of artesunate', *Oncology Letters,* 22(5), article number 750. Available at: https://doi.org/10.3892/ol.2021.13011

Yuan-Ce, Li. *et al.* (2023) 'Artesunate, as an Hsp90 inhibitor, inhibits the proliferation of Burkitt's lymphoma cells by inhibiting AKT and ERK', *Frontiers of Pharmacology,* 14. Available at: https://doi.org/10.3389/fphar.2023.1218467Zhang, S. *et al.* (2011) 'EPLIN Downregulation Promotes Epithelial-Mesenchymal Transition in Prostate Cancer Cells and Correlates with Clinical Lymph Node Metastasis', *Oncogene,* 30, pp. 4941-4952. Available at: https://doi.org/10.1038/onc.2011.199

Zhang, S *et al.* (2020) 'Cervical cancer: Epidemiology, risk factors and screening', *Chinese Journal of Cancer Research,* 32(6), pp. 720-728. Available at: https://doi.org/ 10.21147/j.issn.1000-9604.2020.06.05

Zhao, B *et al.* (2007) 'Inactivation of YAP oncoprotein by the Hippo pathway is involved in cell contact inhibition and tissue growth control', *Gene & Development,* 21(21), pp. 2747-2761. Available at: https://doi.org/10.1101/gad.1602907

Zhao, F. *et al.* (2013) 'Artesunate exerts specific cytotoxicity in retinoblastoma cells via CD71', *Oncology Reports,* 30(3), pp. 1473-1482. Available at: https://doi.org/10.3892/or.2013.2574

Zhao, W. *et al.* (2021) 'Transcriptional co-activators YAP-TAZ: Potential therapeutic targets for metastatic breast cancer', *Biomedicine and Pharmacotherapy,* 133, article number: 110956. Available at: https://doi.org/10.1016/j.biopha.2020.110956

Zhou, H. *et al.* (2007) 'Artesunate inhibits angiogenesis and downregulates vascular endothelial growth factor expression in chronic myeloid leukemia K562 cells', *Vascular Pharmacology,* 47(2-3), pp. 131-138. Available at: https://doi.org/10.1016/j.vph.2007.05.002

Zhou, W. *et al.* (2020) 'Chloroquine against malaria, cancers and viral diseases', *Drug Discovery Today,* 25(11), pp. 2012-2022. Available at: https://doi.org/10.1016/j.drudis.2020.09.010

Zhou, Y. *et al.* (2017) 'Artesunate suppresses the viability and mobility of prostate cancer cells through UCA1, the sponge of miR-184', *Oncotarget,* 8(11), pp. 18260-18270. Available at: https://doi.org/10.18632/oncotarget.15353

Zhou, Z. and Li, M. (2022) 'Targeted therapies for cancer', *BMC Medicine,* 20, article number 90. Available at: https://doi.org/10.1186/s12916-022-02287-3

Zhu, S. *et al.* (2021) 'Ferroptosis: A Novel Mechanism of Artemisinin and its Derivatives in Cancer Therapy', *Current Medicinal Chemistry,* 28(2), pp. 329-345. Available at: https://doi.org/10.2174/0929867327666200121124404

Zhu, S. *et al.* (2014) 'Artemisinin reduces cell proliferation and induces apoptosis in neuroblastoma', *Oncology Reports,* pp.1094-1100. Available at: https://doi.org/10.3892/or.2014.3323

APPENDIX

Materials

Cell Culture Maintenance and Supplements

Material	Manufacturer
RPMI Medium 1640 (1X) [+] L-Glutamine	Gibco™ REF 21875-034 LOT 2726818
Penicillin-Streptomycin 13	Gibco™ REF 15140-122 LOT 2145456
Foetal Bovine Serum (FBS)	Gibco™ REF 16000-044 LOT 2565223RP
0.5% Trypsin-EDTA (10X)	Gibco™ REF 15400-054 LOT 2053183
DPBS (1X) Dulbecco's Phosphate Buffered Saline [-] Calcium Chloride [-] Magnesium Chloride	Gibco™ REF 14190-144 LOT 1234567

Table I

Drug Treatment

Drug Name	Manufacturer
Artemisinin	Sigma-Aldrich, Catalogue no. 361593-100MG
Artesunate	Sigma-Aldrich, Catalogue no. A3731-100MG
Cisplatin	Sigma-Aldrich, Catalogue no 232120-50MG

Table II

MTT Assay

	Manufacturer
Cell Proliferation Kit I (MTT) - MTT labelling reagent (1X) 5mL x 5 - Solubilization buffer (1X) 90mL x 3	Roche, Catalogue no. 11 465 007 001

Table III

Caspase -3 Assay

	Manufacturer
Colorimetric Assay Kit	Millipore, Catalogue no. APT165

Table IV

Western Blotting – Lysis

Lysis Buffer Constitution	Manufacturer
1:10 NuPAGE Sample Reducing Agent (10X)	Invitrogen™, LOT 2190252
1:2 NuPAGE LDS Sample Buffer (4X)	Invitrogen™, LOT 2138054

Table V

SDS-PAGE

Separating Gel	Stacking Gel	Manufacturer
10mL of 30% (w/v) Acrylamide: 0.8% (w/v) Bis-Acryl-amide Stock Solution (37.5:1)	3mL of 30% (w/v) Acrylamide: 0.8% (w/v) Bis-Acryl-amide Stock Solution (37.5:1)	National Diagnostics
7.8mL of 4X ProtoGel Resolving Buffer (1.5M Tris-HCl, 0.4% SDS, pH 8.8)	4mL of Protogel Stacking Buffer (0.5M Tris HCl 0.4% SDS, pH 6.8)	National Diagnostics
9.15mL dH_2O	8.5mL dH_2O	
3.0mL of 1% Ammonium Persulfate (APS)	1.6mL of 1% Ammonium Persulfate (APS)	Sigma-Aldrich
50µL of Tetramethylethylenediamine (TEMED)	50µL of Tetramethylethylenediamine (TEMED)	Sigma-Aldrich

Table VI

Stock Running Buffer (1L)	Transfer Buffer (1L)	Manufacturer
1:10 dilution of Ultra Pure 10X TRIS/GLYCINE/SDS 0.25M Tris – 1.92M Glycine – 1% SDS with dH_2O	1:10 dilution of Ultra Pure 10X TRIS/GLYCINE/SDS 0.25M Tris – 1.92M Glycine – 1% SDS	National Diagnostics
	1:5 Methanol	
	Distilled Water	

Table VII

Immunofluorescence

	Constitution	Manufacturer
Blocking Buffer	1g of 1% BSA powder 0.07f of 20µM Glycine 100mL of 1X PBS	Sigma-Aldrich Fisher Bioreagents Gibco™
16% Formaldehyde Solution (w/v), Methanol Free	10mL of FPA 30mL PBS	ThermoScientific Gibco™
Antibody Dilution/ Permeabilization Buffer	40mL of Blocking Buffer 200µL of 20% Triton	

Table VIII

Antibodies

Antibody	Host	IB*	IF*	IP*	Manufacturer
Phospho-YAP (Ser127)	Rabbit	1:500	-	-	Cell Signalling Technology Catalogue no. 4911S LOT 5
YAP (63.7), IgG_{28}	Mouse Monoclonal	1:500	1:200	5	Santa Cruz Biotechnology Catalogue no. 101199
GAPDH (6C5), IgG_1	Mouse Monoclonal	1:1000	-	-	Santa Cruz Biotechnology Catalogue no. 32233
YAP (H-125), IgG	Rabbit monoclonal	1:500	-	-	Santa Cruz Biotechnology Catalogue no. 15407
IRDye 800 CW	Donkey anti-mouse	1:2500	1:300		LI-COR Catalogue no. 926-68073
IRDye 680 RD	Donkey anti-rabbit	1:2500	-	-	LI-COR Catalogue no. 926-68073

**IB: Immunoblotting, IF: Immunofluorescence, IP: Immunoprecipitation*

Table IX

RNA Extraction

	Manufacturer
RNeasy Mini Kit (50) - Buffer RW1 Wash buffer - Buffer RLT Lysis buffer - Buffer RPE Wash buffer (11mL concentrate) - RNase-free-water	Qiagen, Catalogue no. 74104

Table X

cDNA Synthesis

	Manufacturer
High Capacity RNA-to-cDNA Kit - RT Enzyme Mix - RT Buffer Mix	Applied Biosystems, Catalogue no, 4387406

Table XI

RT-PCR

	Manufacturer
PowerTrack SYBR™ Green Master Mix - 40X Yellow Sample Buffer - SYBR Green Master Mix	Applied Biosystems Catalogue no. A46012
Primers (Forward and Reverse) - CTGF - c-Myc - Cyr61 - GAPDH - Wnt-1 - B-Cat - p53 - mTOR	Sigma-Aldrich

Table XII

Genes		Primers
CYR61	Forward	5'– GGTCAAAGTTACCGGGCAGT – 3'
	Reverse	3'– GGAGGCATCGAATCCCAGC – 5'
CTGF	Forward	5' – CAGCATGGACGTTCGTCTG – 3'
	Reverse	3'– AACCACGGTTTGGTCCTTGG – 5'
c-MYC	Forward	5' – AGGGATCGCGCTGAGTATAA – 3'
	Reverse	3' – TGCCTCTCGCTGGAATTACT – 5'
GAPDH	Forward	5' – CAATGACCCCTTCATTGACC – 3'
	Reverse	3' – GACAAGCTTCCCGTTCTCAG – 5'

Table XIII

Co-Immunoprecipitation

	Manufacturer
Magnetic Beads	MCE® MedChemExpress Protein A/G Magnetic Beads 1mL, Catalogue no. HY-K20202
Inhibitors	Sigma-Aldrich P0044-1mL Phosphatase Inhibitor Cocktail 3, Batch no. 0000080384 Sigma-Aldrich P2714-1BTL Protease Inhibitor Cocktail Powder, LOT no. 068M4099V
Wash Buffer	Sigma-Aldrich, Phosphate Buffered Saline (PBS)
Lysis Buffer	Sigma-Aldrich, Triton X-100 (10mL of PBS)

Table XIV